

Supporting Information

A coordinatively unsaturated iridium complex with an unsymmetrical redox-active ligand: (Spectro)electrochemical and reactivity studies

Sebastian Sobottka, Margarethe van der Meer, Estelle Glais, Uta Albold, Simon Suhr, Cheng-Yong Su, Biprajit Sarkar

Table of Contents

1	NMR Spectroscopy	3
2	X-ray Crystallography	11
3	Hydrogenation of <i>p</i> -benzoquinone	13
4	Cyclic Voltammetry	17
5	CV Simulation for 1.....	19
6	CV Simulation for 2.....	21
7	EPR-Spectroelectrochemistry	23
8	Interconversion of 2 ⁺ to 3 ⁺	24
8.1	Mass spectrum of 2 ⁺ and Fluoroform	25
8.2	Mass spectrometry of 2 ⁺ and Chloroform	26
8.3	Mass spectrometry of 2 ⁺ and Bromoform	27
8.4	Mass spectrometry of 2 ⁺ and Iodoform.....	28
9	IR-spectroelectrochemistry	29
9.1	Spectra for 1 and 1 ²⁺ (experimental and calculated)	31
9.2	IR spectra of 2+.....	33
10	UV-Vis-NIR-Spectroelectrochemistry	38
10.1	Spectra for [2] ⁺	39
10.2	Spectra for [3] ⁺	42
11	(TD)DFT	43
11.1	General remarks	43
11.2	DFT Calculation for [1] (singlet state)	44
11.3	DFT Calculation [1] ⁺ (doublet state).....	45
11.4	DFT Calculation [1] ²⁺ (singlet state)	50
11.5	DFT Calculation for [2] ⁺ (singlet state).....	55
11.6	DFT Calculation for [2] ⁰ (doublet state)	59
11.7	DFT Calculation for [2] ²⁻ (doublet state)	63
11.8	DFT Calculation for [3] ⁺ (singlet state).....	67
11.9	Coordinates of optimized structures	70

1 NMR Spectroscopy

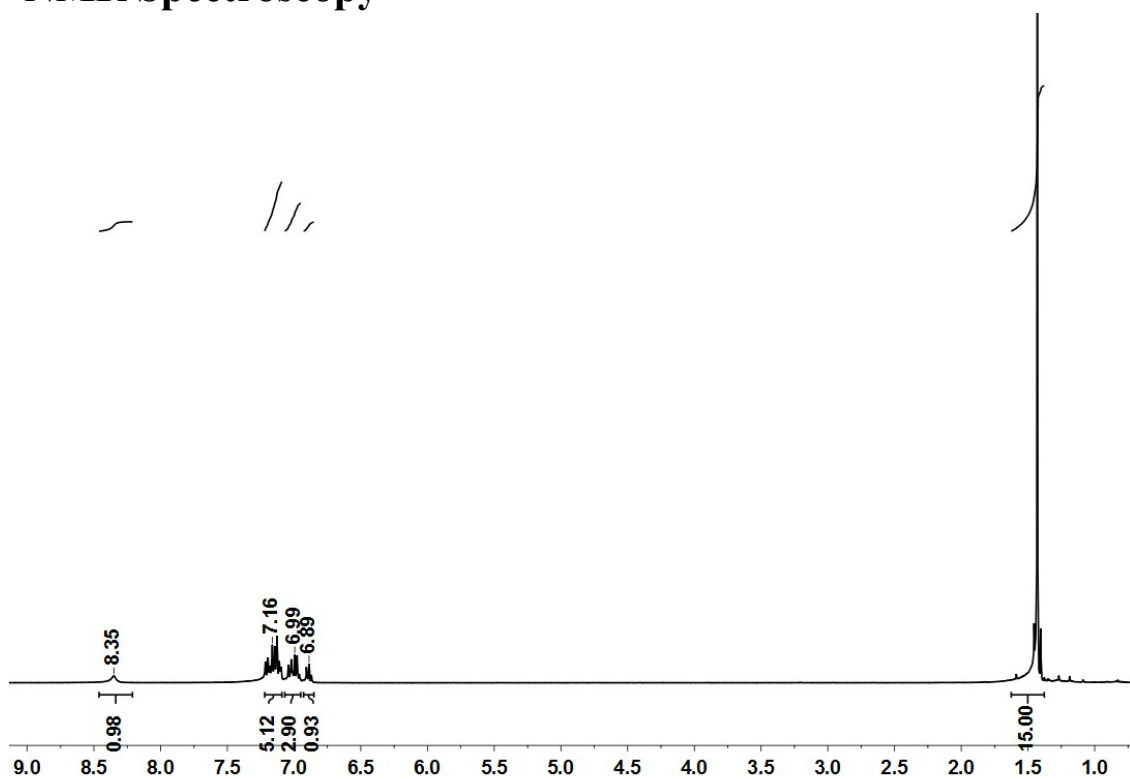


Figure S1: ^1H NMR spectrum of **1** in benzene-d₆.

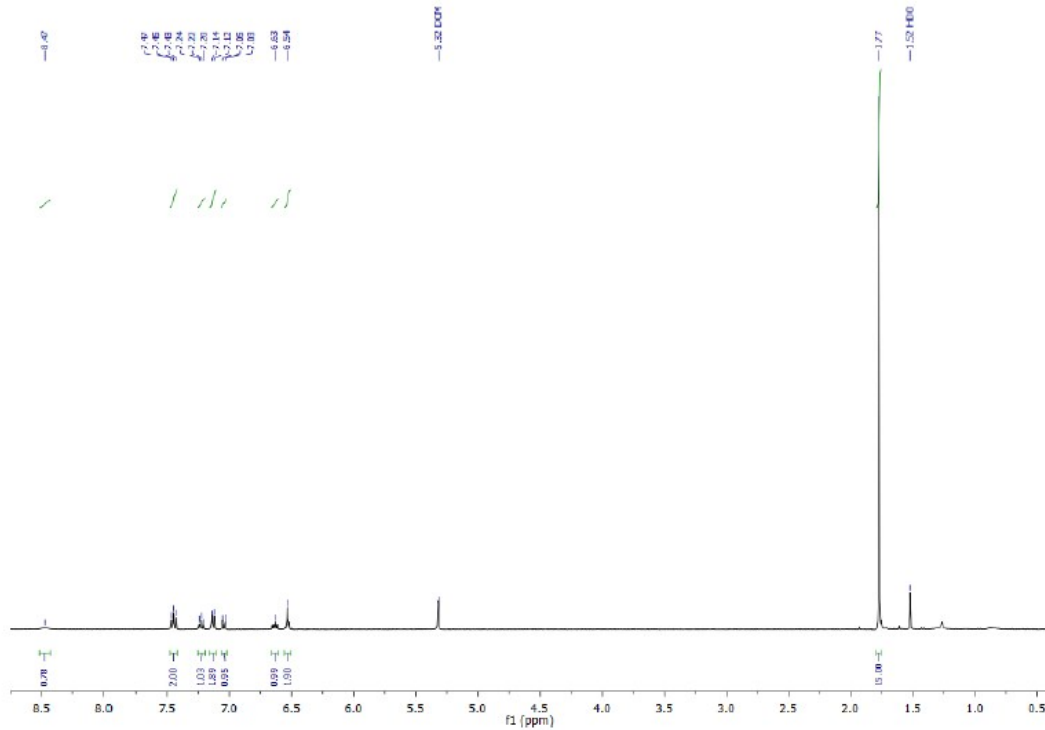


Figure S2: ^1H -NMR of 1 in CD_2Cl_2 .

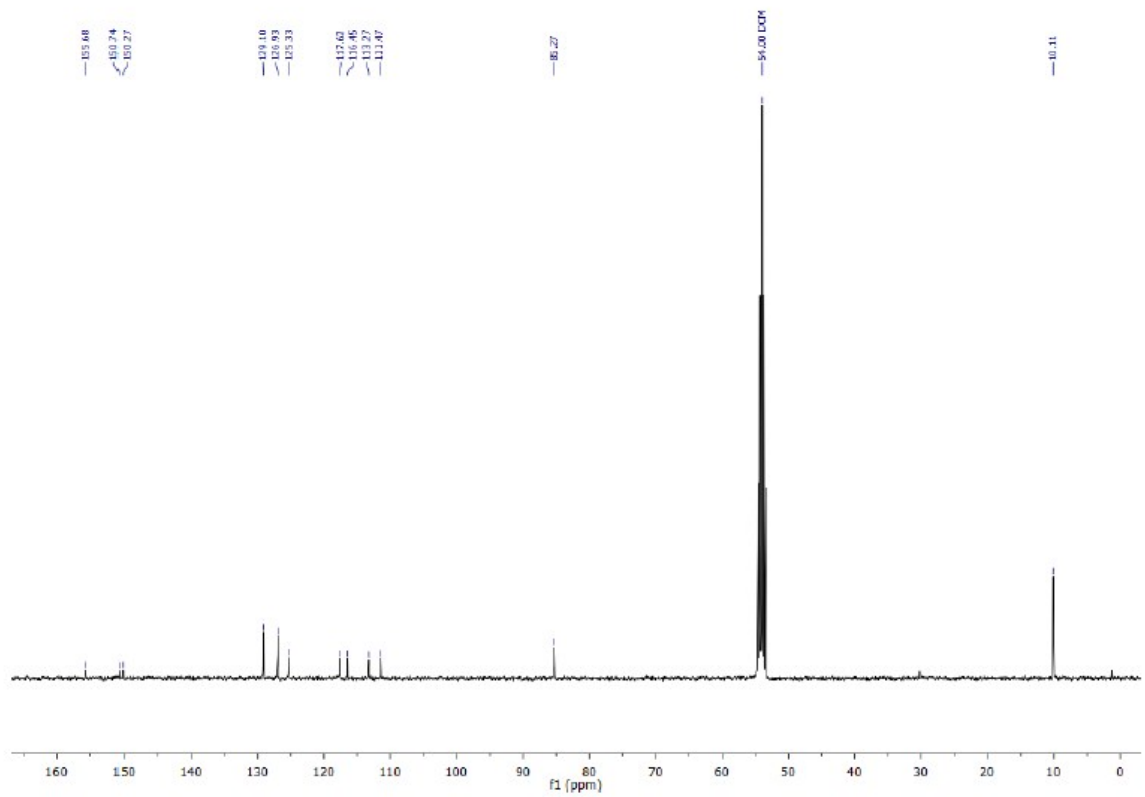


Figure S3: ¹³C-NMR of 1 in CD₂Cl₂.

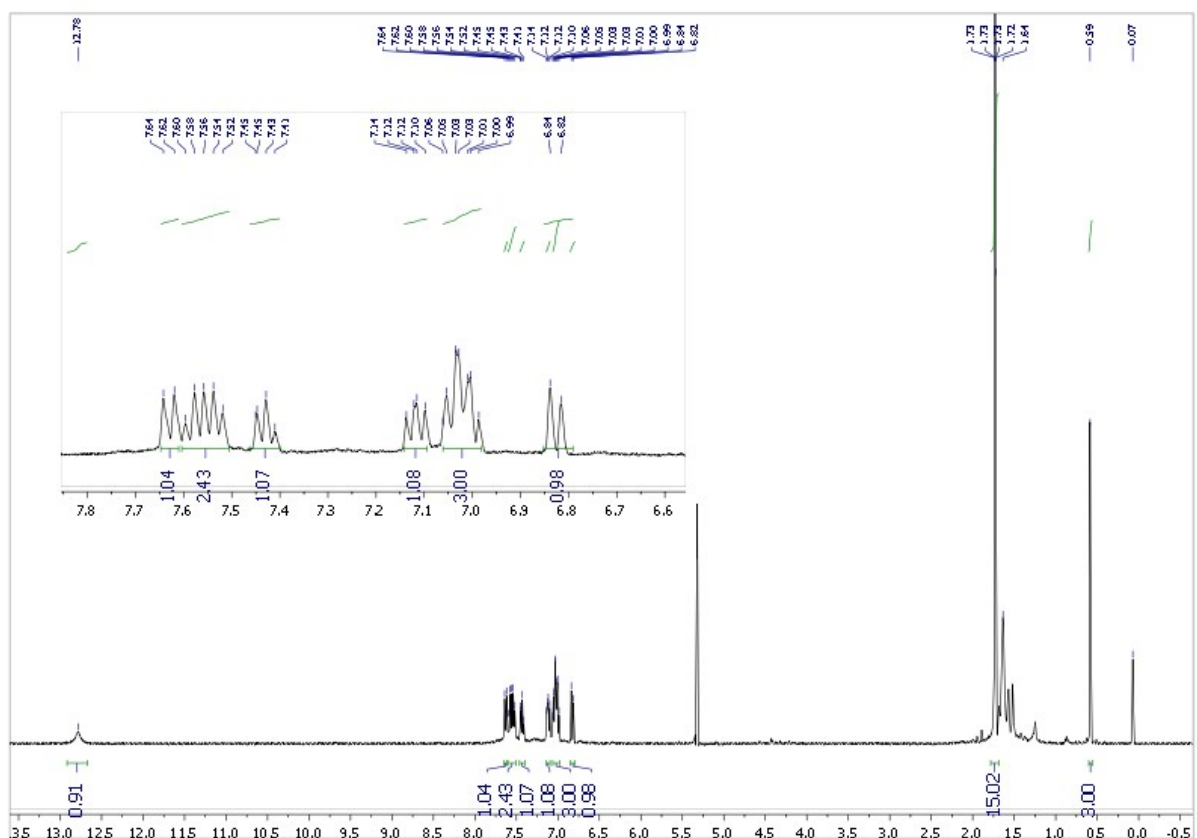


Figure S4: ¹H NMR spectrum of [2]BF₄ in CD₂Cl₂ measured at 283 K.

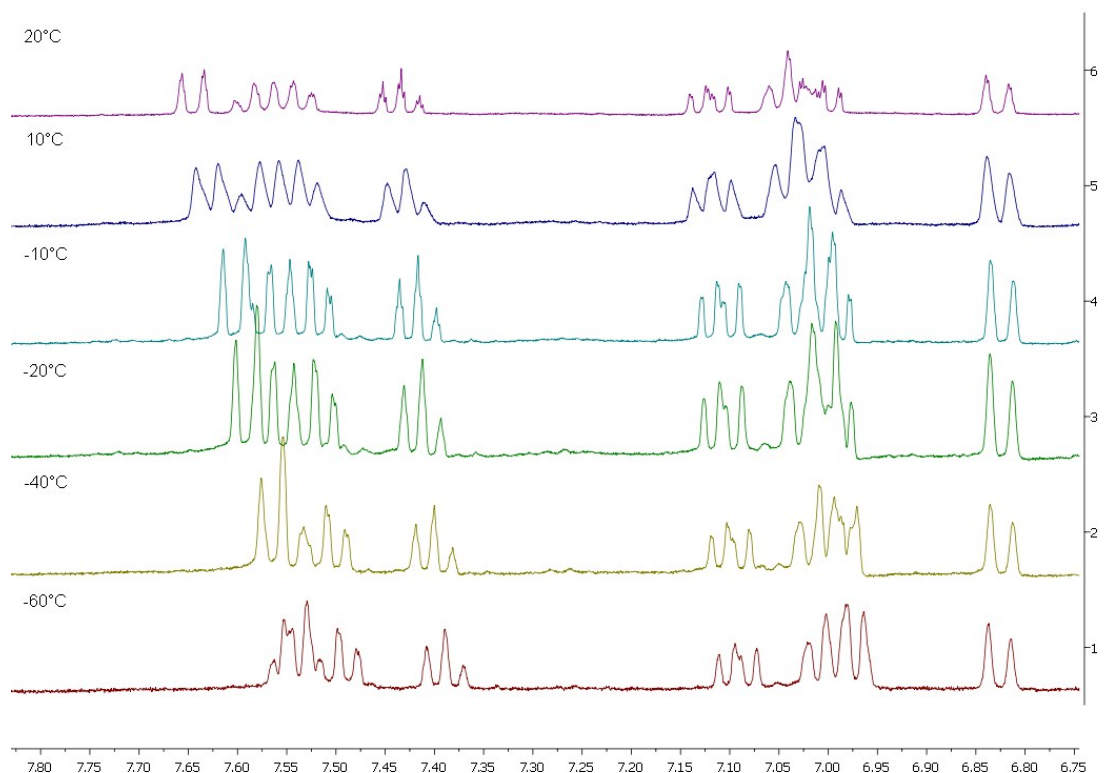


Figure S5: VT-NMR of $[2]\text{BF}_4$ in CD_2Cl_2 .

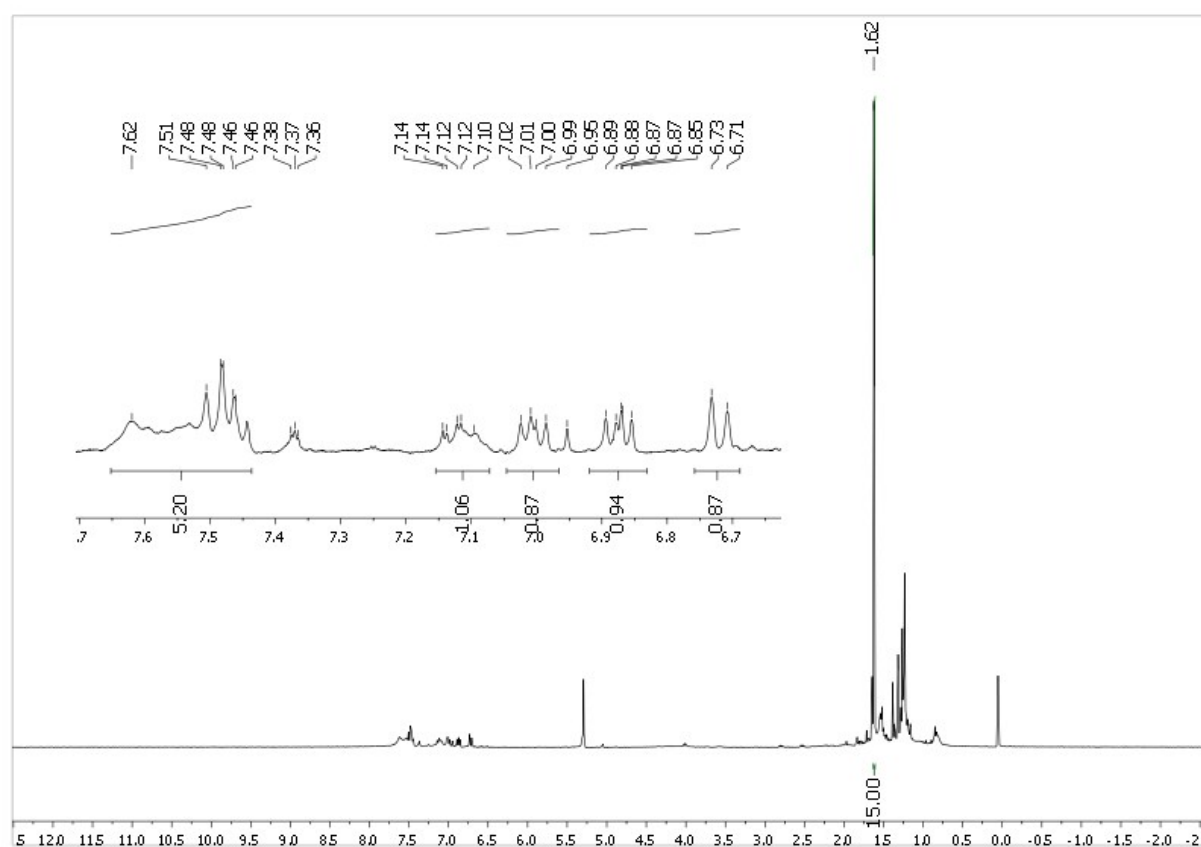


Figure S6: ^1H -NMR of $[3]\text{PF}_6$ in CD_2Cl_2 .

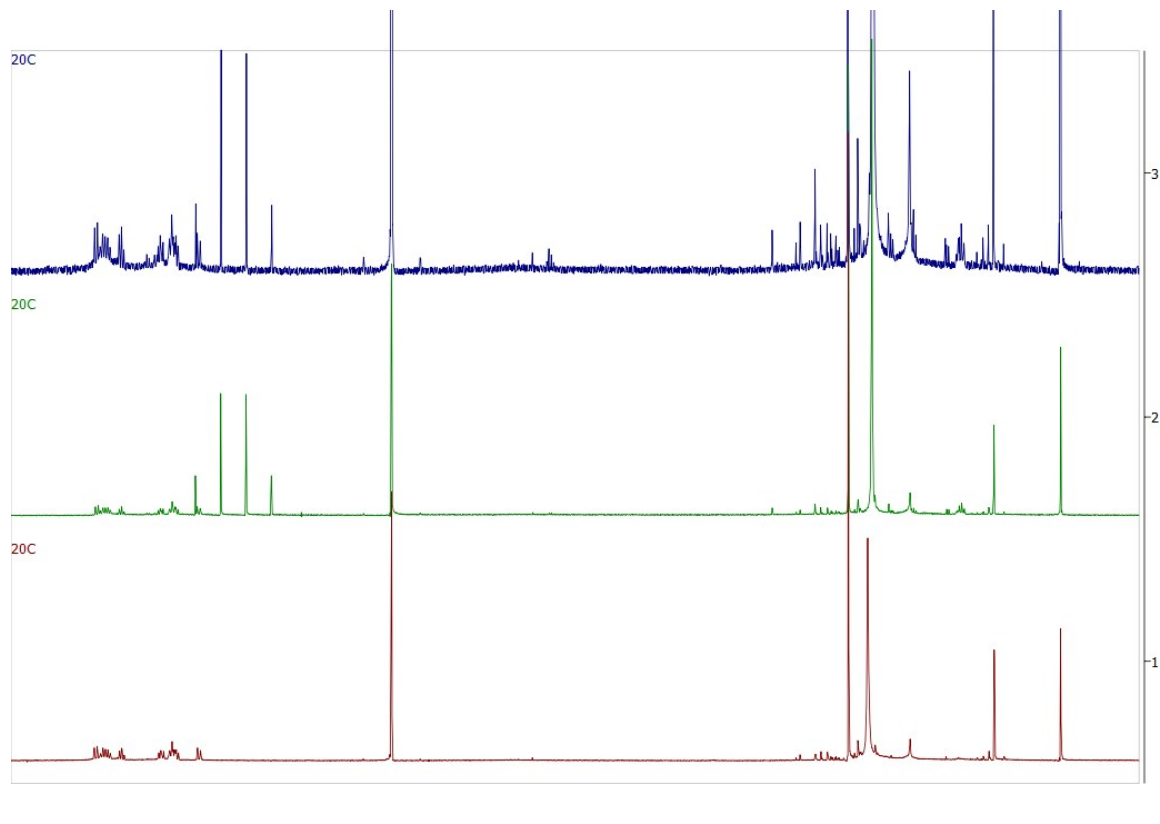


Figure S7: ^1H -NMR of 2+ and Fluoroform in CD_2Cl_2 . Quartet at 6.52 Fluoroform. (1) Spectrum of $[2]\text{BF}_4^-$ without Fluoroform. (2) Immediately after addition of Fluoroform (3) Three weeks after addition of fluoroform, storage at RT.

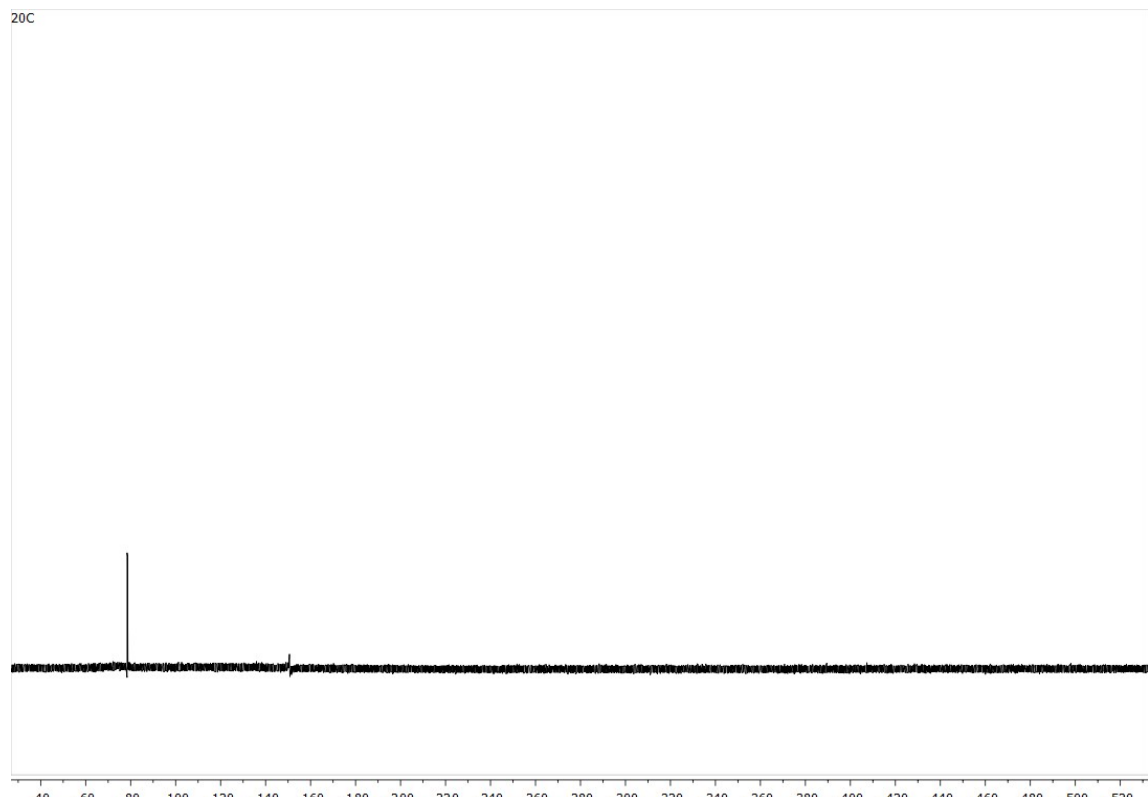


Figure S8: ^{19}F -NMR of $[2]\text{BF}_4^-$ in CD_2Cl_2 in the presence of Fluoroform, immediately after saturation.

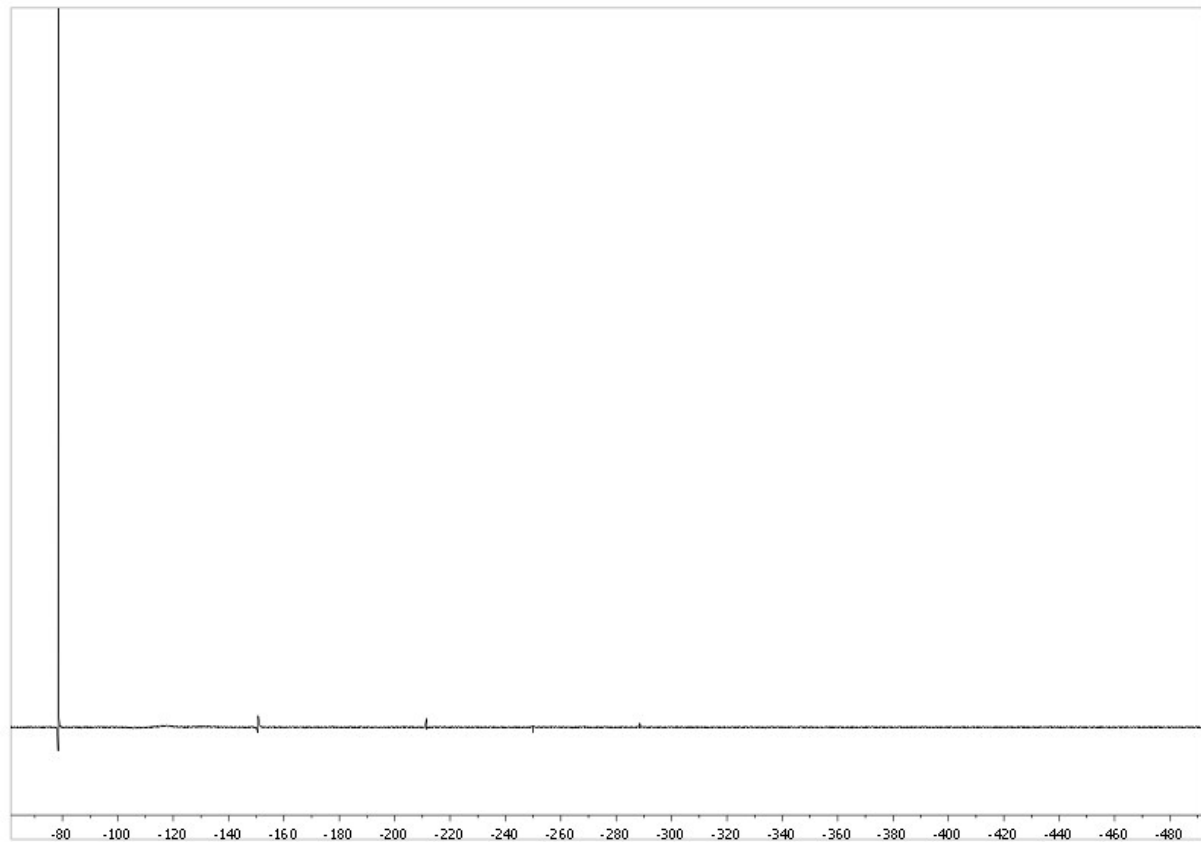


Figure S9: ¹⁹F-NMR of [2]BF₄ in CD₂Cl₂ in the presence of Fluoroform, after three weeks, storage at RT.

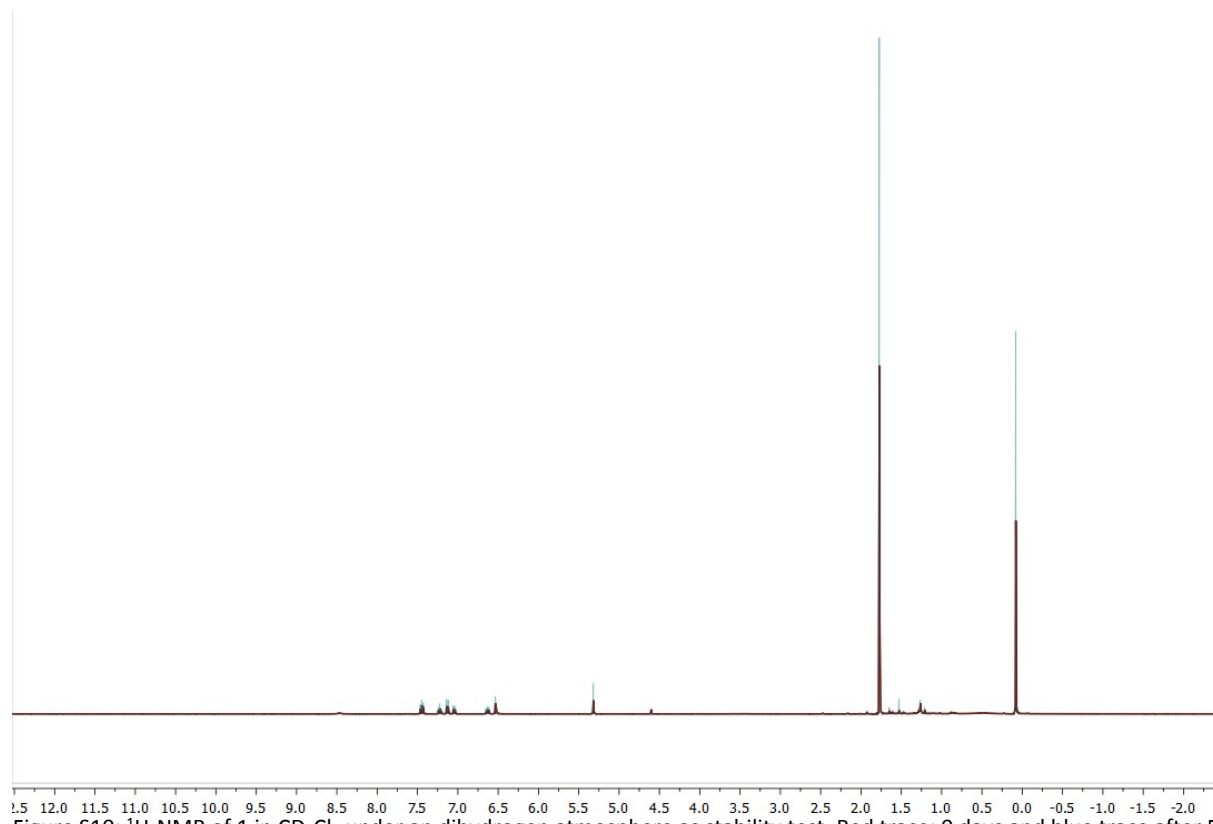


Figure S10: ¹H-NMR of 1 in CD₂Cl₂ under an dihydrogen atmosphere as stability test. Red trace: 0 days and blue trace after 5 days. Zoom on the next page.

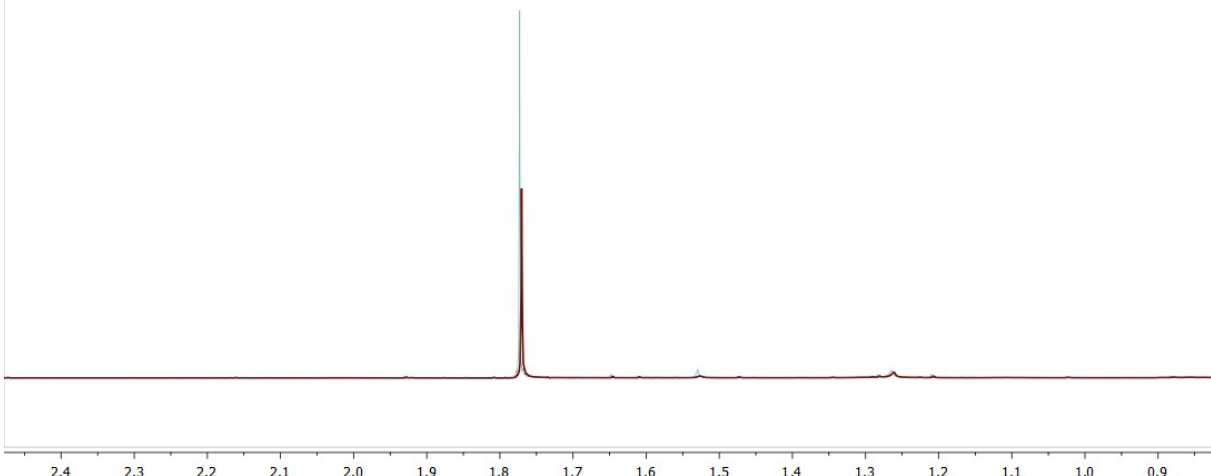


Figure S11: Zoom in of the ^1H -NMR of 1 in CD_2Cl_2 under an dihydrogen atmosphere as stability test. Red trace: 0 days and blue trace after 5 days.

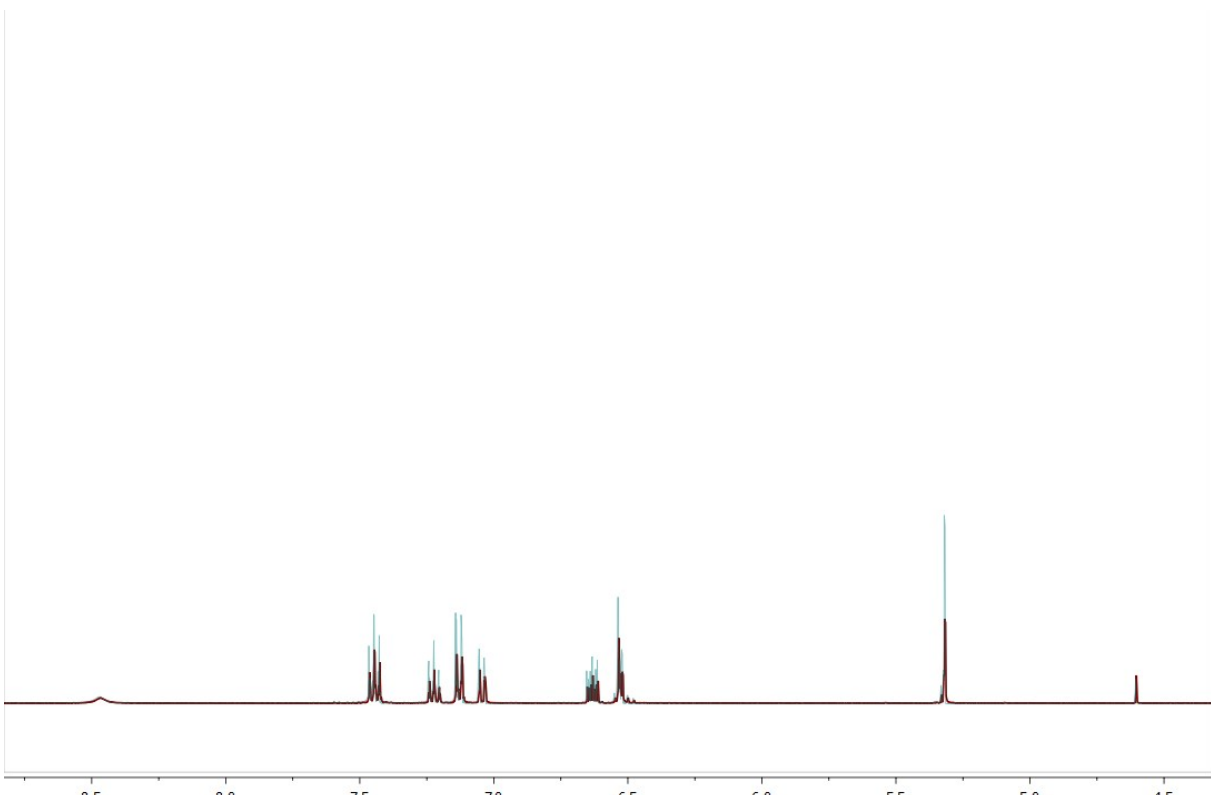


Figure S12: Zoom in of the ^1H -NMR of 1 in CD_2Cl_2 under an dihydrogen atmosphere as stability test. Red trace: 0 days and blue trace after 5 days.

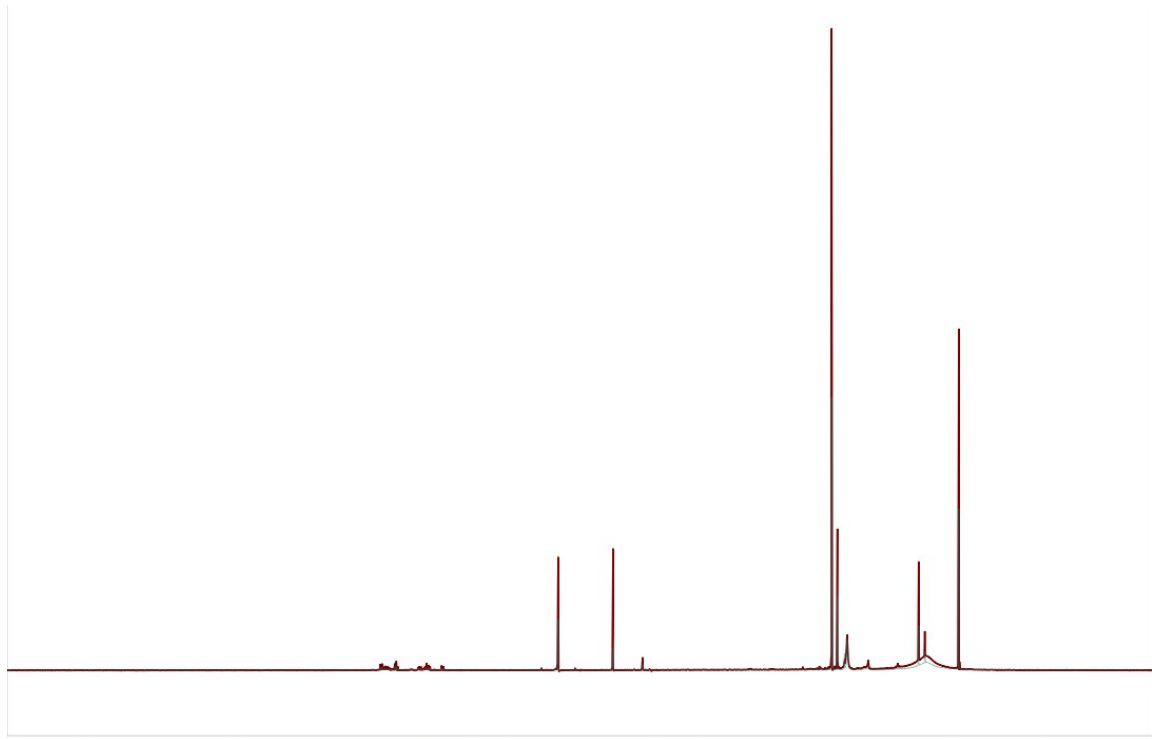


Figure S13: ^1H -NMR of 2^+ in CD_2Cl_2 under an dihydrogen atmosphere as stability test. Blue trace: 0 days and red trace after 3 days. Zoom on the next page.

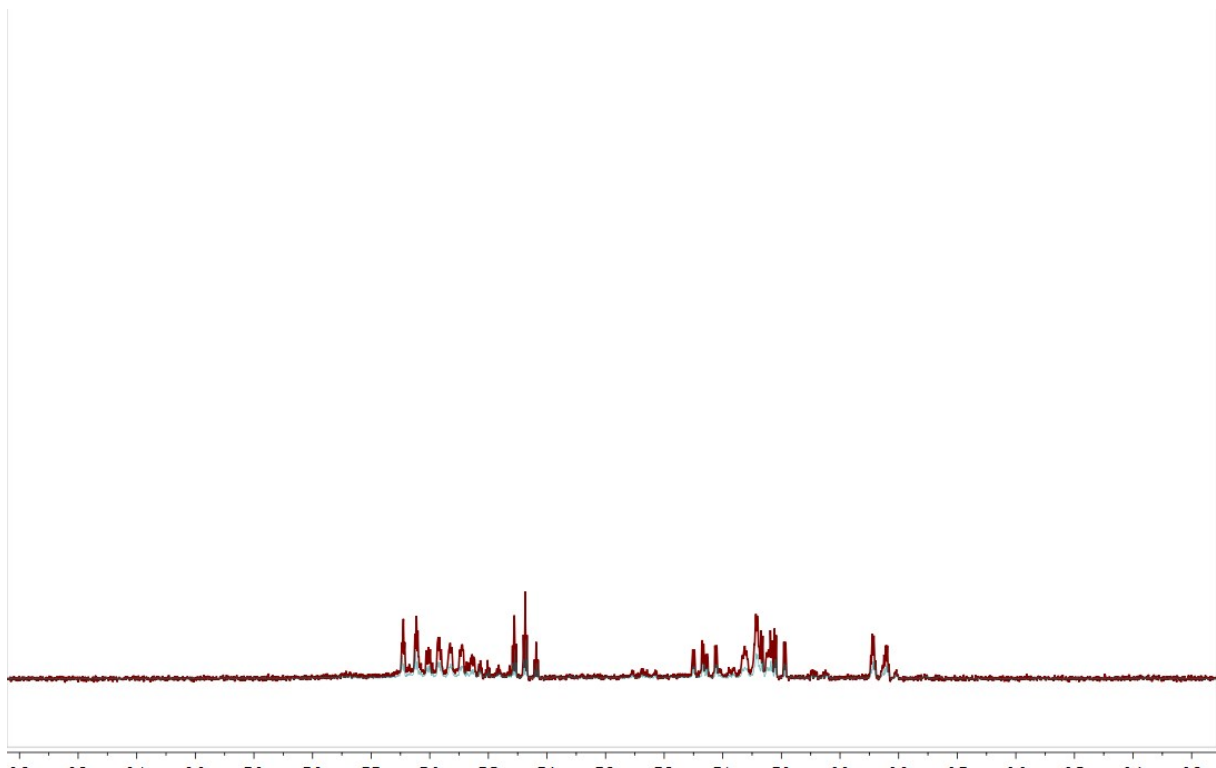


Figure S14: Zoom-in ^1H -NMR of 2^+ in CD_2Cl_2 under an dihydrogen atmosphere as stability test. Blue trace: 0 days and red trace after 3 days. Zoom on the next page.

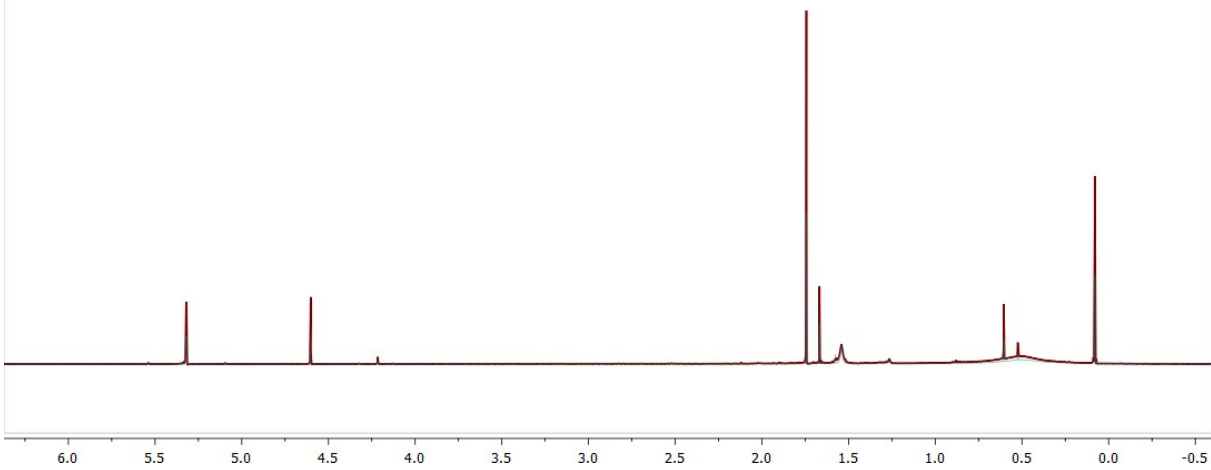


Figure S15: Zoom-in ¹H-NMR of 2⁺ in CD₂Cl₂ under an dihydrogen atmosphere as stability test. Blue trace: 0 days and red trace after 3 days. Zoom on the next page.

2 X-ray Crystallography

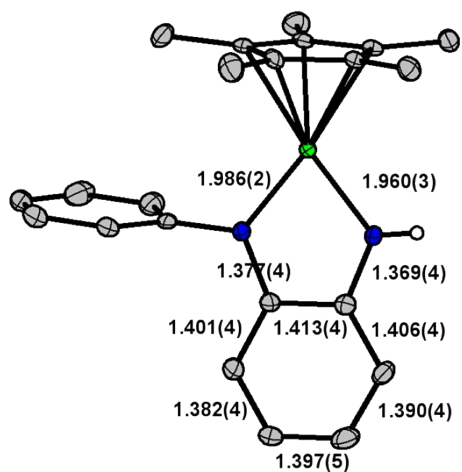


Figure S16: ORTEP representation of **[1]**. Hydrogen atoms are omitted for clarity.

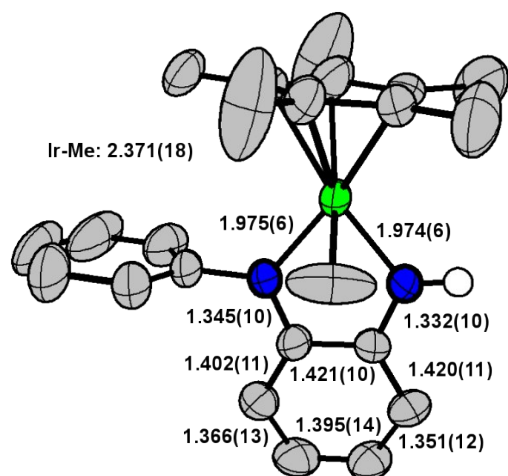


Figure S17: ORTEP representation of **[2]BF₄**. Anions and hydrogen atoms are omitted for clarity.

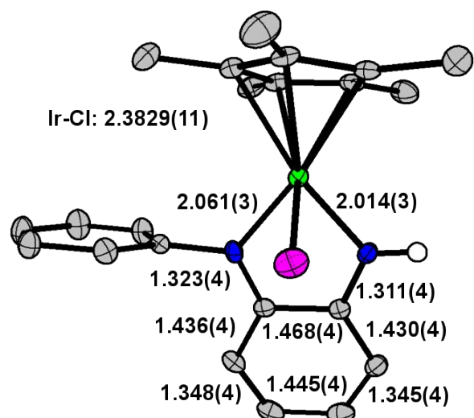


Figure S18: ORTEP representation of **[3]OTf**. Anions and hydrogen atoms are omitted for clarity.

Table S1 Crystallographic details for [1], [2]BF₄ and [3]OTf

	[1]	[2]BF ₄	[3]OTf
Chemical formula	C ₂₂ H ₂₅ IrN ₂	C ₂₃ H ₂₇ B F ₄ IrN ₂	C ₂₃ H ₂₅ ClF ₃ IrN ₂ O ₃ S
M _r	509.64	610.47	694.16
Crystal system	Monoclinic	triclinic	monoclinic
Space group	P2 ₁ /c	P-1	P2 ₁ /c
a (Å)	10.4919(3)	9.8859(17)	14.743(8)
b (Å)	11.4836(4)	10.6665(19)	11.872(5)
c (Å)	15.7162(6)	11.563(2)	28.358(15)
α (°)	90	86.062(4)	90
β (°)	90.245	72.464(4)	96.077(15)
γ (°)	90	89.848(4)	90
V (Å ³)	1893.55(11)	1159.7(4)	4936(4)
Z	4	2	8
D _{calc} (g/cm ³)	1.788	1.748	1.868
Temperature (K)	100	140	100
μ (mm ⁻¹)	7.057	5.800	5.654
Crystal size (mm)	0.21 x 0.07 x 0.03	0.25 x 0.15 x 0.14	0.35 x 0.16 x 0.14
Kα	0.71073 (Mo)	0.71073 (Mo)	0.71073 (Mo)
F(000)	992	594	2704
meas./ indep. refl.	19851/ 4911	12766/ 4100	67206/ 10057
obsvd. [<i>I</i> > 2σ(<i>I</i>)] refl.	4235	3260	8348
R _{int}	0.0376	0.0290	0.0390
R[<i>F</i> ² > 2σ(<i>F</i> ²)]	0.0229	0.0443	0.0218
wR (<i>F</i> ²)	0.0432	0.1137	0.0399
S	1.053	1.102	1.052
Δρ _{max} , Δρ _{min} (e Å ⁻³)	1.371, -1.394	1.439, -1.256	1.116, -0.737

3 Hydrogenation of *p*-benzoquinone

To monitor the reaction of $[1]^+$ with dihydrogen by ^1H NMR, dry THF-d₈ was saturated with H₂ by the freeze and pump method. **1** (9.5 mg, 19 μmol , 1 eq) was dissolved in THF-d₈ (0.5 mL).

A ^1H NMR spectrum was measured (Figure SS14). FcBArF (19.5 mg, 19 μmol , 1 eq) was added and after 30 min a second ^1H NMR spectrum was recorded. Although no hydride signal was detected, the formation of a new complex was observed (Figure SS15). *p*-Benzoquinone (2 mg, 19 μmol , 1 eq) was added three times. After every addition a ^1H NMR spectrum was recorded (Figure SS16). The formation of 1,4-hydroxy benzene was observed.

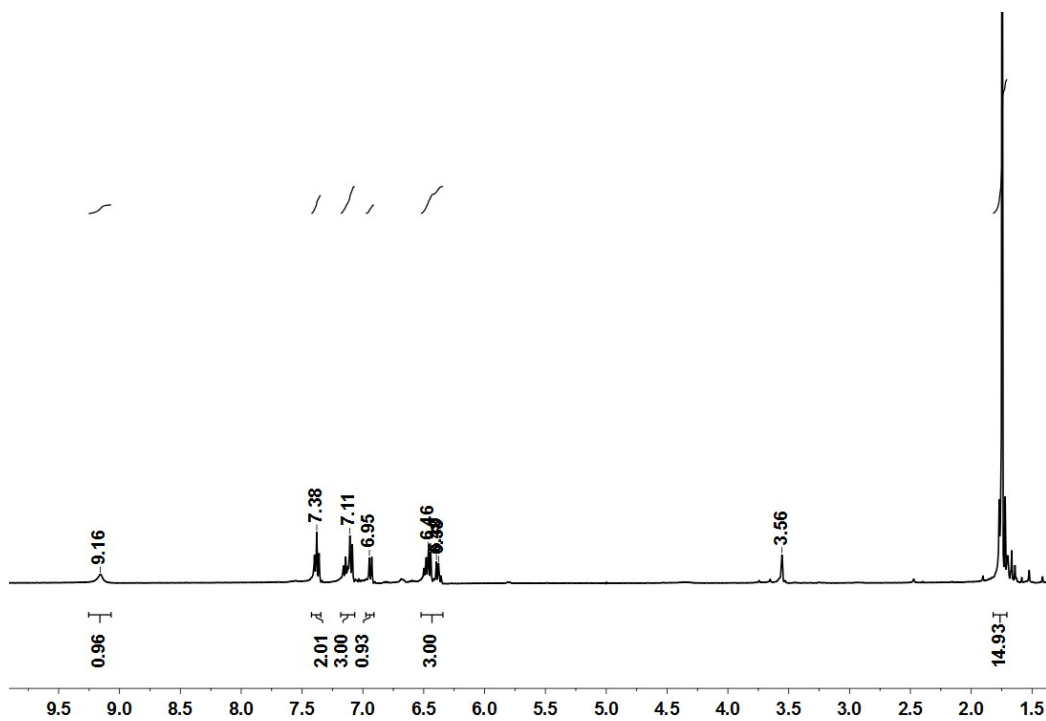


Figure S19: ¹H NMR spectrum of **1** in THF-d₈.

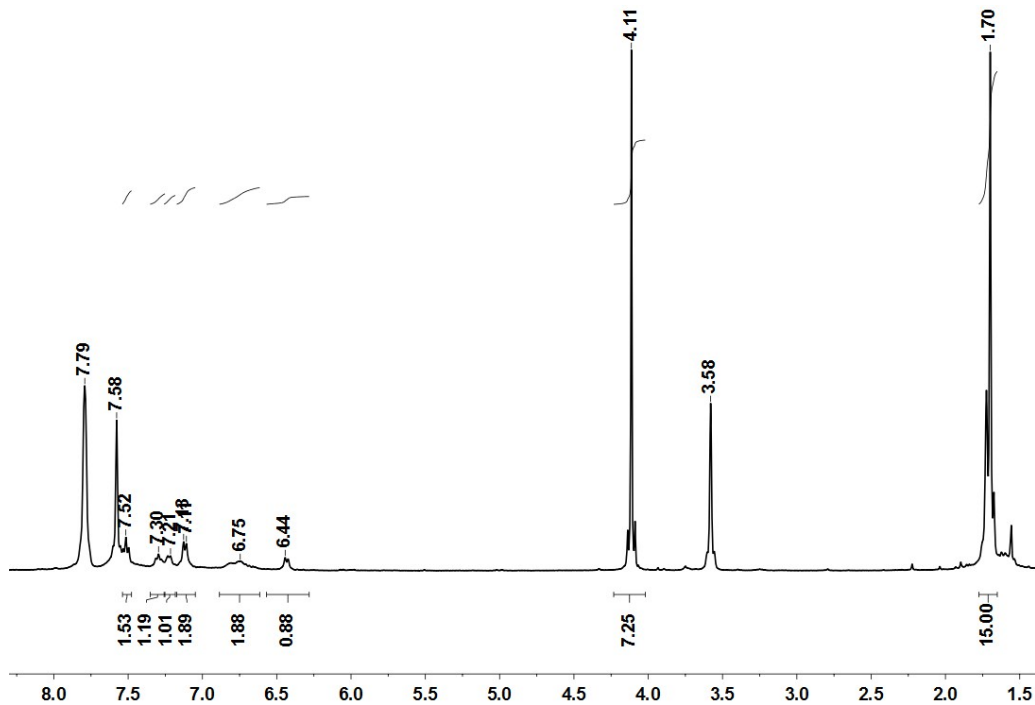


Figure S20: ¹H NMR of **1** after the addition of 1 eq of FcBArF. Signals at 4.11, 7.58 and 7.79 ppm correspond to ferrocene and BArF⁻, signals at 1.70, 6.44, 6.75, 7.18, 7.21, 7.30 and 7.51 ppm correspond to the formed iridium complex.

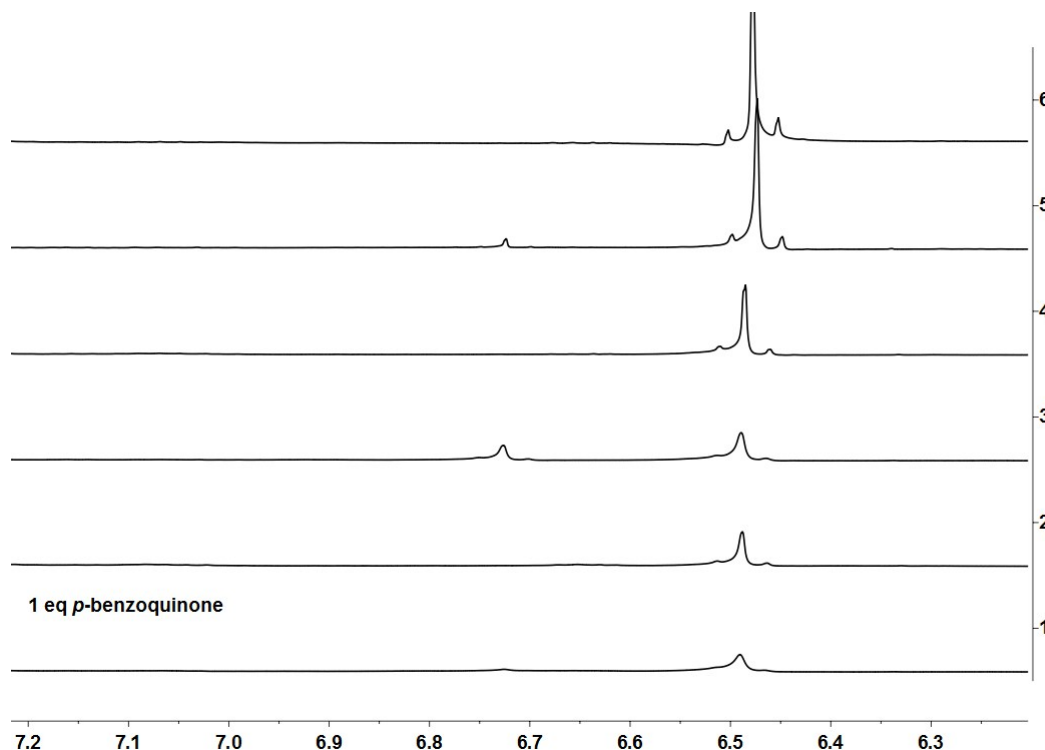


Figure S21:¹H NMR after the addition of 1 eq (1,2) and 2 eq (3, 4) and 3 eq (5, 6) of *p*-benzoquinone. Full conversion to 1,4 dihydroxy benzene was observed.

The solvent (THF) was saturated with dihydrogen before by the freeze and pump method. The reaction was carried out under H₂-atmosphere. **1** (4.0 mg, 7.9 μmol, 5 mol%) was dissolved in THF (2 mL) and FcBArF (8.2 mg, 7.9 μmol, 5 mol%) was added. After the addition of *p*-benzoquinone (17 mg, 0.16 mmol, 1 eq) the reaction mixture was stirred for 20 h at room temperature. The solvent was remove *in vacuum*, the residue was dissolved in CDCl₃ and filtrated of cotton, to remove the residue of the complex. 42 % conversion from *p*-benzoquinone to 1,4-dihydroxy benzene was reached. The conversion was calculated from the NMR integrals.

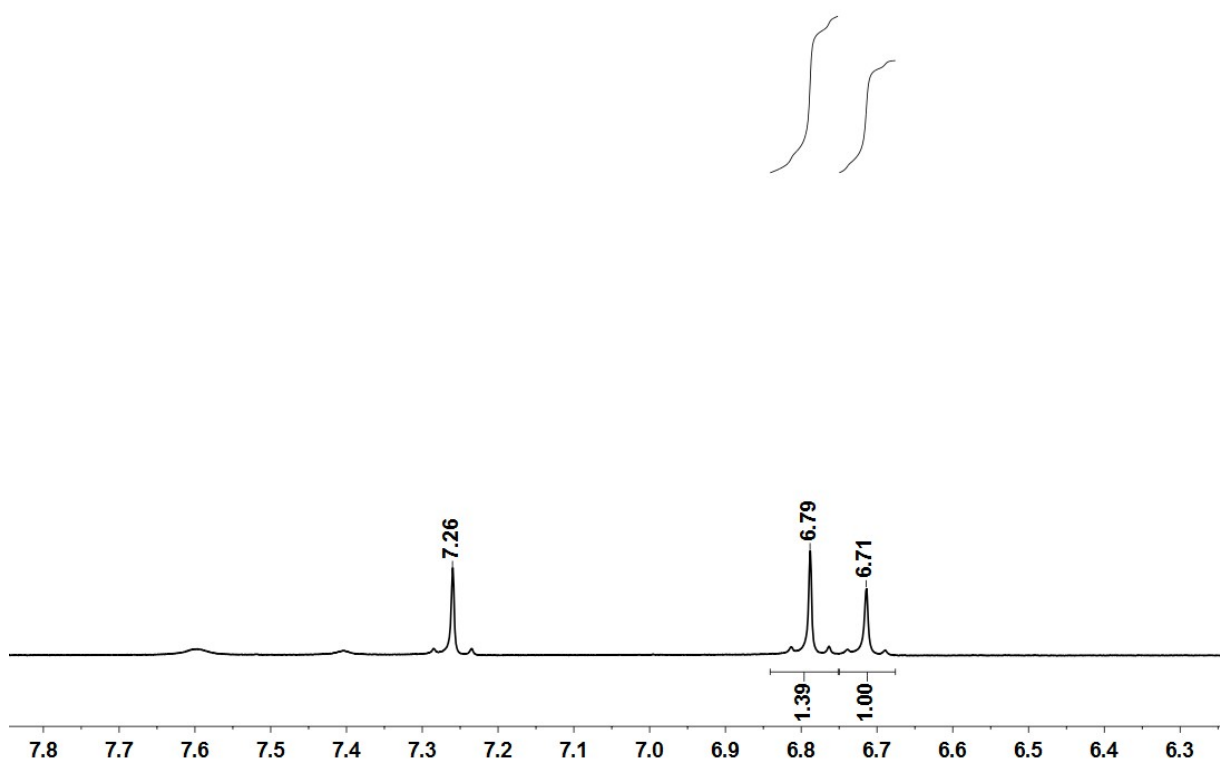


Figure S22: To confirm that [1] is necessary for the hydration of p-benzoquinone, the reaction was repeated in the absence of [1]. No dihydroxy benzene was detected by ¹H NMR.

4 Cyclic Voltammetry

Table S1: Redoxpotentials ($E_{1/2}$) vs Fc/Fc^+ measured in CH_2Cl_2 at 100 mVs^{-1} with $0.1 \text{ M Bu}_4\text{NPF}_6$ at room temperature.

	$E_{1/2}$ (1 st Red)	$E_{1/2}$ (2 nd Ox)	$E_{1/2}$ (2 nd Red)
[1]	--	-0.07 ^[c]	--
[2] ⁺	-1.04 ^[d]	--	-1.98 ^[d]
[3] ⁺	0.64	-0.15	--

^[a]Measured with a gold electrode. ^[b]Potential of the peak current. ^[c]Two electron process as determined by Baranski method.

^[d] First process one electron process, second two electron process as determined by differential pulse voltammetry.

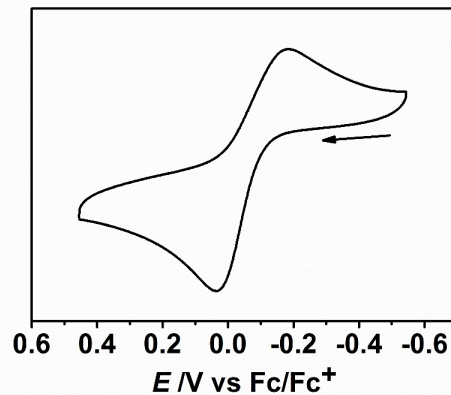


Figure S23: Cyclic voltammogram of **1**. Conditions: THF, glassy carbon working electrode, $0.1 \text{ M Bu}_4\text{NPF}_6$, room temperature and scan rate 100 mVs^{-1} .

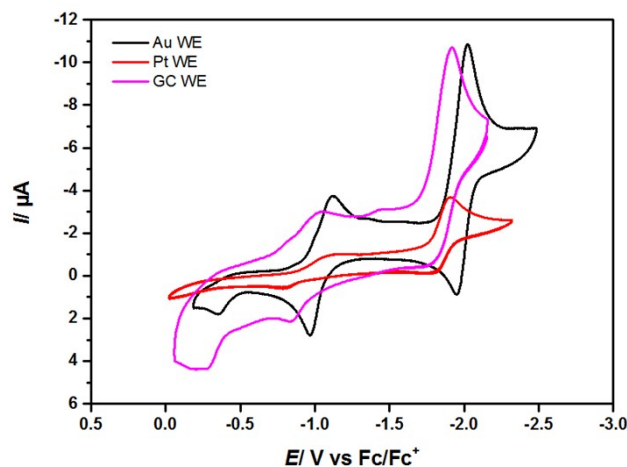


Figure S24: Cyclic voltammograms of **[2]⁺** measured with different working electrodes (gold, platinum, glassy carbon) in $\text{CH}_2\text{Cl}_2 / 0.1 \text{ M Bu}_4\text{NPF}_6$. Different peak currents arise from differences in the surface area of the electrode.

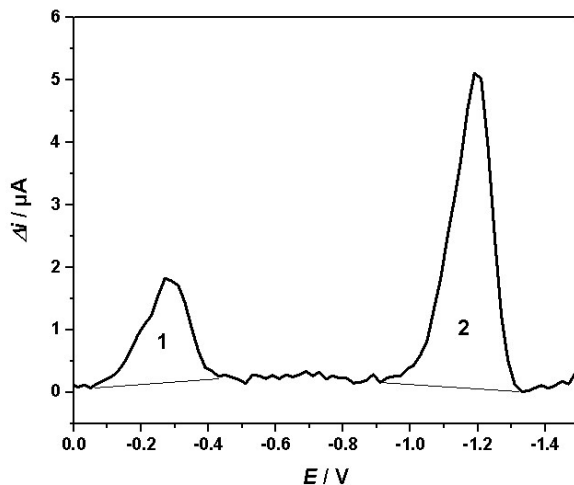


Figure S25: Differential Pulse Voltammogram of $[2]^+$ measured with a gold working electrode in CH_2Cl_2 / 0.1 M Bu_4NPF_6 . The numbers show the normalized areas and correspond to the transferred electrons in the process.

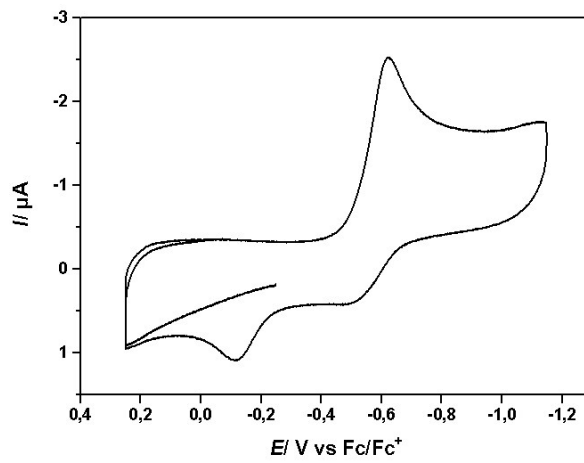


Figure S26: Cyclic voltammogram of 3^+ . Conditions: DCM, glassy carbon working electrode, 0.1 M Bu_4NPF_6 , room temperature and scan rate 100 mVs^{-1} .

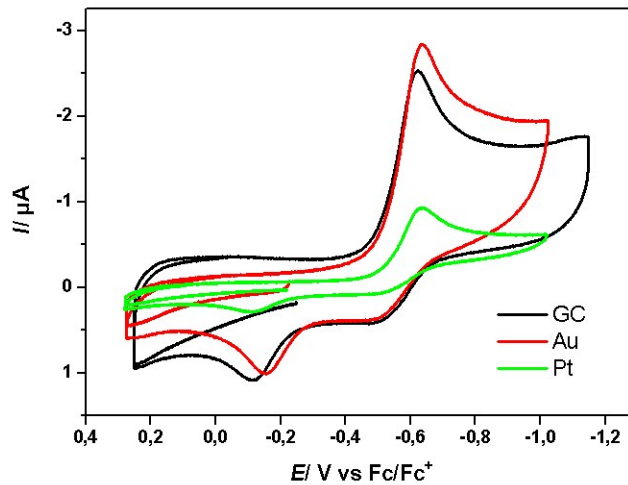


Figure S27: Cyclic voltammograms of $[3]^+$ measured with different working electrodes (gold, platinum, glassy carbon) in CH_2Cl_2 / 0.1 M Bu_4NPF_6 . Different peak currents arise from differences in the surface area of the electrode.

5 CV Simulation for 1

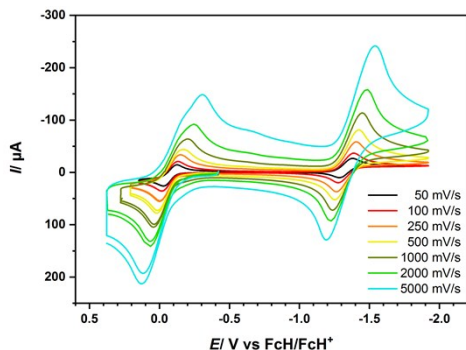


Figure S28. Scan rate dependent CVs of **1** (1.3 mM) and CoCp_2PF_6 (1.4 mM) in 0.1 NBu_4PF_6 / DCM.

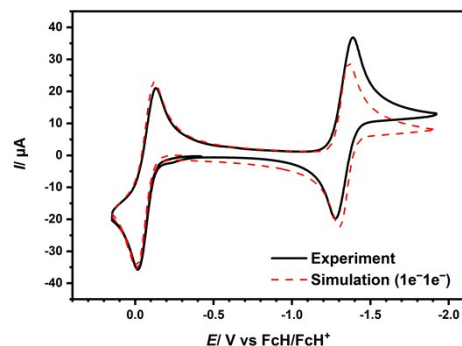


Figure S29. Comparison of the experimental CV at 100 mV/s and the CV simulation for two consecutive one-electron transfers.

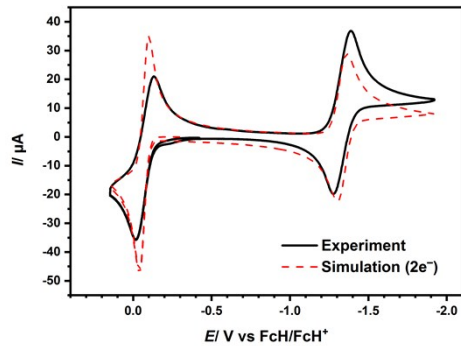


Figure S30. Comparison of the experimental CV at 100 mV/s and the CV simulation for a concerted two-electron transfer.

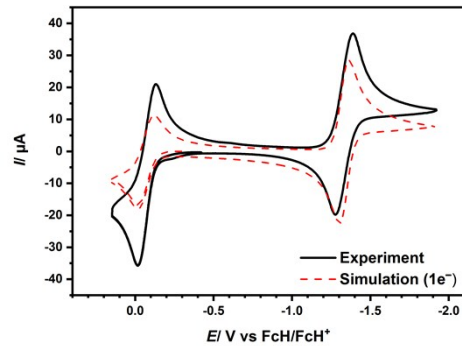


Figure S31. Comparison of the experimental CV at 100 mV/s and the CV simulation for a one-electron transfer.

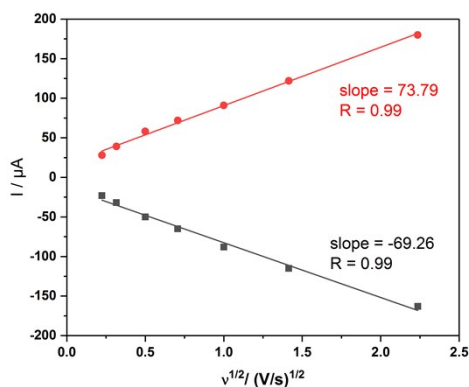


Figure S32. Plot of the anodic and cathodic peak currents over the square root of the scan rate. The slope yielded the diffusion coefficient for the iridium complex **1** and 1^{2+} respectively.

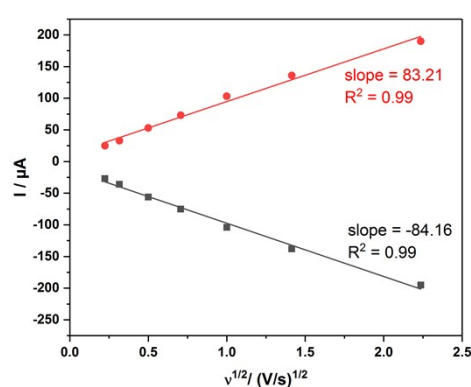


Figure S33. Plot of the anodic and cathodic peak currents over the square root of the scan rate. The slope yielded the diffusion coefficient for CoCp_2^+ and CoCp_2 respectively.

The peak for the oxidation of **1** splits into two close lying waves during the re-reduction in the CV at high scan rates (e.g. 5 V/s) indicating two one-electron steps (see Fig. S28).

The diffusion coefficients have been determined by literature known procedures [A] and yielded the values, which have been used for the CV simulation. It has to be noted that these are only approximations, since the measurements have been conducted in dichloromethane and evaporation of the solvent certainly had a detrimental effect on the accuracy of the measurement (room temperature > 30°C). However the values are in agreement with the expected values (see figures S32+S33).

For comparative purposes three mechanisms have been simulated, one for two successive but very close one-electron oxidations of complex **1**, a one-electron oxidation of complex **1** and a concerted two-electron oxidation of **1**. It can clearly be seen, that the process matches best with two successive one-electron oxidations.

The cyclic voltammogram of **1** was simulated in three segments from -0.30 V to 0.15 V, from 0.15 V to -1.92 V and from -1.92 V to 0.15 V with the software DigiElch Professional [B] by using the Butler-Volmer equation. The surface area of the working electrode was set to 0.07 cm² and the starting concentration of **1** was set to 1.3 mM and of CoCp₂PF₆ to 1.4 mM. The charge transfer coefficients α were left at their initial value of 0.5 and the heterogeneous rate constants k_s were calculated from the peak-to-peak separation [C] and consequently set to 0.005 cm/s. The diffusion coefficients were set to values of 8×10^{-6} cm² s⁻¹ for **1** and 1×10^{-5} cm² s⁻¹ for CoCp₂PF₆. The simulated charge-transfer reactions are described by the following equations for the mechanisms (1)-(3), the E⁰ values for **1** was set to -0.07 V and for CoCp₂PF₆ to -1.33 V. The electrochemical reactions are denoted with (E).

Mechanism	Reaction
(1) Sim. 1e ⁻ 1e ⁻	$1^+ + e^- \rightleftharpoons 1^0$ (E) $1^{2+} + e^- \rightleftharpoons 1^+$ (E) $CoCp_2^+ \rightleftharpoons CoCp_2$ (E)
(2) Sim. 2e ⁻	$1^{2+} + 2 e^- \rightleftharpoons 1^0$ (E) $CoCp_2^+ \rightleftharpoons CoCp_2$ (E)
(3) Sim. 1e ⁻	$1^+ + e^- \rightleftharpoons 1^0$ (E) $CoCp_2^+ \rightleftharpoons CoCp_2$ (E)

A N. Elgrishi, K. J. Rountree, B. D. McCarthy, E. S. Rountree, T. T. Eisenhart, J. L. Dempsey, *J. Chem. Educ.* **2018**, 95, 197–206.

B DigiElch Professional Version 7.FD 2006, ElchSoft GbR, Kleinromstedt, Germany.

C (a) R. S. Nicholson, I. Shain, *Anal. Chem.*, **1965**, 37, 1351. (b) A. S. N. Murthy, K. S. Reddy, *Electrochim. Acta*, **1983**, 28, 1677.

6 CV Simulation for 2

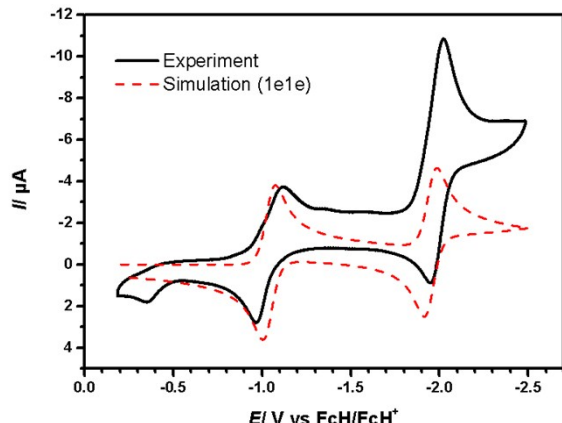


Figure S34: Comparison of experiment and simulation with two consecutive one electron transfer steps (=1e1e) and no chemical reactions.

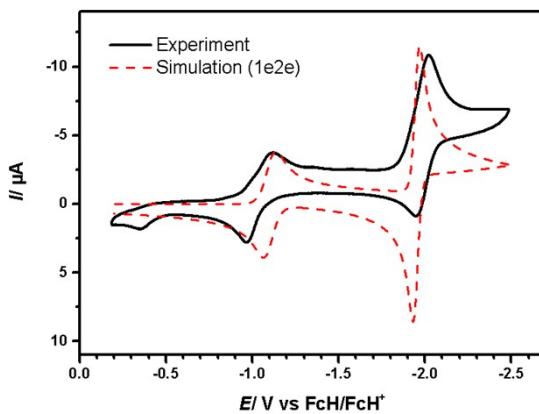


Figure S35: Comparison of experiment and simulation for two consecutive electron transfers, of which the first one is a one electron transfer and the second one is a true two electron transfer (=1e2e).

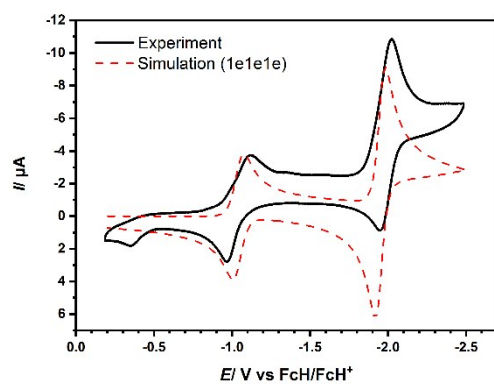


Figure S36: Comparison of experiment and simulation with three one electron transfer steps, of which the two have the same redox potential (=1e1e1e). Rate constant for heterogeneous charge transfer was set to $k_s = 0.02 \text{ cm/s}$.

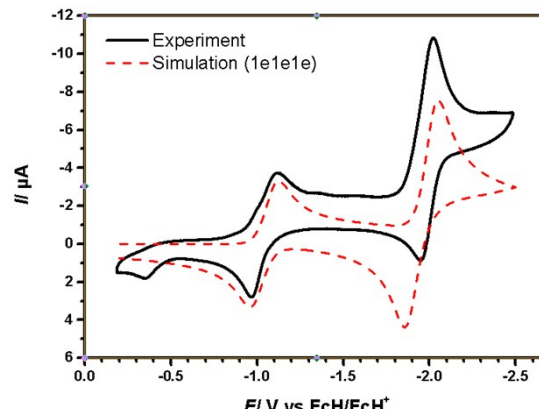


Figure S37: Comparison of experiment and simulation with three one electron transfer steps, of which the two have the same redox potential (=1e1e1e). Rate constant for heterogeneous charge transfer was set to $k_s = 0.002 \text{ cm/s}$.

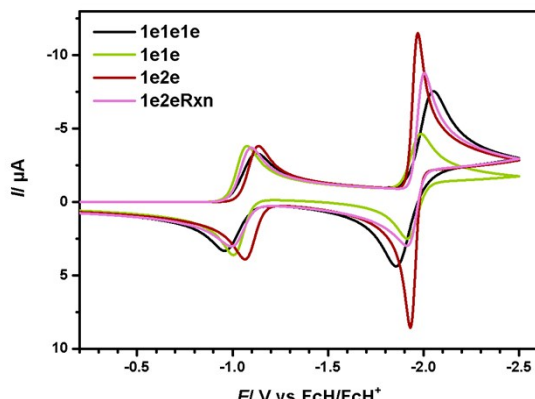


Figure S38: Comparison of all the various simulations.

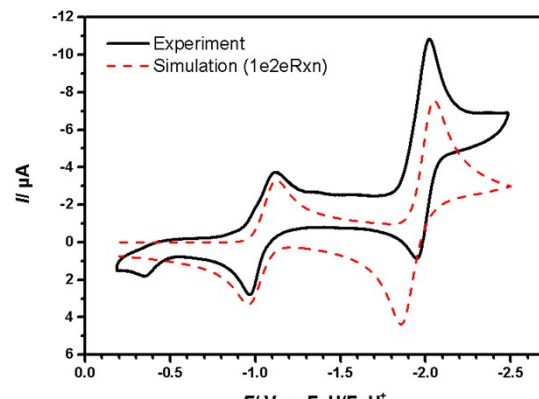


Figure S39: Comparison of experiment and simulation for two consecutive electron transfers, of which the first one is a one electron transfer and the second one is a true two electron transfer and two coupled chemical reaction as shown below (=1e2eRxn).

In order to gain a deeper understanding for the redox processes the cyclic voltammogram of $[2]^+$ was simulated in two segments from -0.20 V to -2.5 V and from -2.5 V to -0.20 V with the software DigiElch Professional [A] by using the Butler-Volmer equation. The surface area of the working electrode was set to 0.07 cm^2 and the starting concentration of $[2]^+$ was set to 0.21 mM . The charge transfer coefficients α were left at their initial value of 0.5 and the heterogeneous rate constants k_s were calculated from the peak-to-peak separation[B] (1^{st} red.: 0.001 cm/s and 2^{nd} red.: 0.015 cm/s) and used as starting values. The shown simulations are above used a k_s of 0.02 cm/s or 0.02 cm/s , where is indicated. The diffusion coefficients were left at their initial values of $1 \times 10^{-5} \text{ cm}^2 \text{ s}^{-1}$. The simulated charge-transfer reactions are described by the following equations for the mechanisms (1)-(4), the E^0 values for $[2]^+$ was set the values shown below. The electrochemical reactions are denoted with (E) and the coupled chemical reactions with (C), which are characterized by the equilibrium constant K_{eq} , and the rate constants for the forward and back reaction k_f and k_b . The asterisk denotes a rearrangement:

Mechanism	Reaction
(1) 1e1e	$[2]^+ + e^- \rightleftharpoons [2]^{0\bullet}$ (E) $E_{1/2} = -1.04 \text{ V}$ $[2]^+ + e^- \rightleftharpoons [2]^-$ (E) $E_{1/2} = -1.95 \text{ V}$
(2) 1e1e1e	$[2]^+ + e^- \rightleftharpoons [2]^{0\bullet}$ (E) $E_{1/2} = -1.04 \text{ V}$ $[2]^{0\bullet} + e^- \rightleftharpoons [2]^-$ (E) $E_{1/2} = -1.95 \text{ V}$ $[2]^- + e^- \rightleftharpoons [2]^{2-}$ (E) $E_{1/2} = -1.95 \text{ V}$
(3) 1e2e	$[2]^+ + e^- \rightleftharpoons [2]^{0\bullet}$ (E) $E_{1/2} = -1.10 \text{ V}$ $[2]^{0\bullet} + 2 e^- \rightleftharpoons [2]^{2-}$ (E) $E_{1/2} = -1.95 \text{ V}$
(4) 1e2eRxn	$[2]^+ + e^- \rightleftharpoons [2]^{0\bullet}$ (E) $E_{1/2} = -1.10 \text{ V}$ $[2]^{0\bullet} + 2 e^- \rightleftharpoons [2]^{2-}$ (E) $E_{1/2} = -1.95 \text{ V}$ $[2]^{0\bullet} \rightleftharpoons [2]^{0\bullet*}$ (C) $K_{\text{eq}} = 8; k_f = 10^3; k_b = 125$ $[2]^{2-} \rightleftharpoons [2]^{2-*}$ (C) $K_{\text{eq}} = 5; k_f = 20; k_b = 4$

[A] DigiElch Professional Version 7.FD 2006, ElchSoft GbR, Kleinromstedt, Germany.

[B] R. S. Nicholson, I. Shain, *Anal. Chem.*, **1965**, 37, 1351.

7 EPR-Spectroelectrochemistry

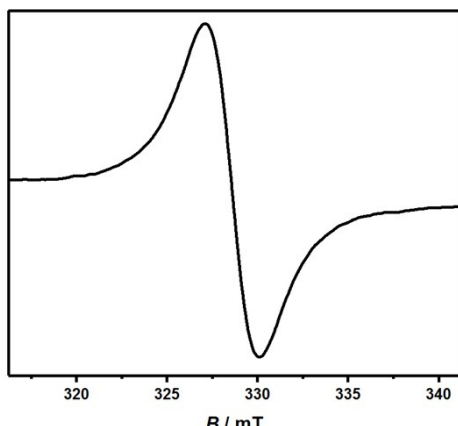


Figure S40: EPR spectrum of $[1]^+$, generated in-situ in $\text{CH}_2\text{Cl}_2 / 0.1 \text{ M } \text{NBu}_4\text{PF}_6$ at a platinum working electrode. $[1]^+$ shows a g-value of 2.056 at 9.46 GHz.

Table S2: Loewdin spin populations [%] for selected compounds from B3LYP/def2-TZVP level of theory.

Compound	ρ_{Ir}	$\rho_{\text{N}1(\text{NH})}$	$\rho_{\text{N}2(\text{NPhN})}$	ρ_{Me}	ρ_{Cl}
1^{+}	7	10	14	--	--
2^0	19	21	18	4	--
2^{2-}	36	2	2	1	--
3^0	12	22	20	--	5

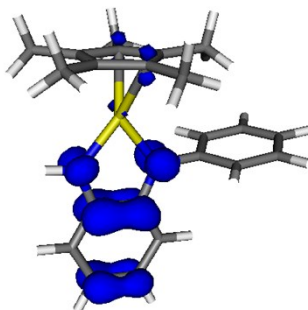


Figure S41: Loewdin spin density population for $[1]^+$, iso value = 0,005.

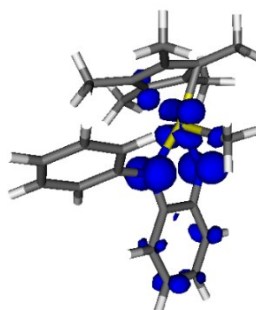


Figure S42: Loewdin spin density population for $[2]^0$ iso value = 0,005.

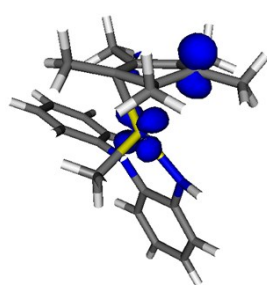


Figure S43: Loewdin spin density of $[2]^{2-}$ Iso value = 0.01

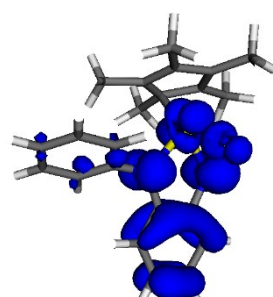
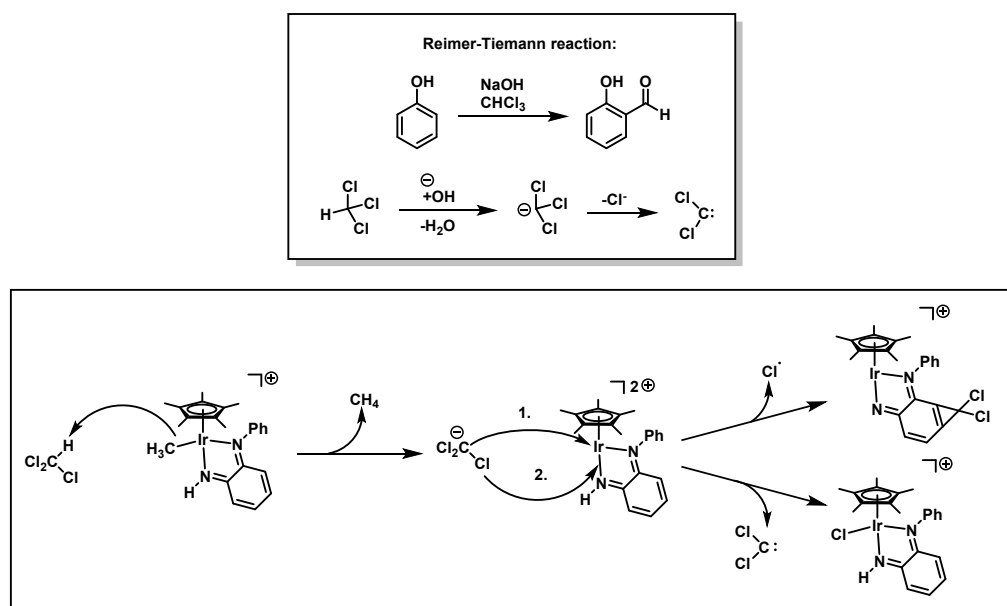


Figure S44: Loewdin spin density population for $[3]^0$, iso value = 0.002

8 Interconversion of 2^+ to 3^+



Scheme S1: Proposed mechanism for the interconversion of $[2]^+$ into $[3]^+$. References: K. Reimer, F. Tiemann, *Ber. Dtsch. Chem. Ges.* **1876**, 9, 1268. H. Wynberg, *Chem. Rev.* **1960**, 60, 169.

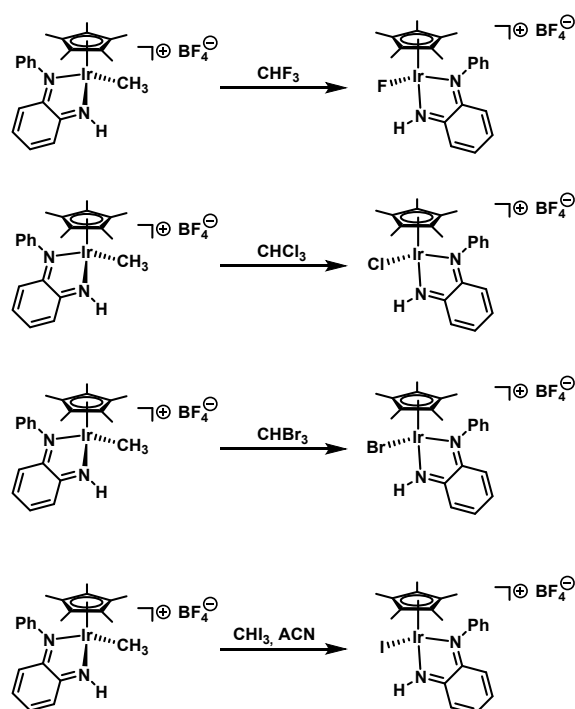


Figure S45: Haloform activation with $[2]\text{BF}_4^-$.

8.1 Mass spectrum of 2⁺ and Fluoroform

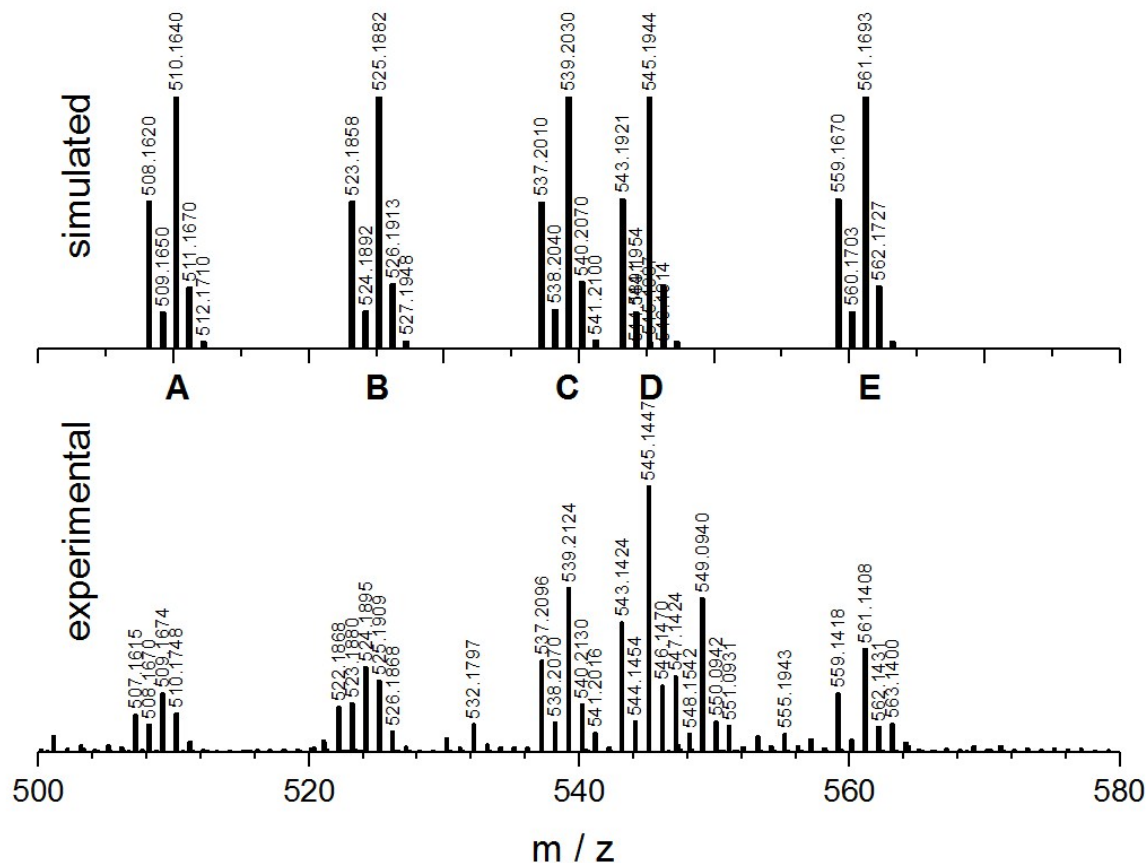


Figure S46: Mass spectrum (simulation and experiment) of [2]BF₄ in MeCN solution in the presence of Fluoroform.

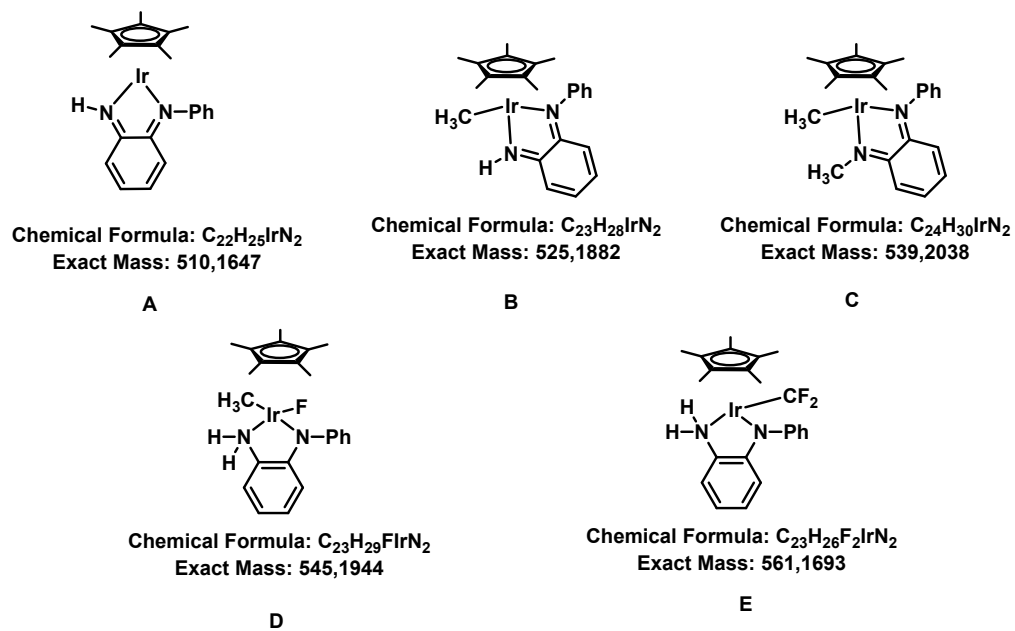


Figure S47: Proposed intermediates for the reaction of [2]BF₄ and Fluoroform.

8.2 Mass spectrometry of 2⁺ and Chloroform

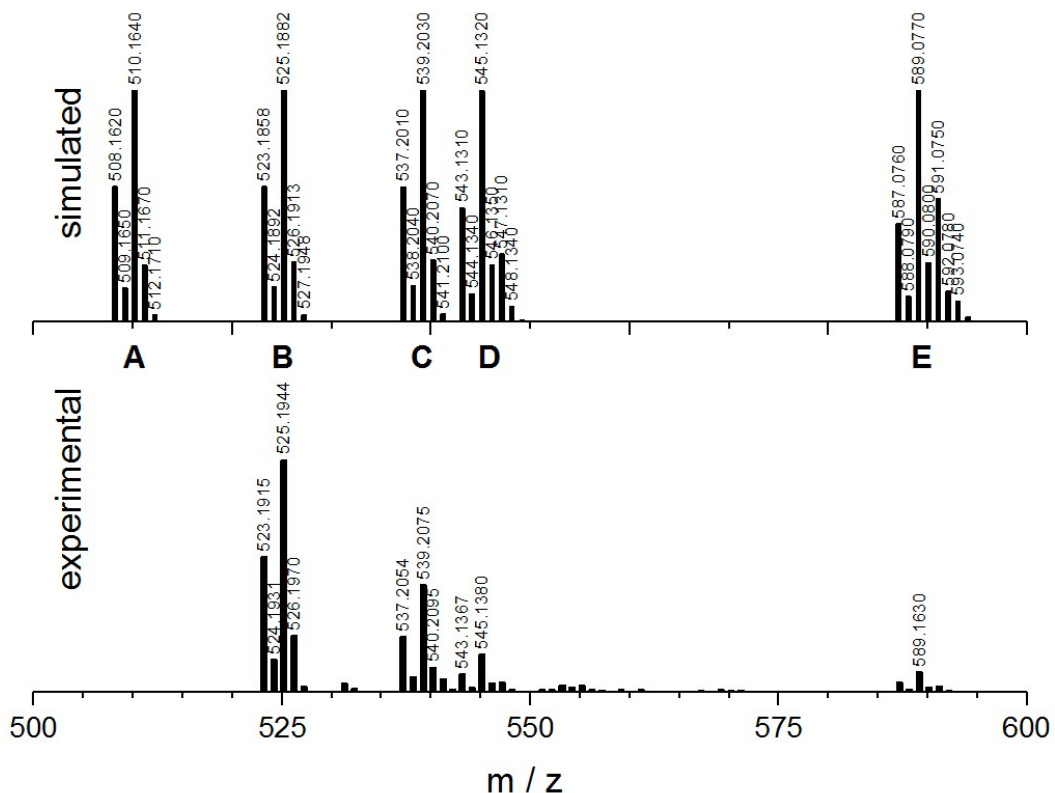


Figure S48: Mass spectrum (simulation and experiment) of [2]BF₄ in Chloroform solution.

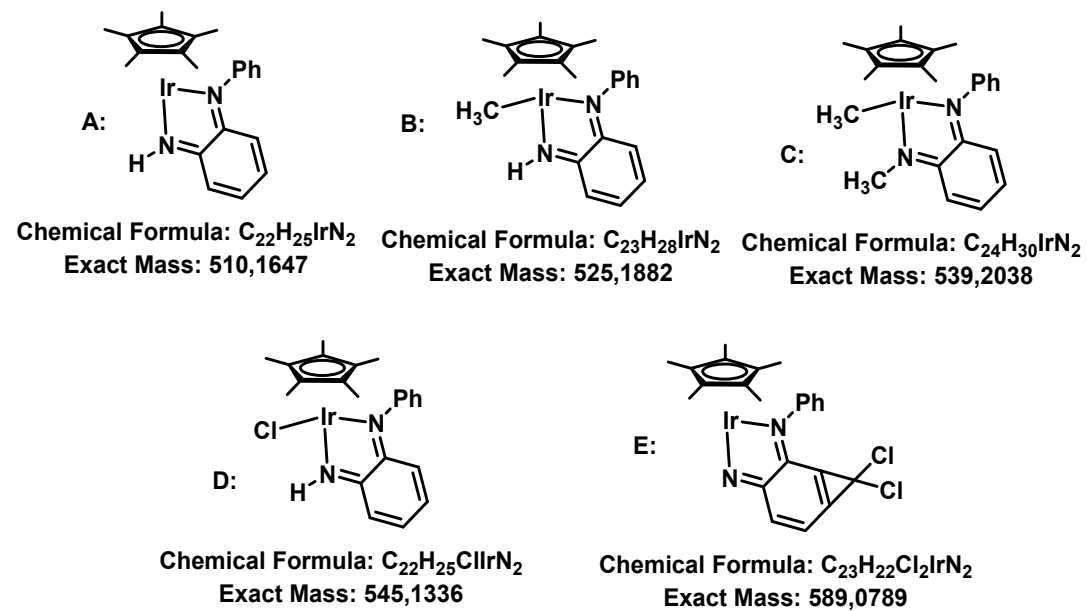


Figure S49: Proposed intermediates for the reaction of [2]BF₄ and Chloroform.

8.3 Mass spectrometry of 2^+ and Bromoform

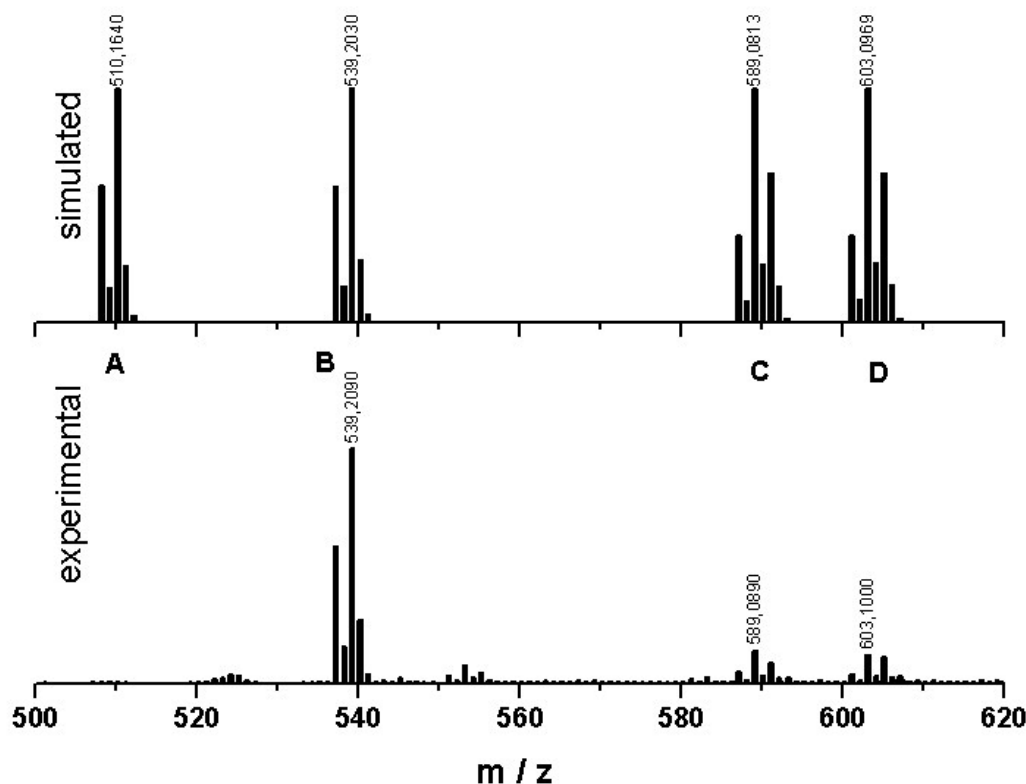


Figure S50: Mass spectrum (simulation and experiment) of $[2]\text{BF}_4$ in Bromoform solution.

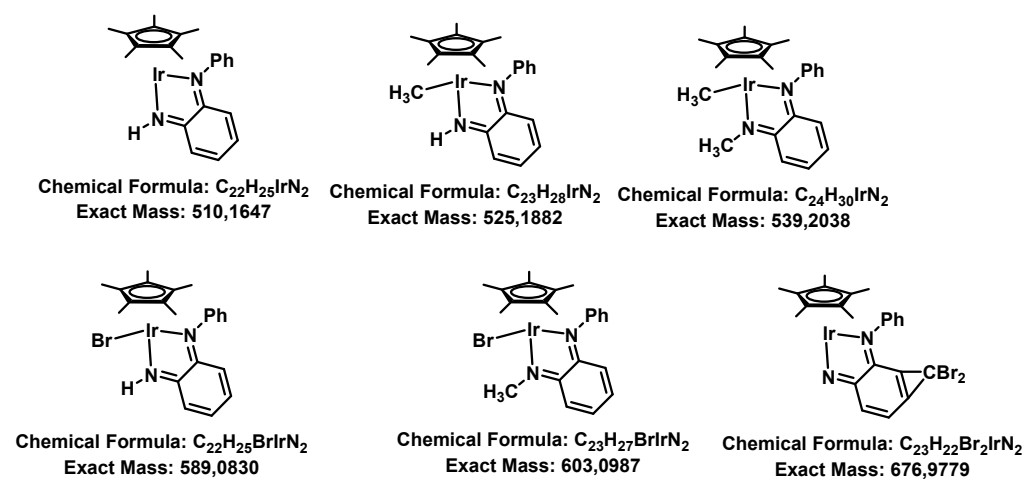


Figure S51: Proposed intermediates for the reaction of $[2]\text{BF}_4$ and Bromoform.

8.4 Mass spectrometry of 2^+ and Iodoform

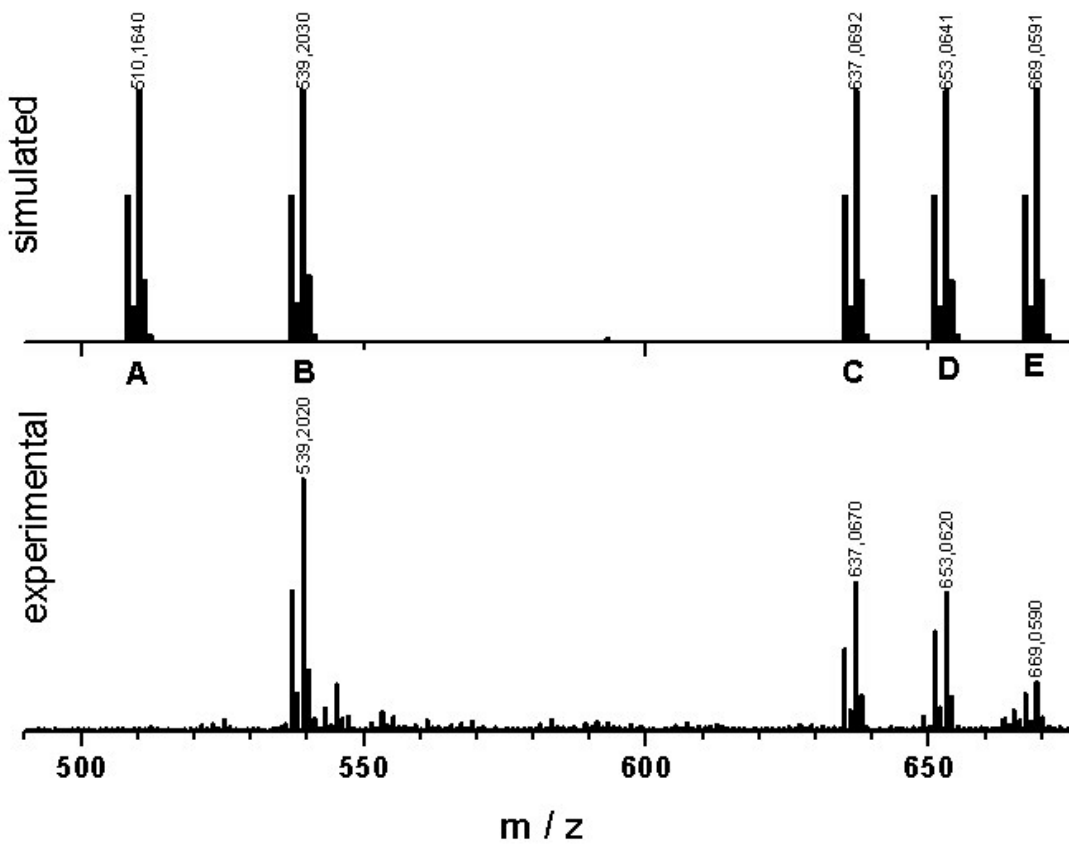


Figure S52: Zoom-in of the mass spectrum (simulation and experiment) of $[2]\text{BF}_4^-$ in MeCN solution in the presence of Iodoform.

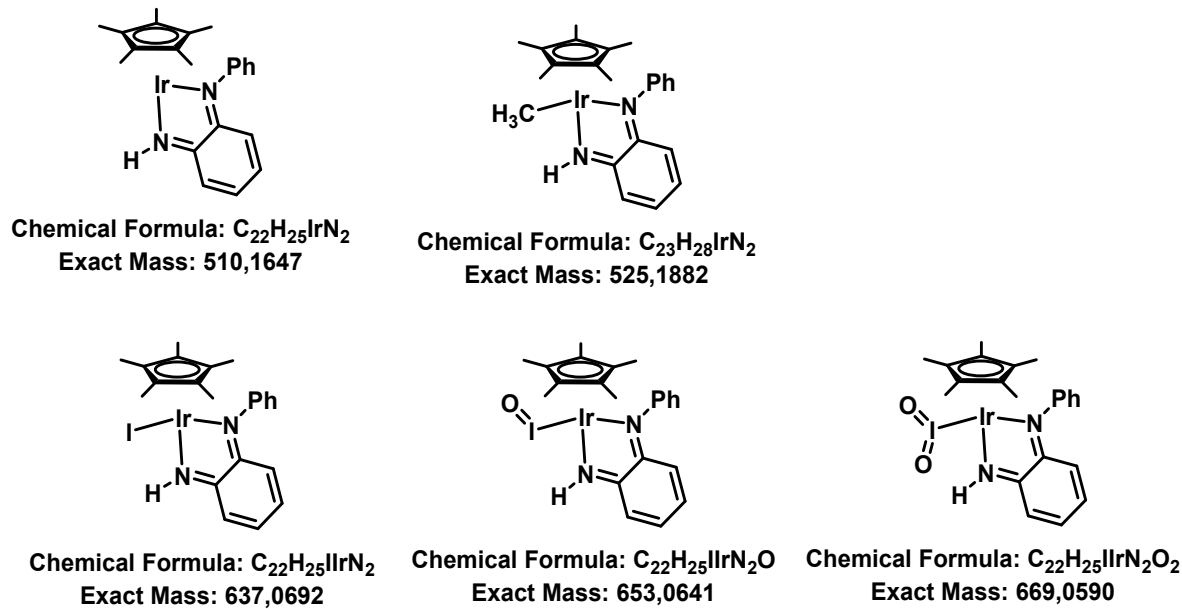


Figure S53: Proposed intermediates for the reaction of $[2]\text{BF}_4^-$ and Iodoform.

9 IR-spectroelectrochemistry

Table S3: IR data for compounds [1] and [2]⁺ from OTLE-spectroelectrochemistry in DCM with 0.1 NBu₄PF₆ measured with a gold mesh working electrode.

Compound	Peaks / cm ⁻¹
1	1591 w, 1577 w, 1483 s, 1461 sh, 1382m, 1361 m, 1324 s, 1228 m, 1191 w, 1147w, 1095 s, 1024s
1 ²⁺	1591 w, 1486 m, 1454 m, 1382m, 1361w, 1324 w, 1095 s, 1024s
2 ⁺	1483m, 1469m, 1459m, 1423s, 1382 w, 1274s, 1255s,
2 ²⁻	1483m, 1469m, 1459m, 1423m, 1382w, 1272m, 1253m

Table S4: Comparison of calculated and experimental peaks for the IR spectra of various species. Calculated at the RI-BP86/def2-TZVP level of DFT.

Compound	Peak(exp.)	Peak(calc.)	Assignment
1	1483	1474.21	Methyl groups of Cp* mostly, bit of C-N and Aromativ
		1474.84	Asym C-N stretch; quite a bit of Cp*, aromatic C=C
	1361	1388.93	Symmetric c-n stretch; Cp* frame deformation; C=C of aromatic ring
	1324	1326.8	asymmetric C-N stretch; N-H deformation; C=C of aromatic rings
		1334.93	Symmetric C-N stretch; N-H deformation; C=C of aromatic rings
1^{2+}	1486 &	1462.47	Sym C=N and aromatic C=C stretch,
	1454	1453.34	Cp* Me; bit aromatic rings
		1464.18	Cp* Me; bit aromatic rings
		1479.2	Cp* Me Deformation
		1491.62	Asym. C=N stretch; C=C stretch; bit of Cp*
	1384	1383.41	Cp*Me deform; bit C=N; C-H deform
		1386.01	Sym. C=N; C=C stretch, bit of Cp*; C-H deform.
2^+	1483-1423	1487.23	More deform, less C=N/C=C
		1485.36	Asym C=N; C=C stretch MeCp* deform
		1480.34	Same
		1466.36	IrMe deform, MeCp*deform
		1415.37	Sym C=N; C=C, bit MeCp* deform
		till1461.87	Various MeCp* deform; and IrMe
	1274+1255	1292.28	C=N sym; C=C stretch; IrMe derform, NH deform
2^{-}		1280.01	IrMe deform
		1274.96	IrMe leicht deform,C=N, NH deform
		1234.7	NH deform, N=C stretch asym
	1483	1538.64	C=N asym stretch; C=C
			Phenylenediaminobenzene stretch asym
		1516.01	
	1420	1490.84	C=N sym stretch; sym benzeneNN sym stretch; Cp* deform
	1276	1344.06	C=NPh stretch with benzene strech
	1253	1313.55	C=NH stretch with benzene stretch

9.1 Spectra for $\mathbf{1}$ and $\mathbf{1}^{2+}$ (experimental and calculated)

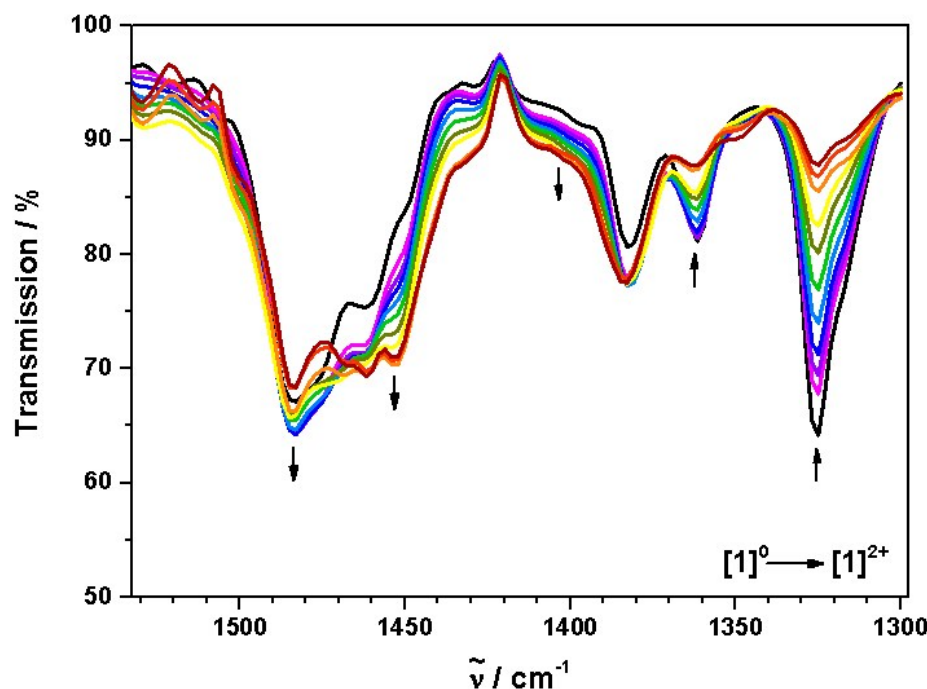


Figure S54: Changes in the IR spectrum of 1 during OTTLE-spectroelectrochemistry in $\text{CH}_2\text{Cl}_2/0.1 \text{ M } \text{NBu}_4\text{PF}_6$.

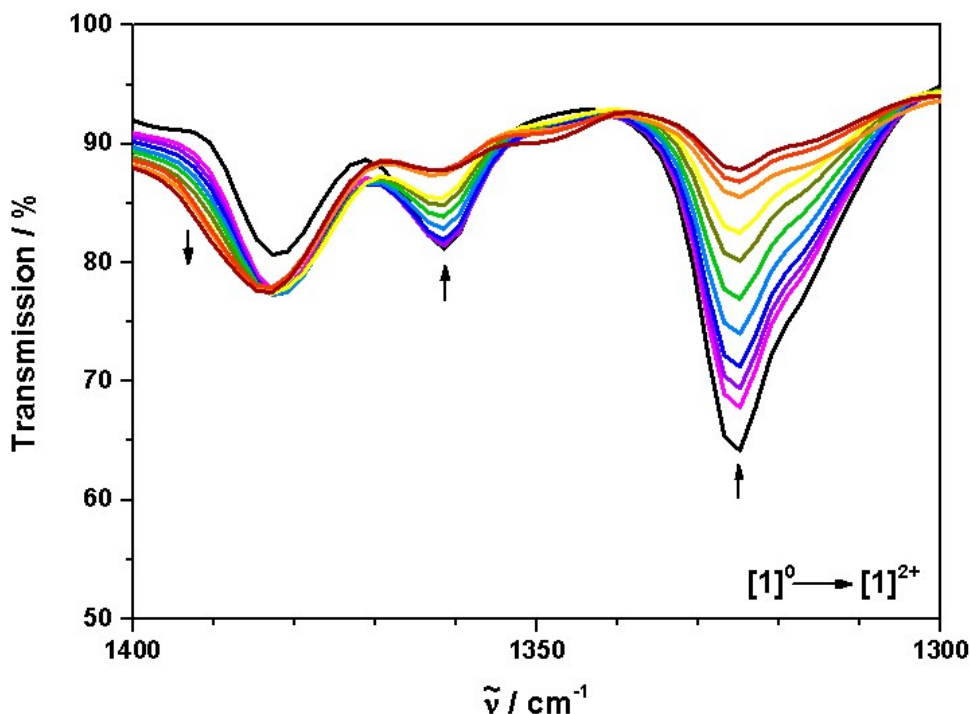


Figure S55: Zoom-in of the changes of the IR spectrum of 1 during OTTLE-spectroelectrochemistry in $\text{CH}_2\text{Cl}_2/0.1 \text{ M } \text{NBu}_4\text{PF}_6$.

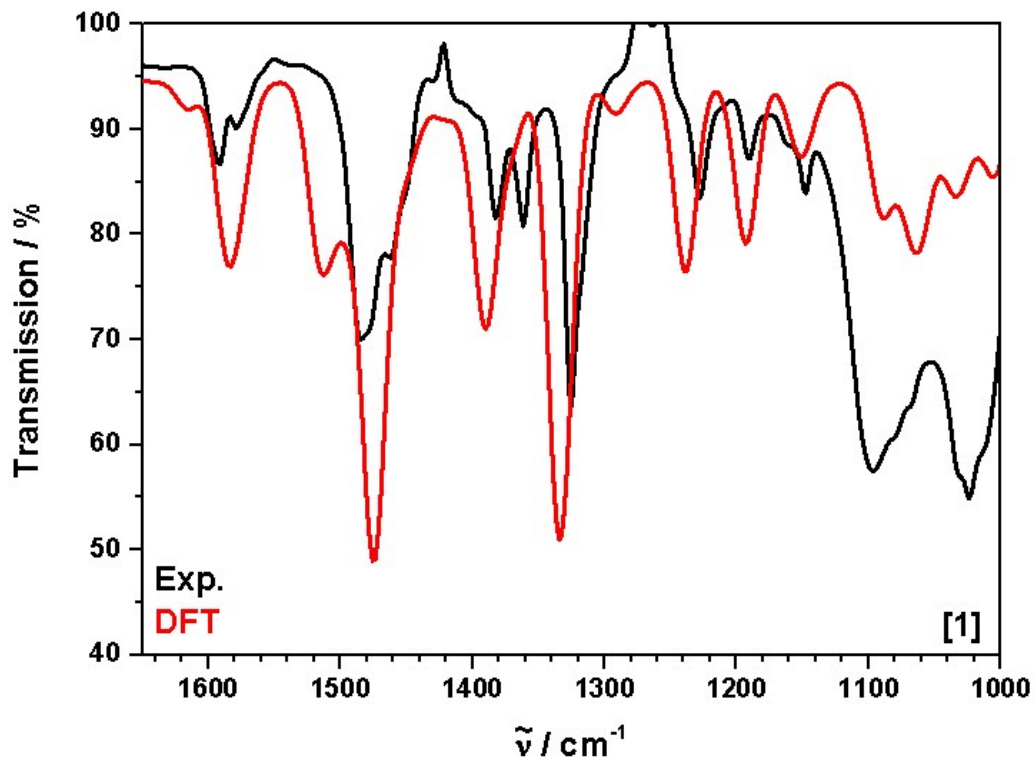


Figure S56: Comparison of the calculated (red) and experimental (black) IR spectrum of 1.

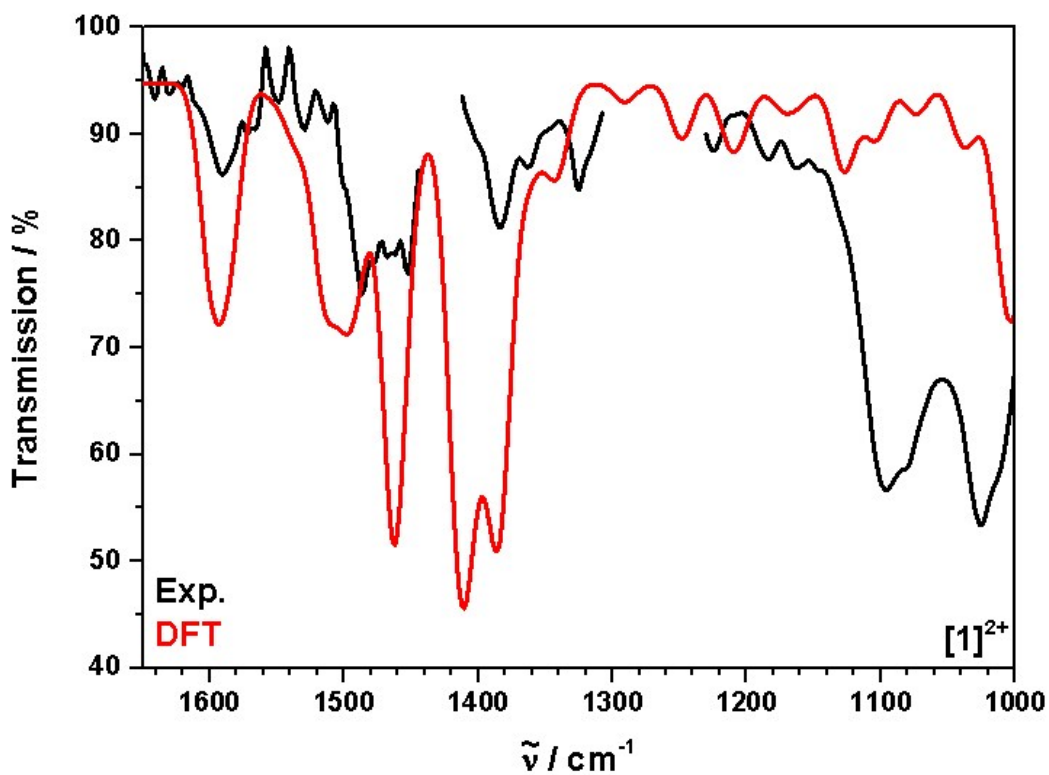


Figure S57: Comparison of the calculated (red) and experimental (black) IR spectrum of 1²⁺.

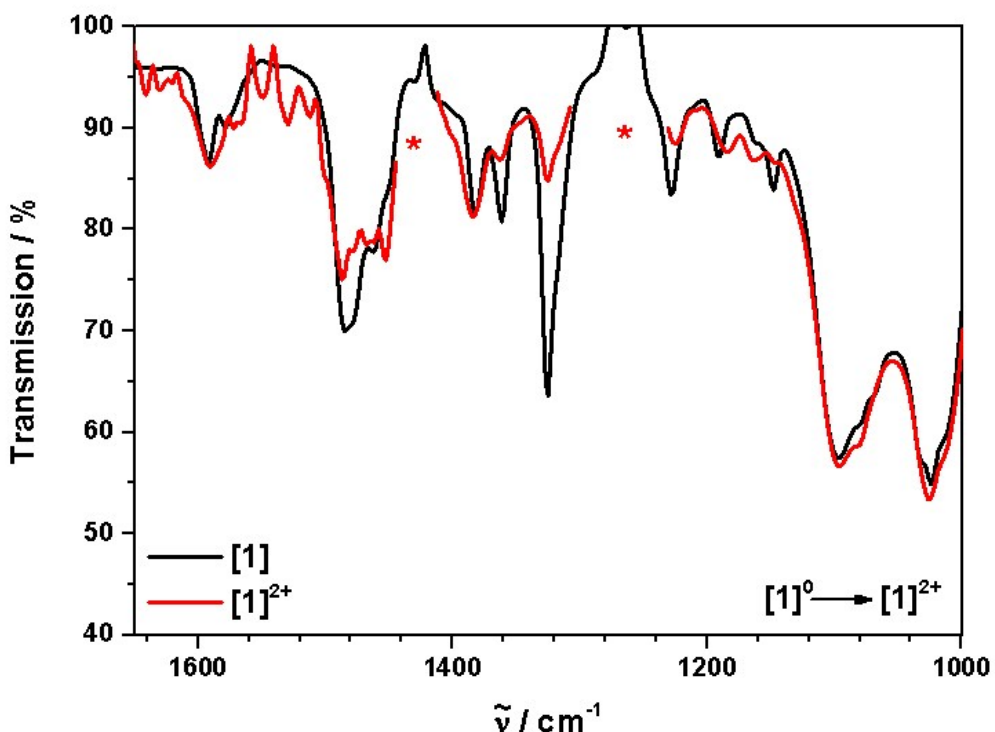


Figure S58: Comparison of the IR spectra of 1 and 1²⁺, asterisks indicate region of strong solvent absorptivity during the electrolysis.

9.2 IR spectra of 2⁺

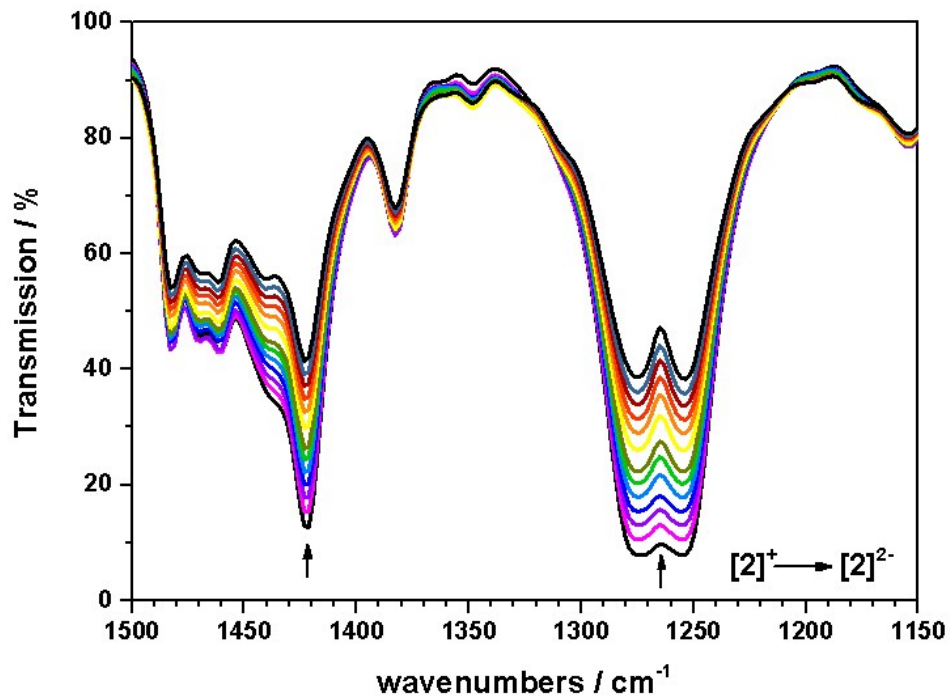


Figure S59: Changes of the IR spectrum of 2⁺ during OTTLE-spectroelectrochemistry in CH₂Cl₂/0.1 M NBu₄PF₆.

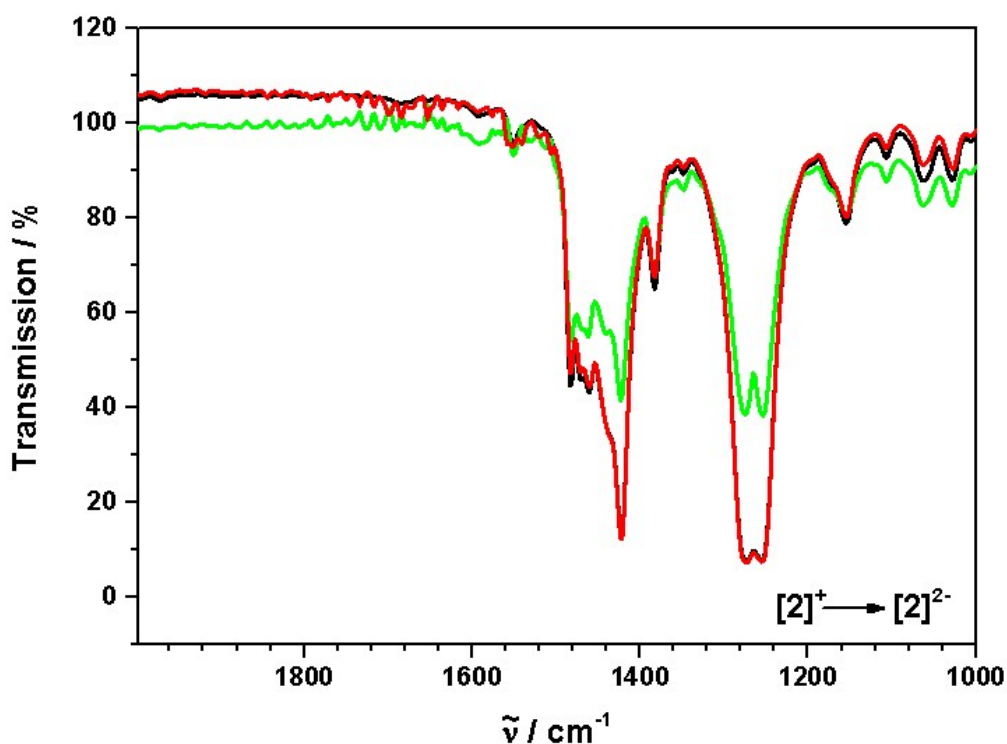


Figure S60: IR spectra of 2^+ before and after electrolysis and 2^{2-} OTTLE-spectroelectrochemistry in $\text{CH}_2\text{Cl}_2/0.1 \text{ M } \text{NBu}_4\text{PF}_6$.

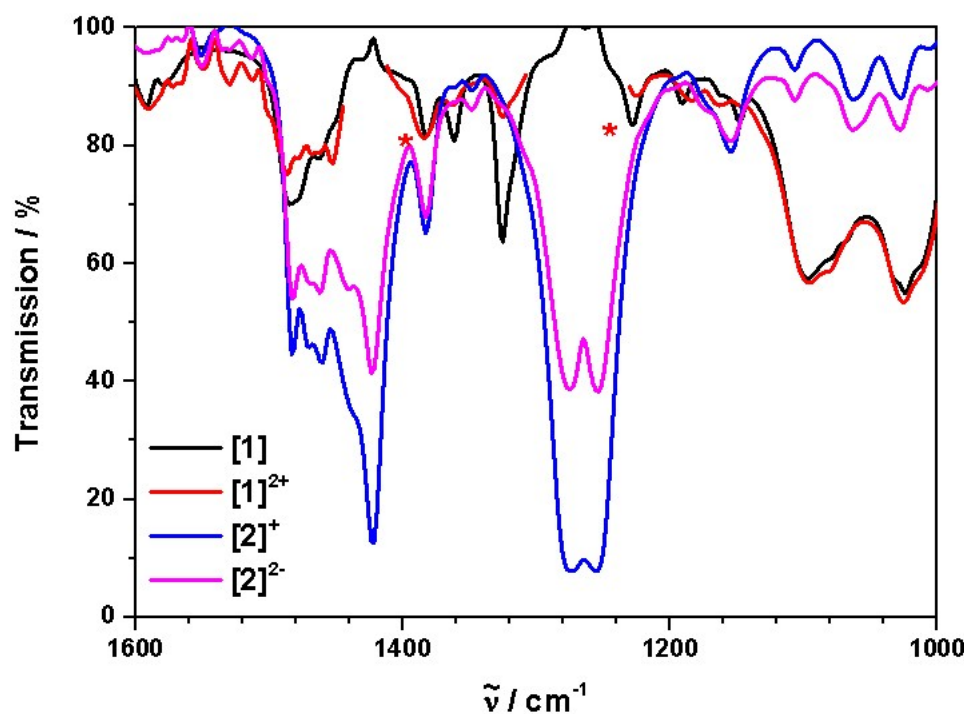


Figure S61: IR spectra of 1 , 1^{2+} , 2^+ and 2^{2-} during OTTLE-spectroelectrochemistry in $\text{CH}_2\text{Cl}_2/0.1 \text{ M } \text{NBu}_4\text{PF}_6$.

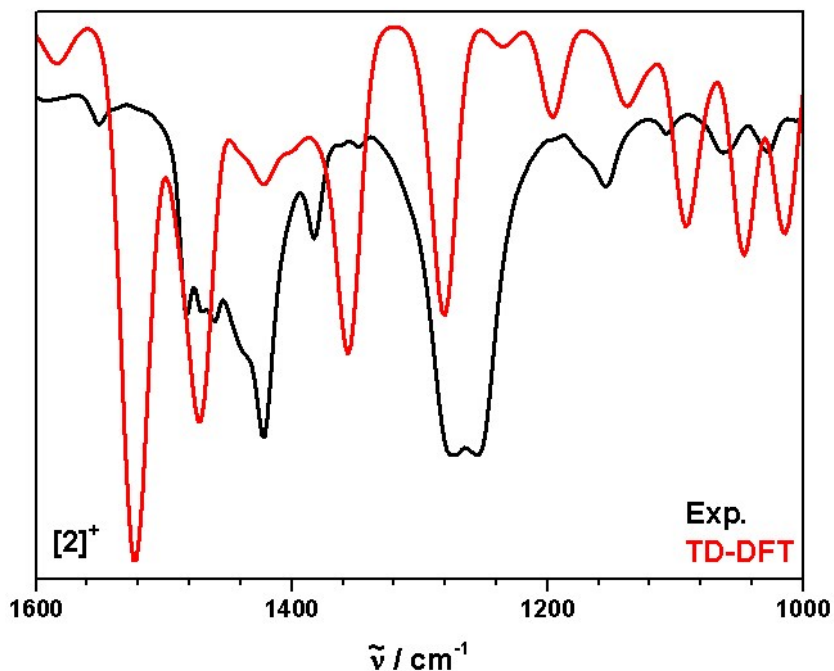


Figure S62: Comparison of the experimental (black) and calculated (red) IR spectra of $[2]^+$.

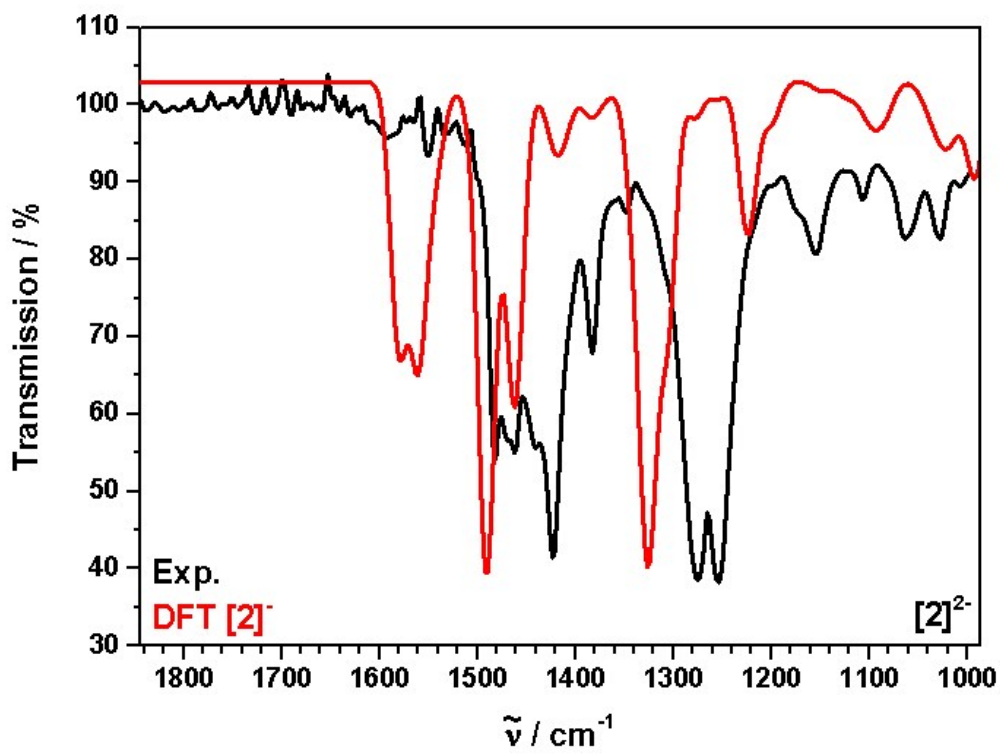


Figure S63: Comparison of the experimental (black) of $[2]^{2-}$ and calculated (red) IR spectrum of $[2]^-$.

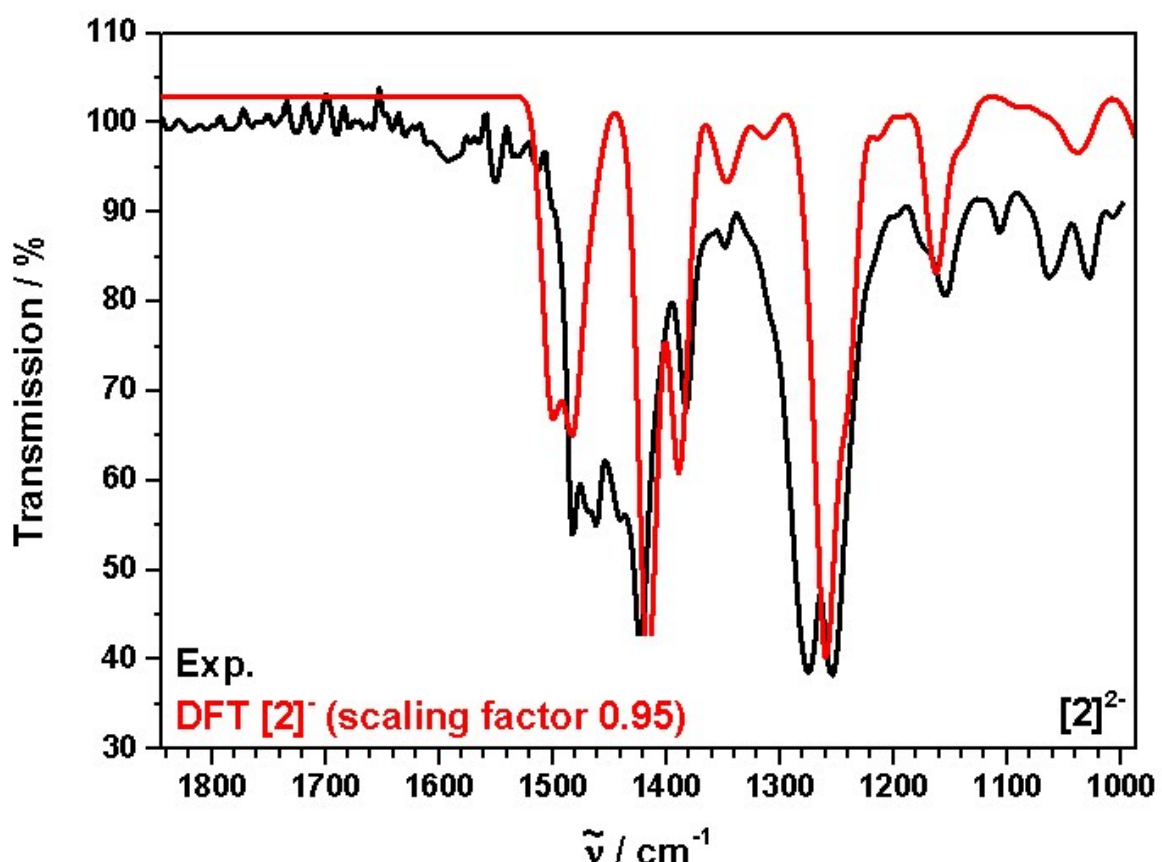


Figure S64: Comparison of the experimental (black) of $[2]^{2-}$ and scaled calculated (red) IR spectrum of $[2]^{2-}$.

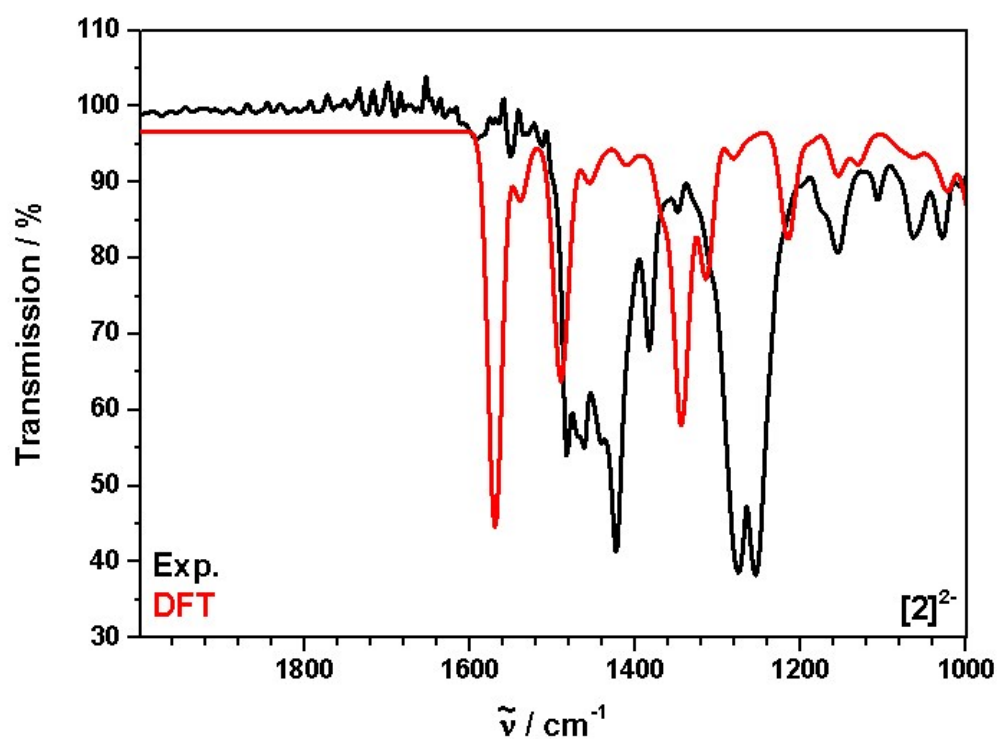


Figure S65: Comparison of the experimental (black) and calculated (red) IR spectra of $[2]^{2-}$.

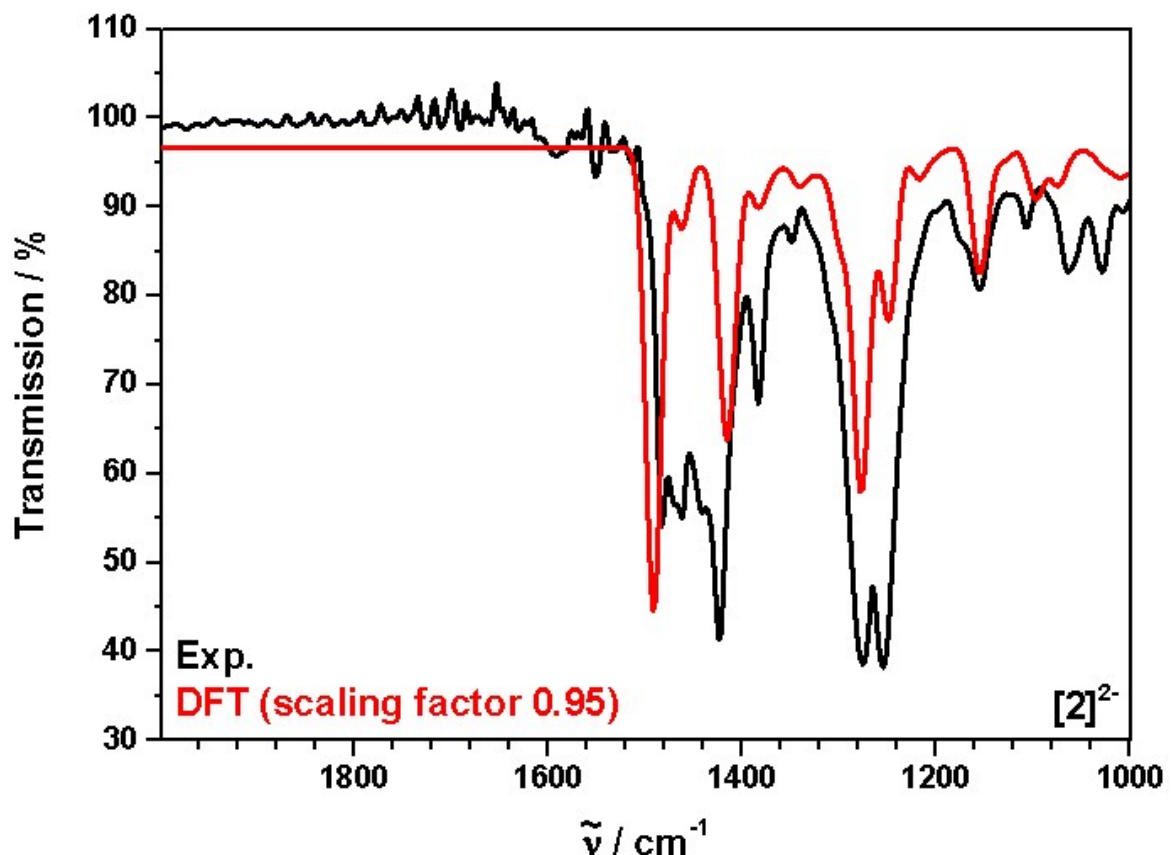


Figure S66: Comparison of the experimental (black) and scaled calculated (red) IR spectra of $[2]^+$.

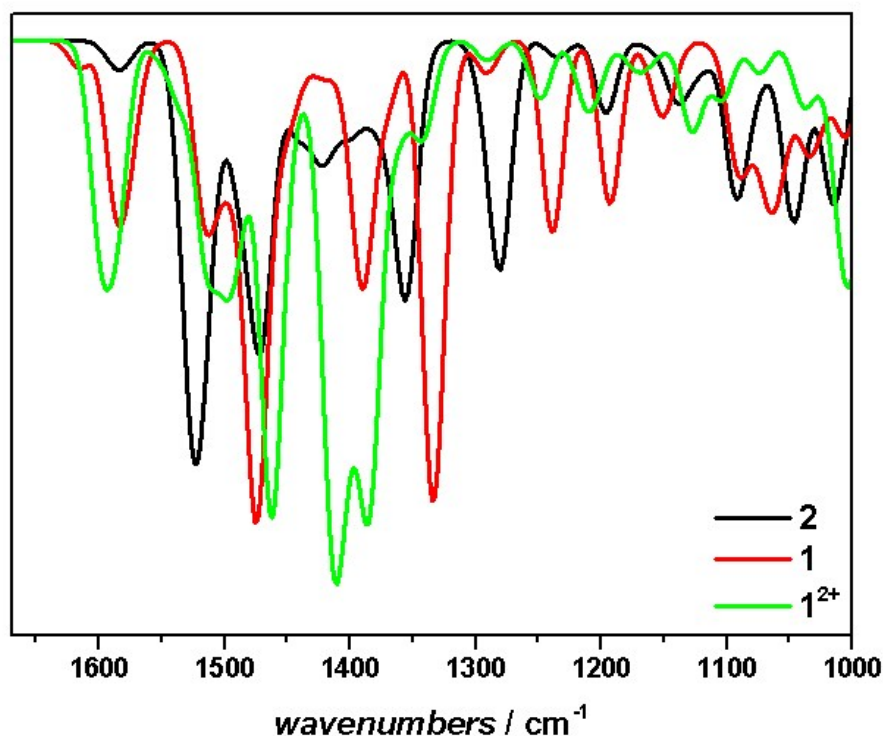


Figure S67: Comparison of the calculated IR spectra of 1, 1^{2+} and 2 $^+$ at the RI-BP86/def2-TZVP level of theory.

10 UV-Vis-NIR-Spectroelectrochemistry

Table S5: (UV-)Vis-NIR data for compounds [1], [2]⁺ and [3]⁺ from OTTLE-spectroelectrochemistry in DCM with 0.1 NBu₄PF₆ measured with agold or platinum mesh working electrode.

λ [nm] (e [10^3 M ⁻¹ • cm ⁻¹])	
[1]	304 (4.2), 434 (9.4), 504 (1.7) sh
[1] ⁺	424 (4.4) br, 504 (1.7) sh, 638 (0.9) sh, 1044 (0.3) br
[1] ²⁺	341 (1.9), 449 (3.7), 513 (1.9) sh, 663 (0.3) br , 955 (0.2) br
[2] ⁺	315 (3.9), 486 (12.9), 608 (1.6) sh
[2] ⁰	308 (4.5), 443 (9.5), 486 (10.7), 608 (1.4) sh
[2] ²⁻	307 (5.5), 437 (9.9), 568 (4.0), 842 (0.6) br
[3] ⁻	308 (2.5), 469 (2.5), 776 br (2.1)
[3] ²⁻	See [1]
Obtained from spectroelectrochemical measurements using an OTTLE-cell with a gold working electrode in CH ₂ CL ₂ /0.1 M NBu ₄ PF ₆ at 295K.	

10.1 Spectra for $[2]^+$

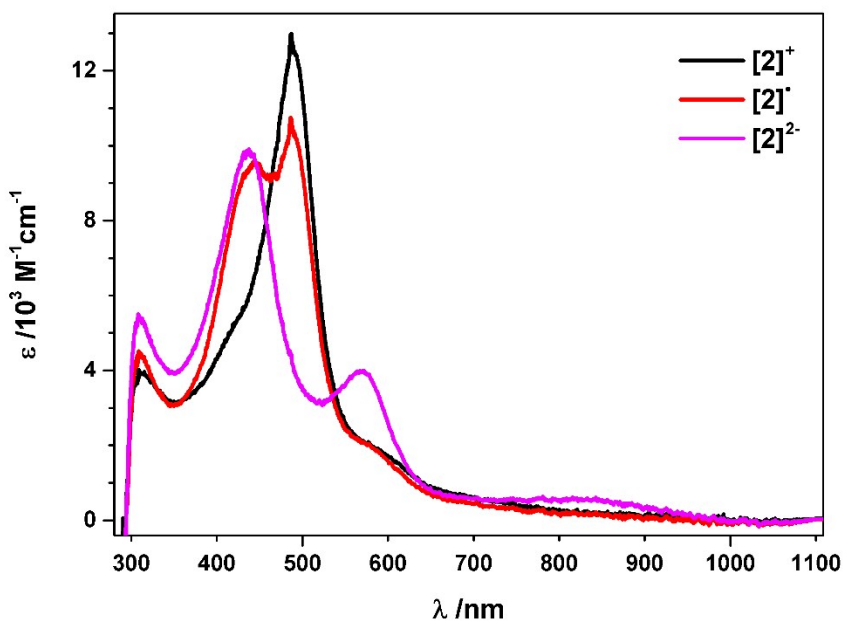


Figure S68: UV-Vis-NIR spectra of 2^+ , 2^\cdot and 2^{2-} .

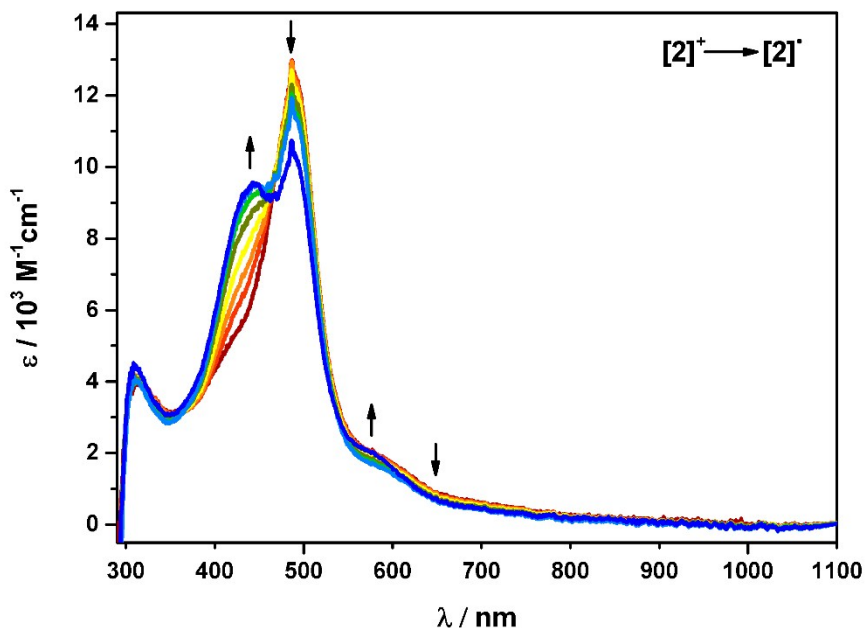


Figure S69: Changes in the UV-Vis-NIR spectrum of 2^+ during OTTLE-spectroelectrochemistry in $\text{CH}_2\text{Cl}_2/0.1 \text{ M } \text{NBu}_4\text{PF}_6$.

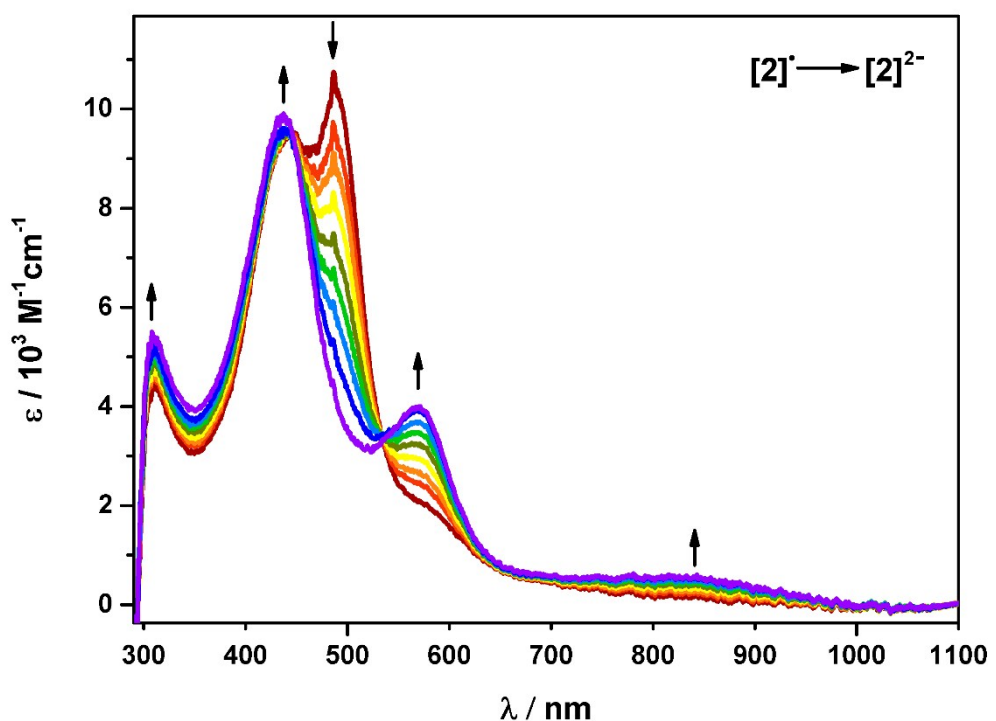


Figure S70: Changes in the UV-Vis-NIR spectrum of 2^0 during OTTLE-spectroelectrochemistry in $\text{CH}_2\text{Cl}_2/0.1 \text{ M } \text{NBu}_4\text{PF}_6$.

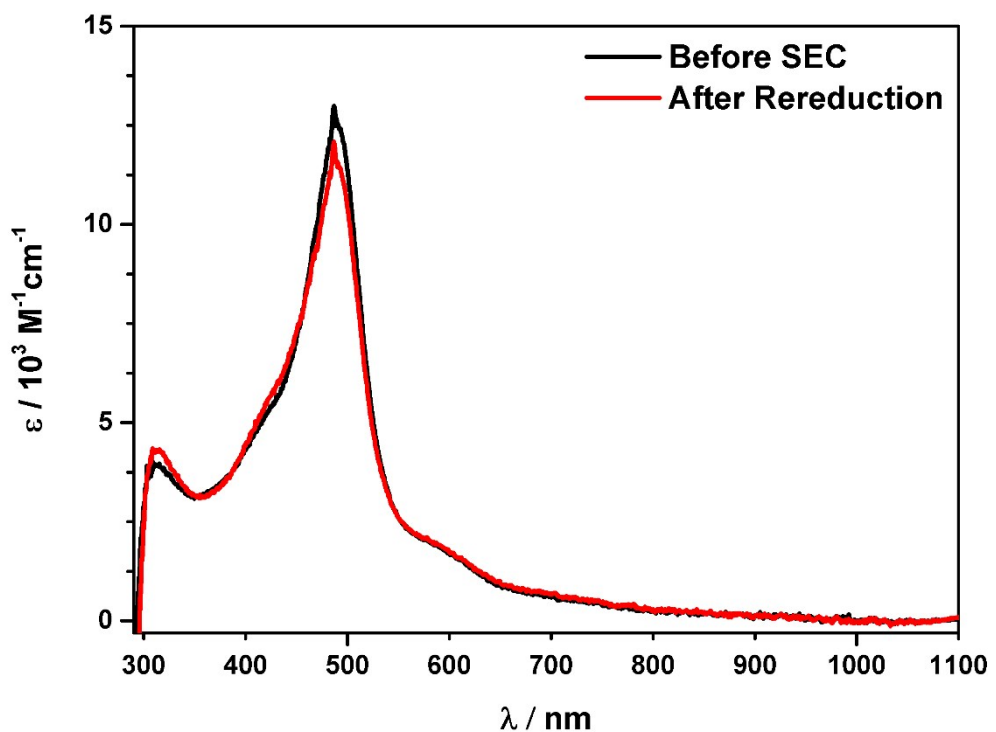


Figure S71: Comparison of the UV-Vis-NIR spectrum of 2 before and after oxidative OTTLE spectroelectrochemistry.

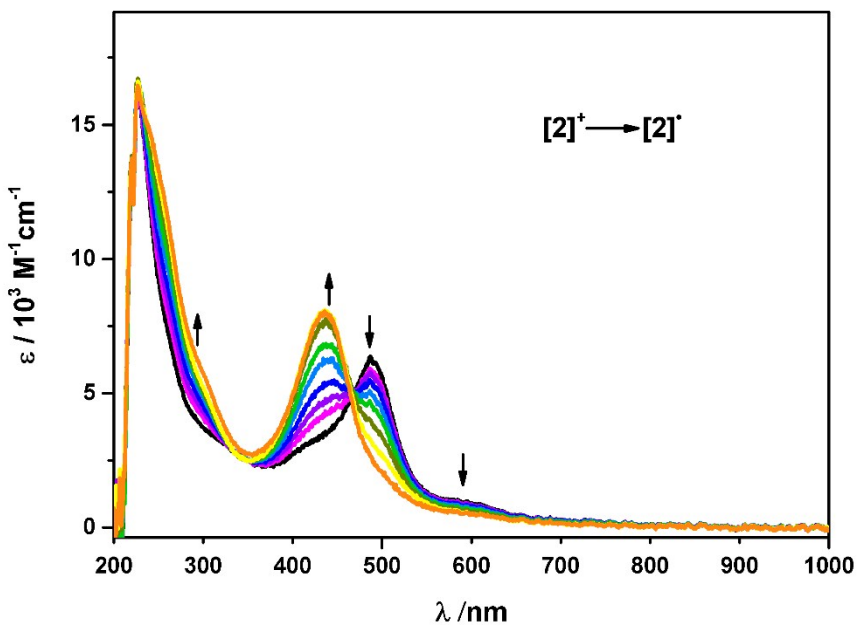


Figure S72: Changes in the UV-Vis-NIR spectrum of 2 during OTTLE spectroelectrochemistry in $\text{CH}_2\text{Cl}_2 / 0.1 \text{ M } \text{NBu}_4\text{PF}_6$.

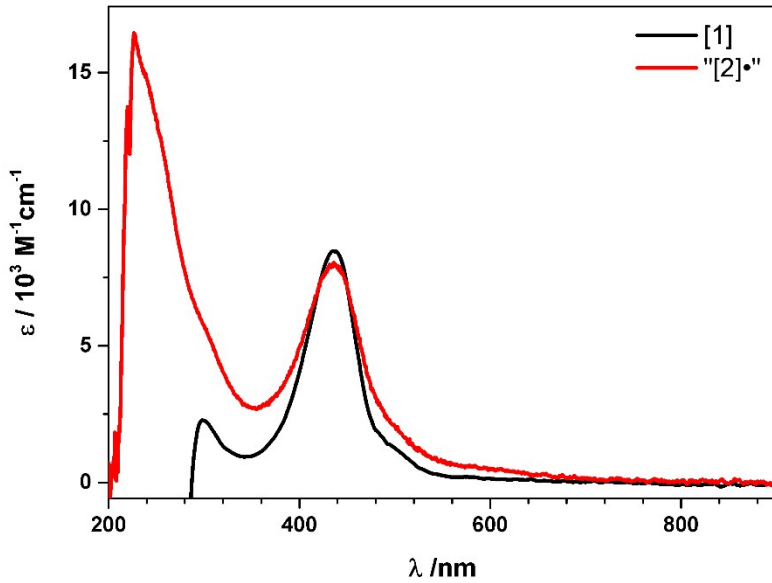


Figure S73: Comparison of the UV/Vis-NIR spectrum of [1] in the absence of the middle UV part of the spectrum and the spectrum of $[2]^+$ after electrochemical reduction.

10.2 Spectra for $[3]^+$

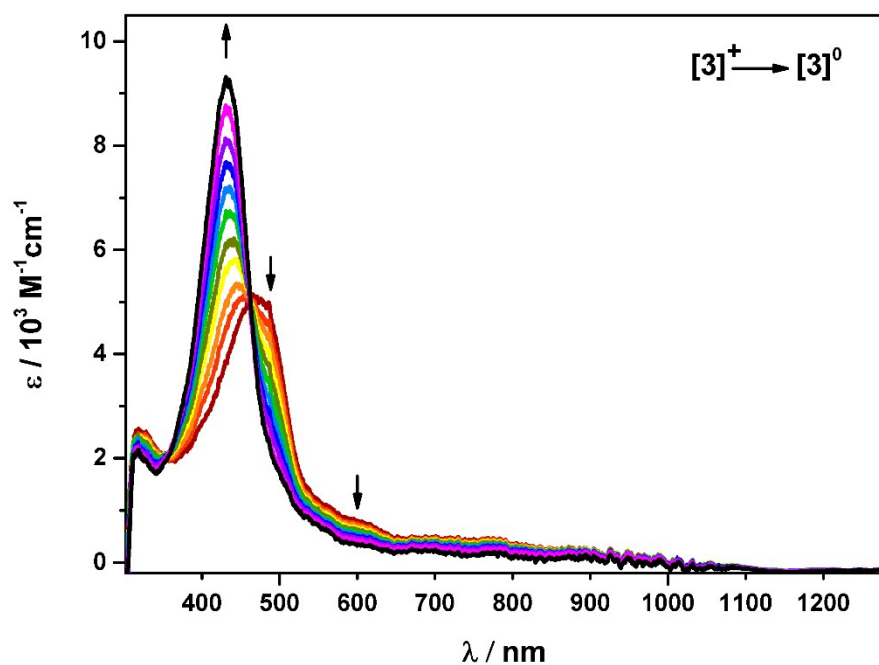


Figure S74: Changes in the UV-Vis-NIR spectrum of 3 during OTTLE spectroelectrochemistry in $\text{CH}_2\text{Cl}_2 / 0.1 \text{ M } \text{NBu}_4\text{PF}_6$.

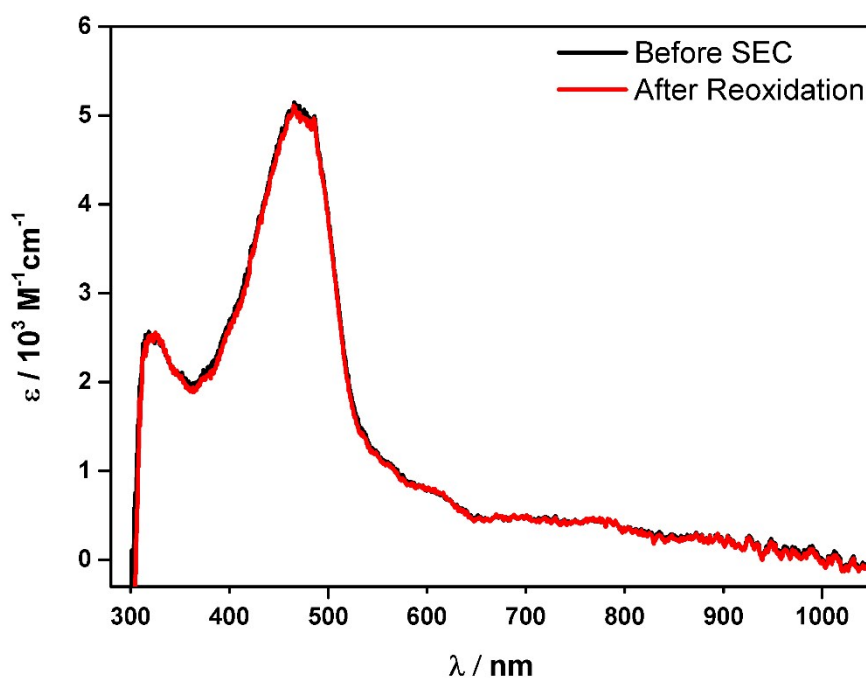


Figure S75: Comparison of the UV-Vis-NIR spectrum of 3 before and after reductive OTTLE spectroelectrochemistry.

11 (TD)DFT

11.1 General remarks

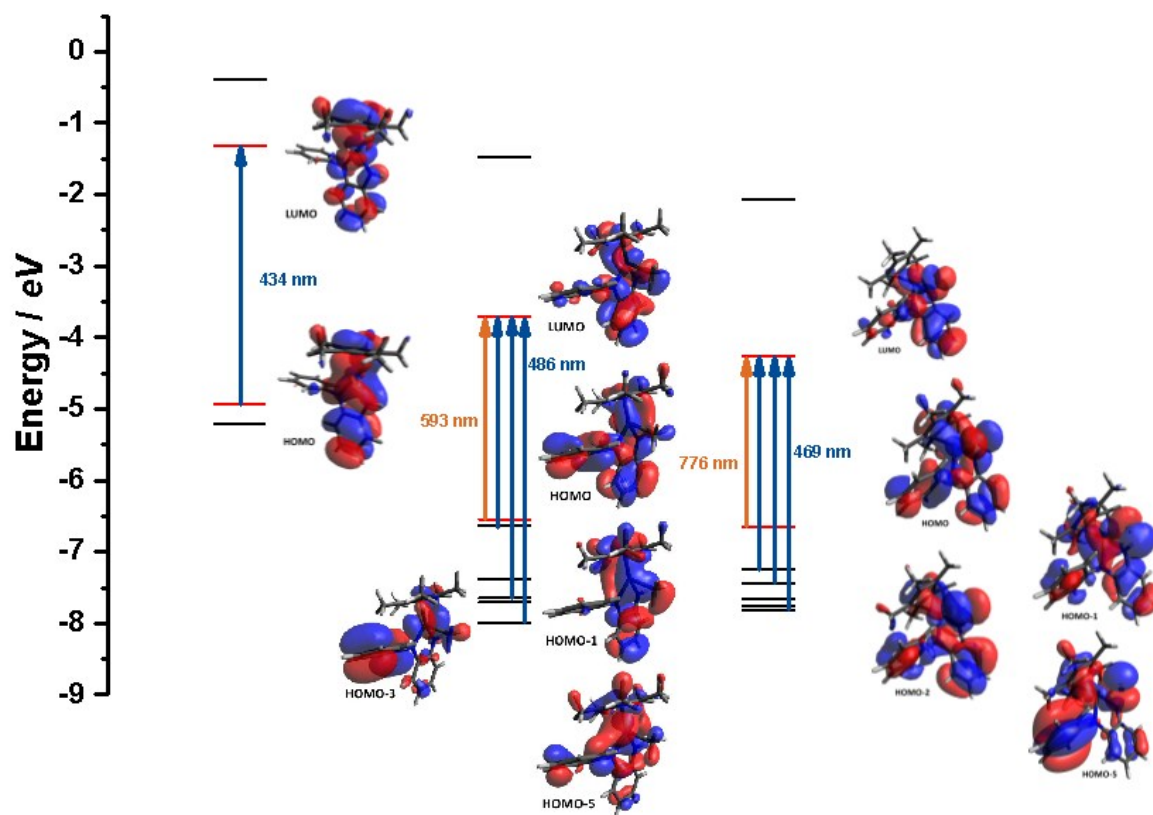


Figure S76: Comparison of frontier orbitals and main contributions to transitions observed in (UV-)Vis-NIR spectroscopy. HOMO and LUMO marked in red.

11.2 DFT Calculation for [1] (singlet state)

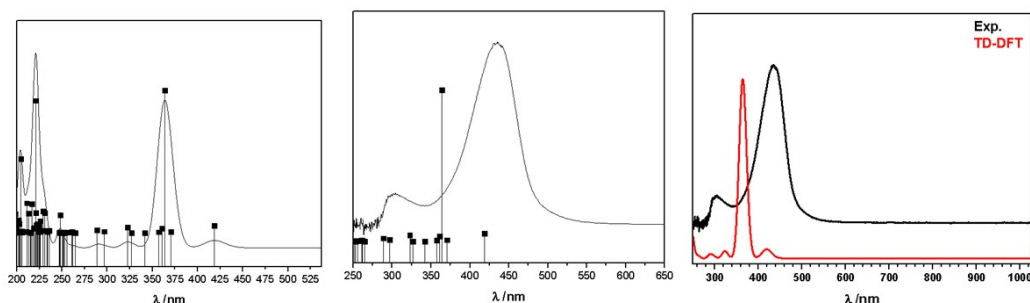


Figure S77: Calculated TD-DFT spectrum with discrete transitions (left), experimental spectrum with discrete calculated transitions (middle) and experimental (black) and calculated TD-DFT spectrum (red) (left).

Table S6: TD-DFT transitions for 1

State	Difference density (iso value 0.004)	Transition	Transition homo lumo	Calculated Transition energy	Oscillator strength	Experimental transition energy	Molar absorption coefficient 10^3
3		123->124 (0.89)	HOMO → LUMO	363.9	0.5171	434	9.3

Table S7: Selected molecular orbitals for 1.

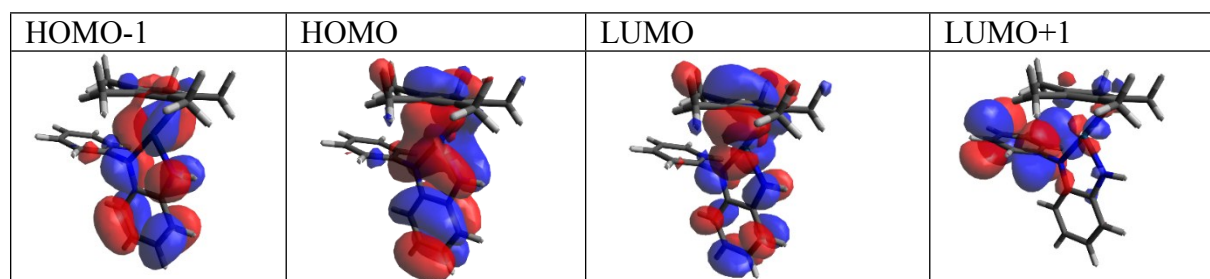


Table S8: Selected molecular orbital energies for 1.

Orbital No.	HOMO/LUMO	Energy (Eh)	Energy (eV)
122	HOMO-1	-0.191448	-5.2096
123	HOMO	-0.180974	-4.9245
124	LUMO	-0.048281	-1.3138
125	LUMO+1	-0.014316	-0.3896

11.3 DFT Calculation [1]⁺ (doublet state)

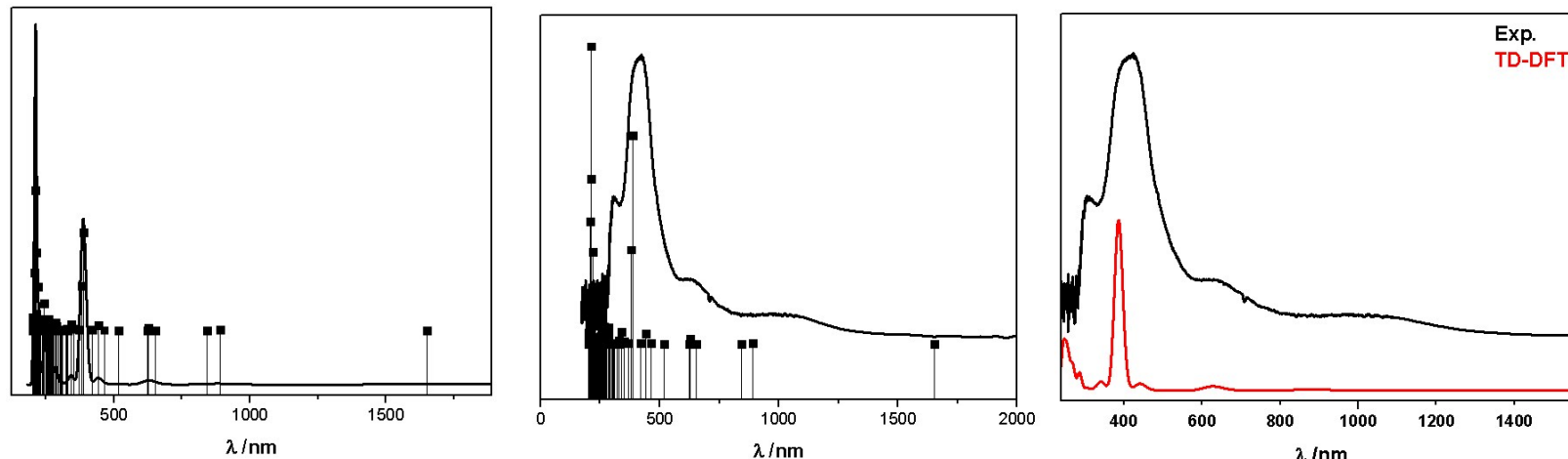
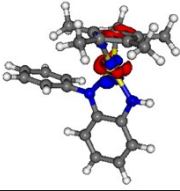
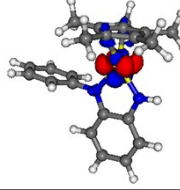
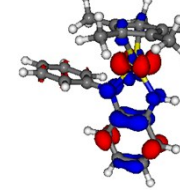
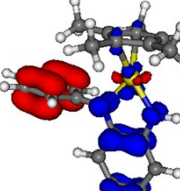


Figure S78: Calculated TD-DFT spectrum with discrete transitions (left), experimental spectrum with discrete calculated transitions (middle) and experimental (black) and calculated TD-DFT spectrum (red) (left).

Table S9: TD-DFT transitions for [1]⁺ (doublet state) (raw data) iso 0.004

State		Transition	Transition homo lumo	Calculated Transition energy	Oscillator strength	Experimental transition energy	Molar absorption coefficient 10^3
11		123a -> 124a (0.25) 115b -> 123b (0.42) 122b -> 124b (0.16)	HOMO α -> LUMO α (0.25) HOMO β -7 -> LUMO β (0.42) HOMO β -> LUMO β +1 (0.16)	388.9	0.2633	424	4.4
12		122a -> 124a (0.14) 123a -> 124a (0.10) 115b -> 123b (0.11) 122b -> 124b (0.47)	HOMO α -1 -> LUMO α (0.14) HOMO α -> LUMO α (0.10) HOMO β -7 -> LUMO β (0.11) HOMO β -> LUMO β +1 (0.47)	380.1	0.1197		
4		117b -> 123b (0.43) 119b -> 123b (0.42)	HOMO β -5 -> LUMO β (0.43) HOMO β -3 -> LUMO β (0.42)	626.8	0.0072	638	0.9
6		117b -> 123b (0.35) 119b -> 123b (0.56)	HOMO β -5 -> LUMO β (0.35) HOMO β -3 -> LUMO β (0.56)	652.6	0.0006		

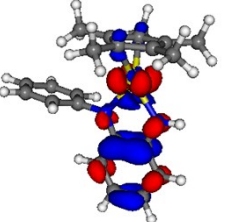
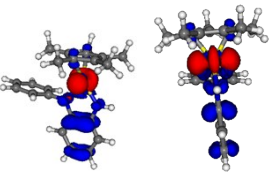
1		122b -> 123b (0.97)	HOMO β -> LUMO β (0.97)	1652.6	0.0007	1044	0.3
2		120b -> 123b (0.64) 121b -> 123b (0.29)	HOMO β -2 -> LUMO β (0.64) HOMO β -1 -> LUMO β (0.29)	890.4	0.0017		

Table S10: Selected molecular orbitals for [2]⁺.

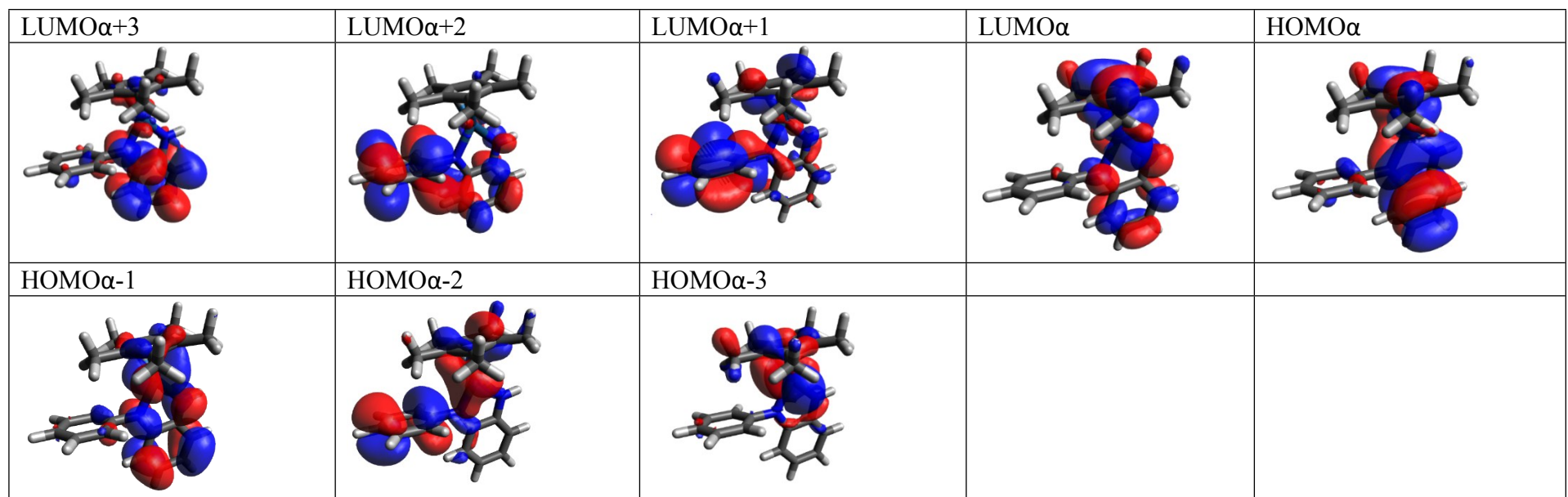


Table S11: Selected molecular orbitals for $[2]^+$.

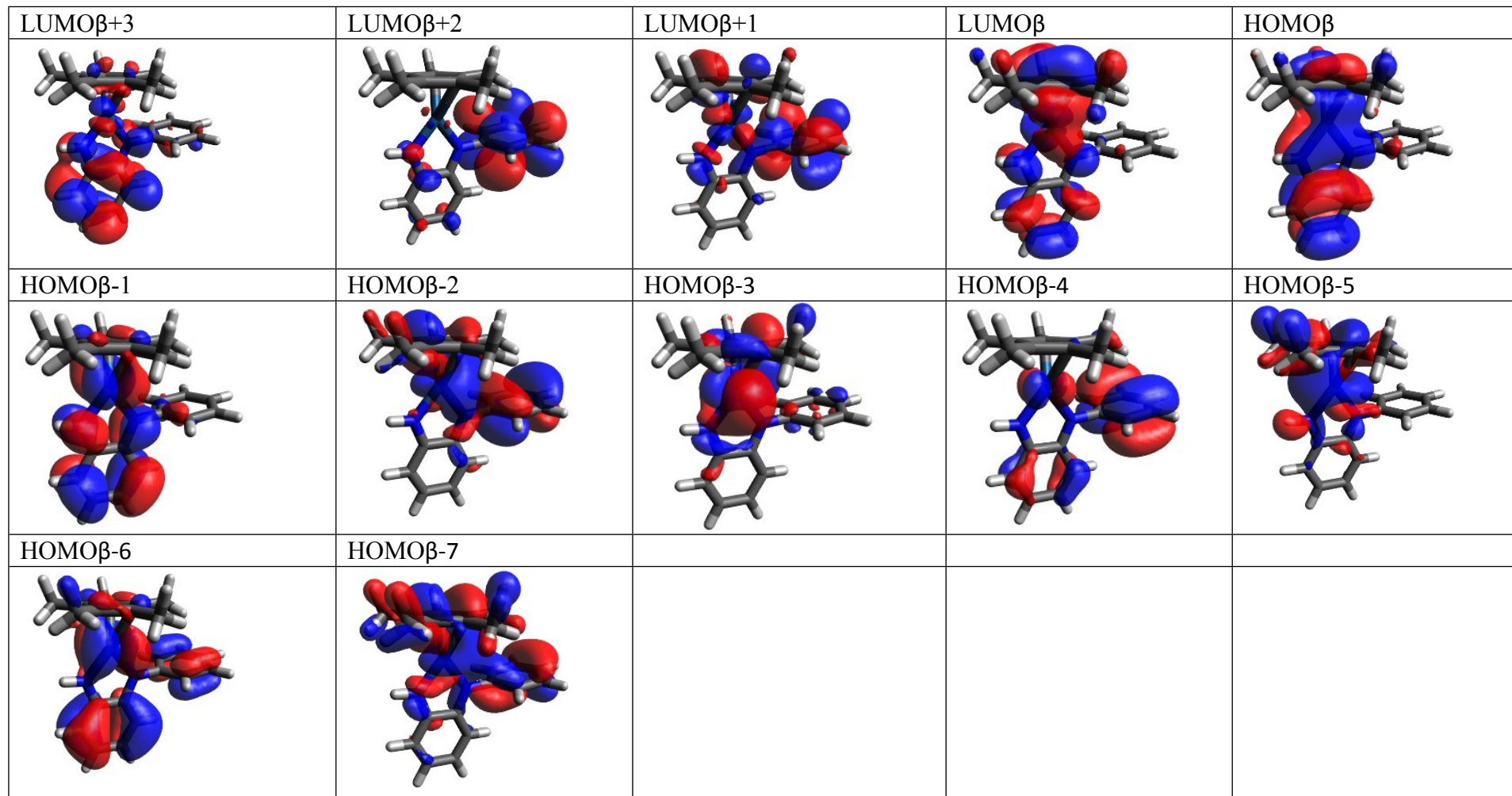


Table S12: Orbital energies for [1]⁺ (doublet state)

Spin up Orbitals alpha				Spin down orbitals beta			
Orbital No.	Orbital	Energy (Eh)	Energy (eV)	Orbital No.	Orbital	Energy (Eh)	Energy (eV)
114	HOMO α -9	-0.355101	-9.6628	114	HOMO β -8	-0.344884	-9.3848
115	HOMO α -8	-0.321275	-8.7423	115	HOMO β -7	-0.313018	-8.5177
116	HOMO α -7	-0.299267	-8.1435	116	HOMO β -6	-0.298623	-8.1259
117	HOMO α -6	-0.295000	-8.0274	117	HOMO β -5	-0.291469	-7.9313
118	HOMO α -5	-0.290216	-7.8972	118	HOMO β -4	-0.289554	-7.8792
119	HOMO α -4	-0.278126	-7.5682	119	HOMO β -3	-0.277392	-7.5482
120	HOMO α -3	-0.271645	-7.3918	120	HOMO β -2	-0.270393	-7.3578
121	HOMO α -2	-0.263343	-7.1659	121	HOMO β -1	-0.262364	-7.1393
122	HOMO α -1	-0.246584	-6.7099	122	HOMO β	-0.239958	-6.5296
123	HOMO α	-0.229292	-6.2394	123	LUMO β	-0.172193	-4.6856
124	LUMO α	-0.094578	-2.5736	124	LUMO β^+	-0.083993	-2.2856
125	LUMO α +1	-0.044587	-1.2133	125	LUMO β^+	-0.044150	-1.2014

11.4 DFT Calculation $[1]^{2+}$ (singlet state)

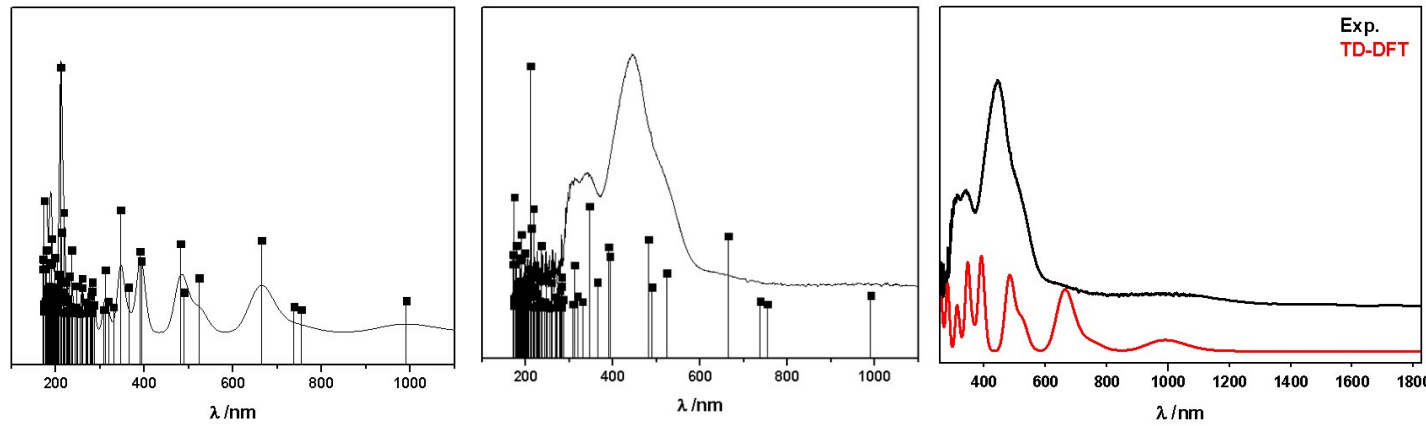
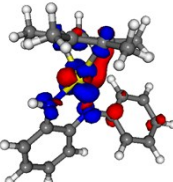
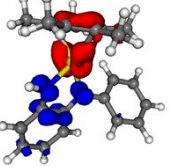
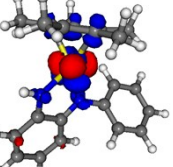
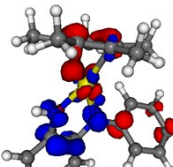


Figure S79: Calculated TD-DFT spectrum with discrete transitions (left), experimental spectrum with discrete calculated transitions (middle) and experimental (black) and calculated TD-DFT spectrum (red) (right).

Table S13: TD-DFT transitions for [1]²⁺ (singlet state) (raw data)

State		Transition	Transition homo lumo	Calculated Transition energy	Oscillator strength	Experimental transition energy	Molar absorption coefficient 10^3
11		119a -> 124a (0.19) 121a -> 124a (0.40) 122a -> 124a (0.17)	HOMO-3 -> LUMO+1 (0.19) HOMO-1 -> LUMO+1 (0.40) HOMO -> LUMO+1 (0.17)	346.6	0.1407	341	1.9
9		115a -> 123a (0.74) 121a -> 124a (0.16)	HOMO-7 -> LUMO (0.74) HOMO-1 -> LUMO+1 (0.16)	389.8	0.0850	449	3.7
8		122a -> 124a (0.63)	HOMO -> LUMO+1 (0.63)	393.2	0.0718		
7		116a -> 123a (0.38) 118a -> 123a (0.42)	HOMO-6 -> LUMO (0.38) HOMO-4 -> LUMO (0.42)	481.9	0.0951		

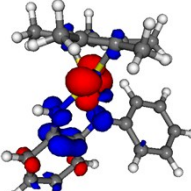
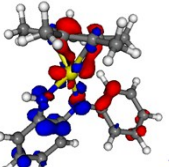
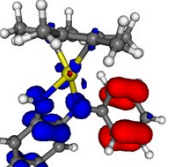
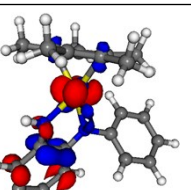
5		117a -> 123a (0.76) 118a -> 123a (0.14)	HOMO-5 -> LUMO (0.76) HOMO-4 -> LUMO (0.14)	523.9	0.0489	
3		121a -> 123a (0.67) 122a -> 123a (0.11)	HOMO-1 -> LUMO (0.67) HOMO -> LUMO (0.11)	663.9	0.0999	663sh 1.9
4		119a -> 123a (0.16) 120a -> 123a (0.78)	HOMO-3 -> LUMO (0.16) HOMO-2 -> LUMO (0.78)	737.4	0.0098	995 0.2
1		121a -> 123a (0.17) 122a -> 123a (0.75)	HOMO-1 -> LUMO (0.17) HOMO -> LUMO (0.75)	990.7	0.0181	

Table S14: Selected molecular orbitals for [2].

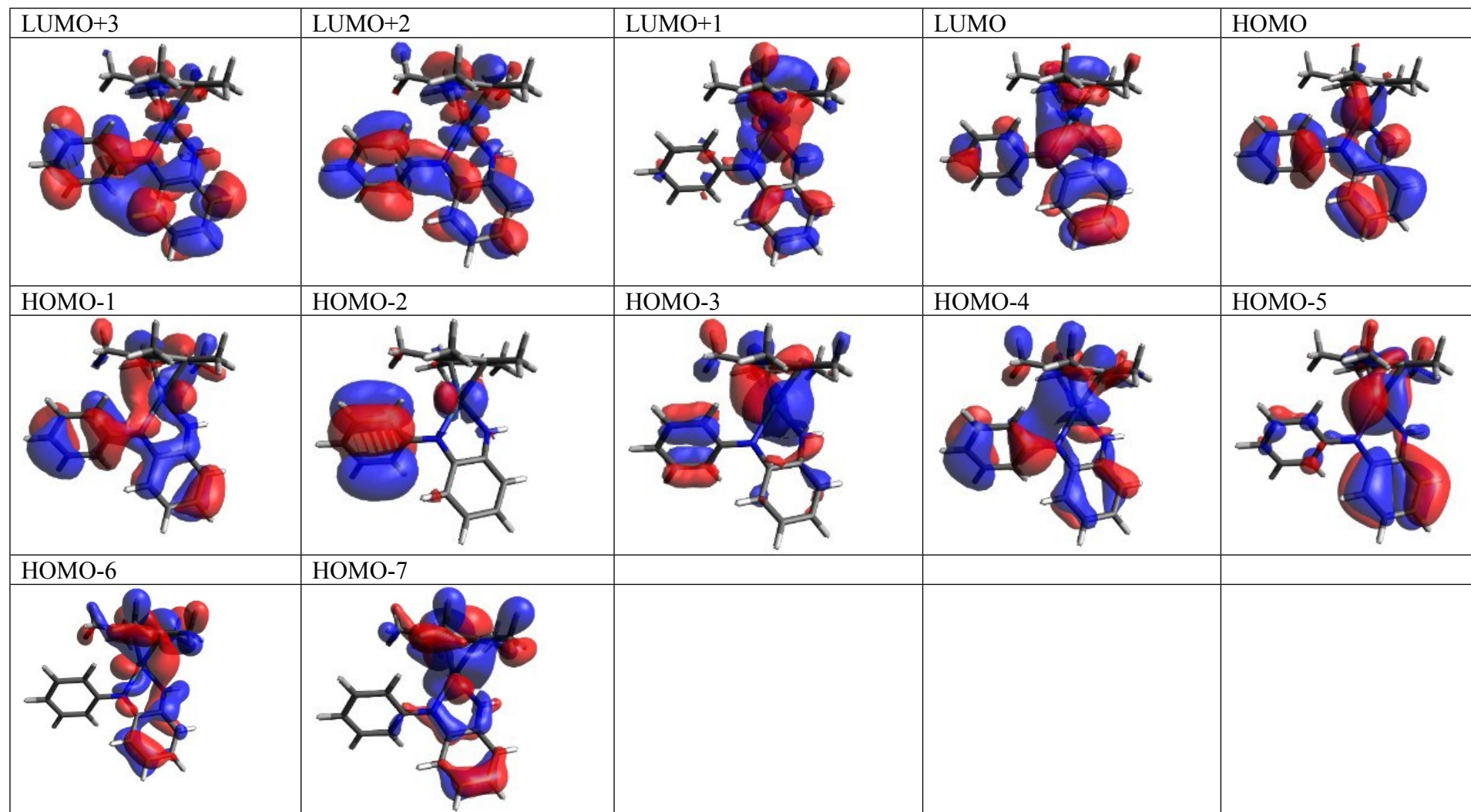


Table S15: Selected molecular orbital energies for [2].

Orbital No.	HOMO/LUMO	Energy (Eh)	Energy (eV)
115	HOMO-7	-0.358431	-9.7534
116	HOMO-6	-0.340761	-9.2726
117	HOMO-5	-0.335119	-9.1191
118	HOMO-4	-0.333889	-9.0856
119	HOMO-3	-0.316401	-8.6097
120	HOMO-2	-0.313341	-8.5265
121	HOMO-1	-0.303275	-8.2525
122	HOMO	-0.283697	-7.7198
123	LUMO	-0.216146	-5.8816
124	LUMO+1	-0.138525	-3.7695
125	LUMO+2	-0.092869	-2.5271

11.5 DFT Calculation for $[2]^{+}$ (singlet state)

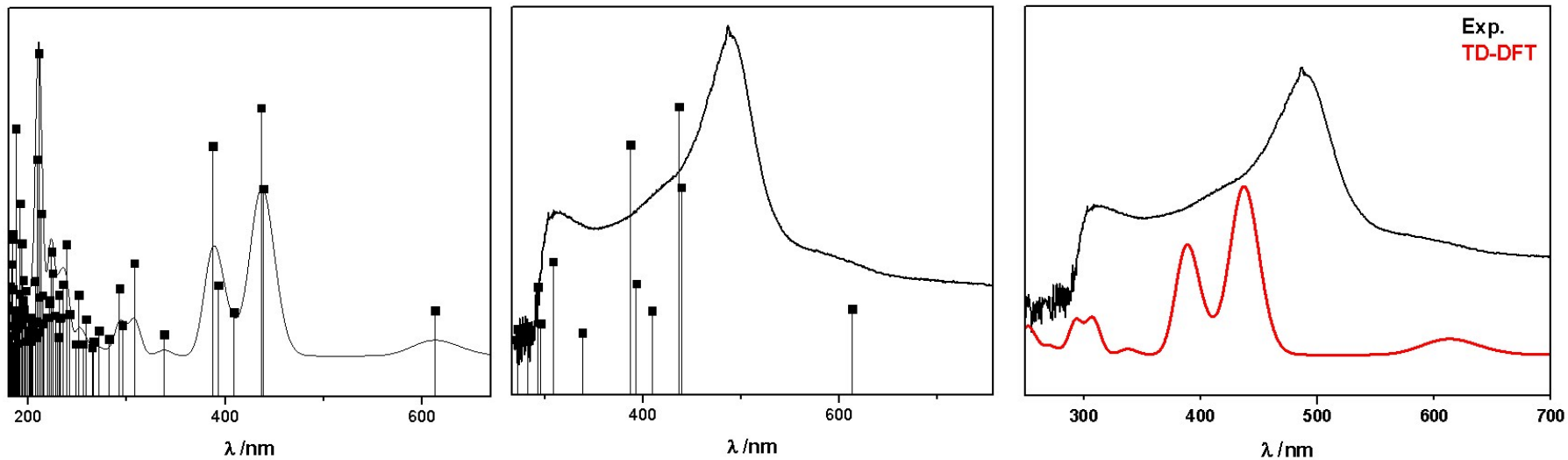
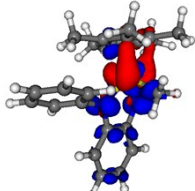
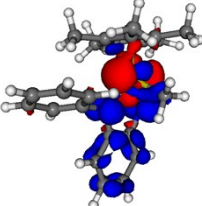
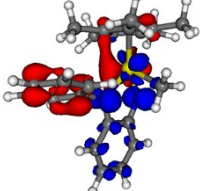
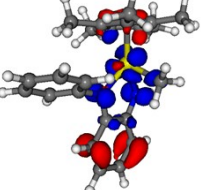


Figure S80: Calculated TD-DFT spectrum with discrete transitions (left), experimental spectrum with discrete calculated transitions (middle) and experimental (black) and calculated TD-DFT spectrum (red) (left).

Table S16: TD-DFT transitions for [2]⁺ (singlet state).k

State	Difference densities (iso 0,004; red negative, blue positive)	Transition	Transition homo lumo	Calculated Transition energy	Oscillator strength	Experimental transition energy	Molar absorption coefficient 10^3
1		127a -> 128a (0.81)	HOMO -> LUMO (0.81)	613.3	0.0267	593	1.0
2		122a -> 128a (0.40) 123a -> 128a (0.13) 124a -> 128a (0.11) 126a -> 128a (0.25)	HOMO-5 -> LUMO (0.40) HOMO-4 -> LUMO (0.13) HOMO-3 -> LUMO (0.11) HOMO-1 -> LUMO (0.25)	438.9	0.1135	486	6.4
3		124a -> 128a (0.38) 125a -> 128a (0.10) 126a -> 128a (0.39)	HOMO-3 -> LUMO (0.38) HOMO-2 -> LUMO (0.10) HOMO-1 -> LUMO (0.39)	436.5	0.1710		
4		125a -> 128a (0.72)	HOMO-2 -> LUMO (0.72)	409.1	0.0255	413	3.1

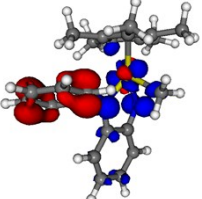
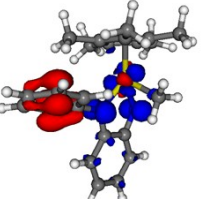
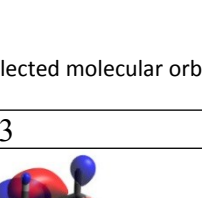
						
6		122a -> 128a (0.42) 123a -> 128a (0.44)	HOMO-5 -> LUMO (0.42) HOMO-4 -> LUMO (0.44)	392.9	0.0450	
5		123a -> 128a (0.37) 124a -> 128a (0.29) 126a -> 128a (0.14)	HOMO-4 -> LUMO (0.37) HOMO-3 -> LUMO (0.29) HOMO-1 -> LUMO (0.14)	387.2	0.1439	

Table S17: Selected molecular orbitals for $[2]^+$.

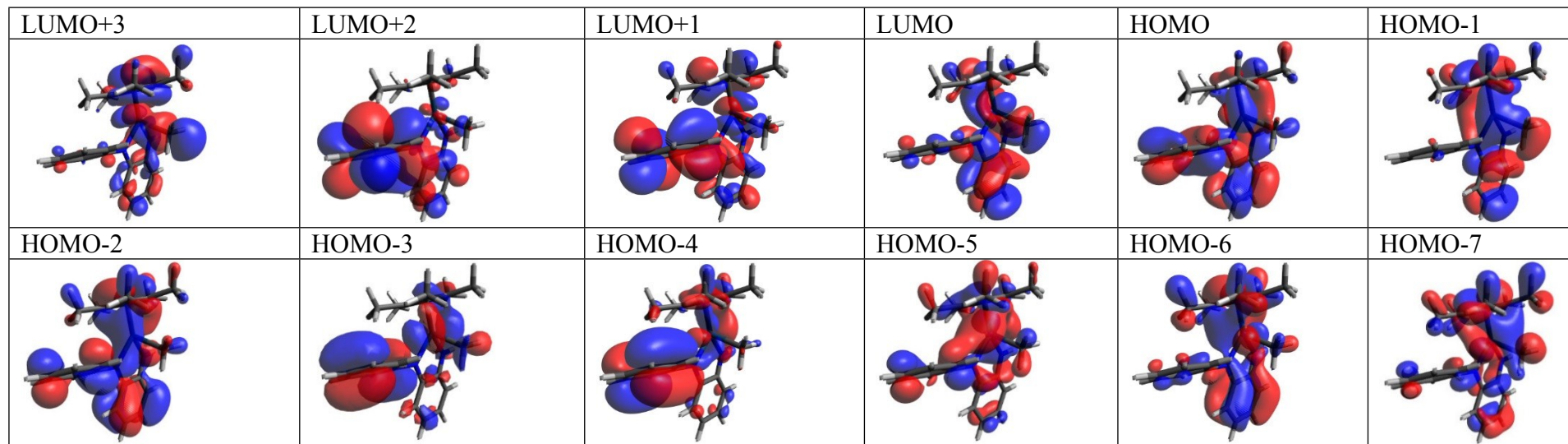


Table S18: Selected molecular orbital energies for [1]²⁺.

Orbital No.	HOMO/LUMO	Energy (Eh)	Energy (eV)
120	HOMO-7	-0.311020	-8.4633
121	HOMO-6	-0.305476	-8.3124
122	HOMO-5	-0.293880	-7.9969
123	HOMO-4	-0.283206	-7.7064
124	HOMO-3	-0.281052	-7.6478
125	HOMO-2	-0.271251	-7.3811
126	HOMO-1	-0.243830	-6.6349
127	HOMO	-0.240521	-6.5449
128	LUMO	-0.136344	-3.7101
129	LUMO+1	-0.054350	-1.4790
130	LUMO+2	-0.042796	-1.1645
131	LUMO+3	-0.037464	-1.0195

11.6 DFT Calculation for $[2]^0$ (doublet state)

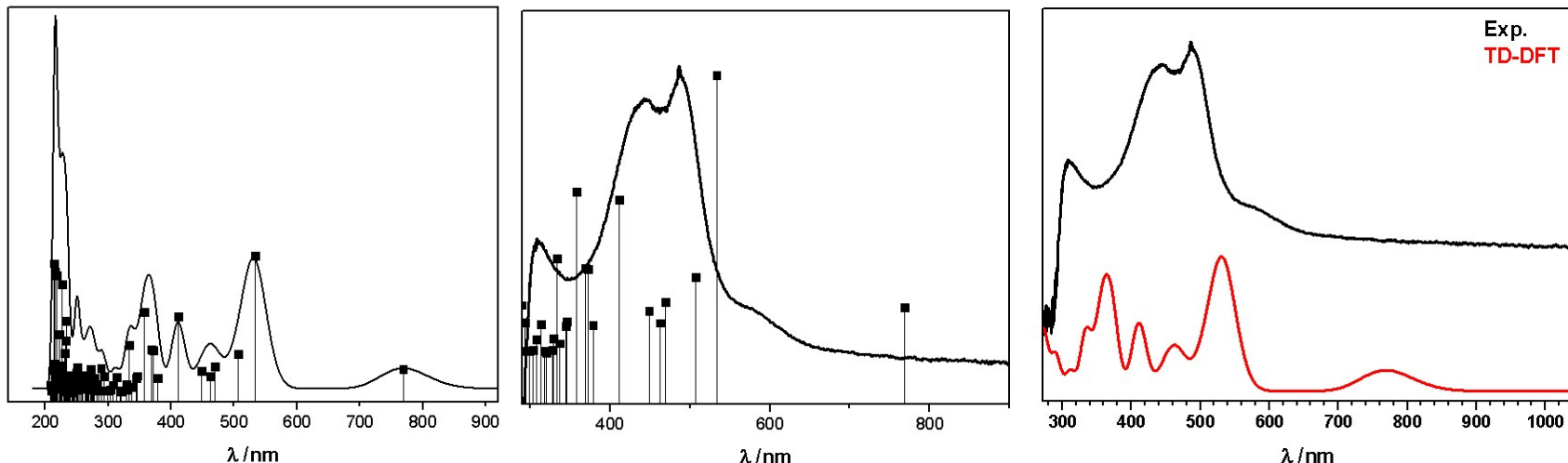


Figure S81: Calculated TD-DFT spectrum with discrete transitions (left), experimental spectrum with discrete calculated transitions (middle) and experimental (black) and calculated TD-DFT spectrum (red) (left).

Table S19: TD-DFT transitions for [2]⁰ (doublet state) (raw data)

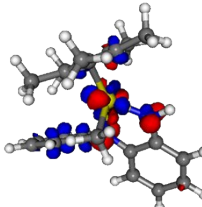
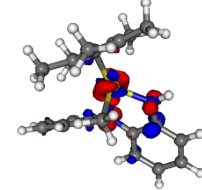
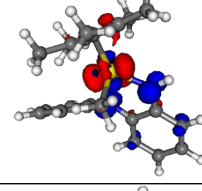
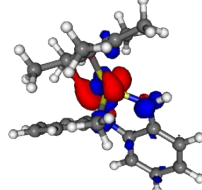
State	Difference densities	Transition	Transition homo lumo	Calculated Transition energy	Oscillator strength	Experimental transition energy	Molar absorption coefficient 10^3
7		128a -> 131a (0.59)	HOMO α -> LUMO $\alpha+2$ (0.59)	411.2	0.0545	443	9.5
11		128a -> 132a (0.25) 128a -> 133a (0.30)	HOMO α -> LUMO $\alpha+3$ (0.25) HOMO α -> LUMO $\alpha+4$ (0.30)	358.0	0.0575		
2		126b -> 128b (0.82)	HOMO $\beta-1$ -> LUMO β (0.82)	533.4	0.0984	486	10.7
1		127b -> 128b (0.93)	HOMO β -> LUMO β (0.93)	768.9	0.0168	608	1.4

Table S20: Composition of selected spin up and spin down molecular orbitals of $[2]^0$.

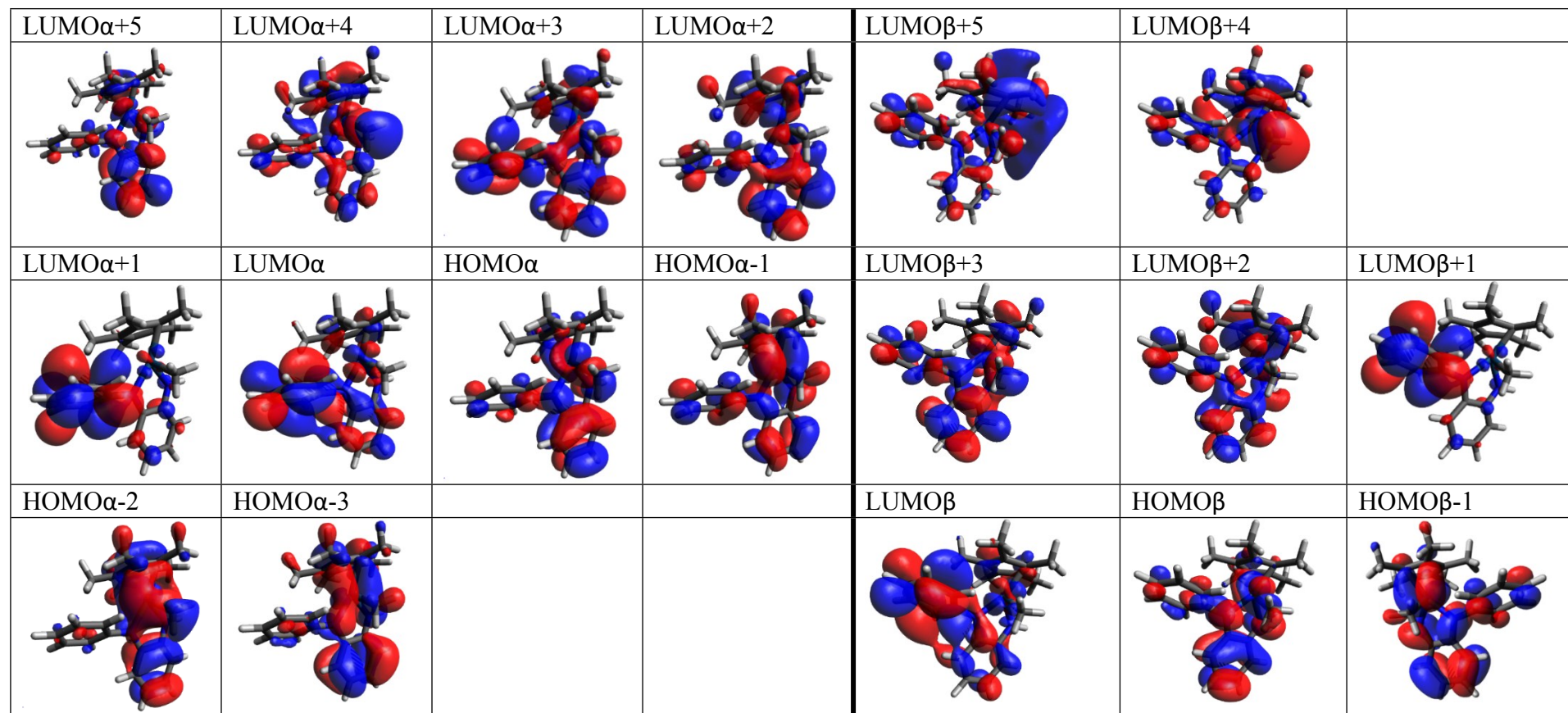


Table S21: Orbital energies of [2]⁰ from DFT-calculation

Spin up Orbitals alpha				Spin down orbitals beta			
Orbital No.	Orbital	Energy (Eh)	Energy (eV)	Orbital No.	Orbital	Energy (Eh)	Energy (eV)
126	HOMO α -2	-0.212939	-5.7944	126	HOMO β -1	-0.199963	-5.4413
127	HOMO α -	-0.194693	-5.2979	127	HOMO β	-0.183648	-4.9973
128	HOMO α	-0.146421	-3.9843	128	LUMO β	-0.086230	-2.3464
129	LUMO α	-0.020399	-0.5551	129	LUMO β +1	-0.018420	-0.5012
130	LUMO α +1	-0.014510	-0.3948	130	LUMO β +2	-0.013372	-0.3639
131	LUMO α +2	0.002959	0.0805	131	LUMO β +3	0.007712	0.2099
132	LUMO α +3	0.012268	0.3338	132	LUMO β +4	0.019694	0.5359
133	LUMO α +4	0.017902	0.4871	133	LUMO β +5	0.021276	0.5789
134	LUMO α +5	0.023008	0.6261	134	LUMO β +6	0.027368	0.7447

11.7 DFT Calculation for [2]²⁻ (doublet state)

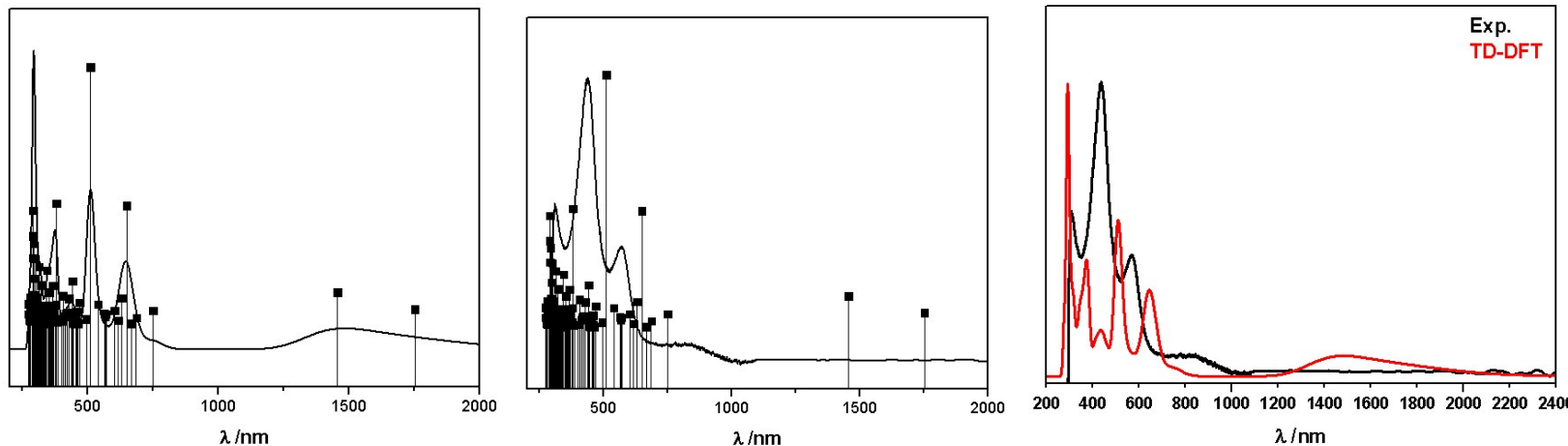


Figure S82: Calculated TD-DFT spectrum with discrete transitions (left), experimental spectrum with discrete calculated transitions (right) and experimental (black) and calculated TD-DFT spectrum (red) (below).

Table S22: TD-DFT transitions for [2]²⁻ (doublet state)

State	Difference densities	Transition	Transition homo lumo	Calculated Transition energy	Oscillator strength	Experimental transition energy	Molar absorption coefficient 10^3
14		128a → 130a (0.20) 128b → 131b (0.25)	HOMO α -1 → LUMO α (0.20) HOMO β → LUMO β +2 (0.25)	509.8	0.1409	437	9.9
31		128a → 133a (0.21) 128b → 133b (0.14) mixed	HOMO α -1 → LUMO α +3 (0.21) HOMO β → LUMO β +4 (0.14) mixed	378.7	0.0663		
5		129a → 133a (0.25) 128b → 129b (0.34) **	HOMO α → LUMO α +3 (0.25) HOMO β → LUMO β (0.34)	648.6	0.0651	568	4.0
7		129a → 133a (0.41)	HOMO α → LUMO α +3 (0.41)	629.4	0.0143		

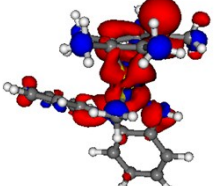
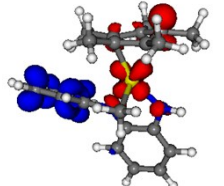
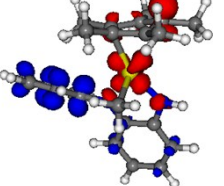
3	 **	129a → 132a (0.88)	HOMO α → LUMO $\alpha+2$ (0.88)	748.6	0.0073	842	0.6
1		129a → 130a (0.69) 129a → 131a (0.28)	HOMO α → LUMO α (0.69) HOMO α → LUMO $\alpha+1$ (0.28)	1752.9	0.0080		
2		129a → 130a (0.26) 129a → 131a (0.69)	HOMO α → LUMO α (0.26) HOMO α → LUMO $\alpha+1$ (0.69)	1455.4	0.0173		

Table S23: Selected molecular orbitals for $[2]^{2-}$.

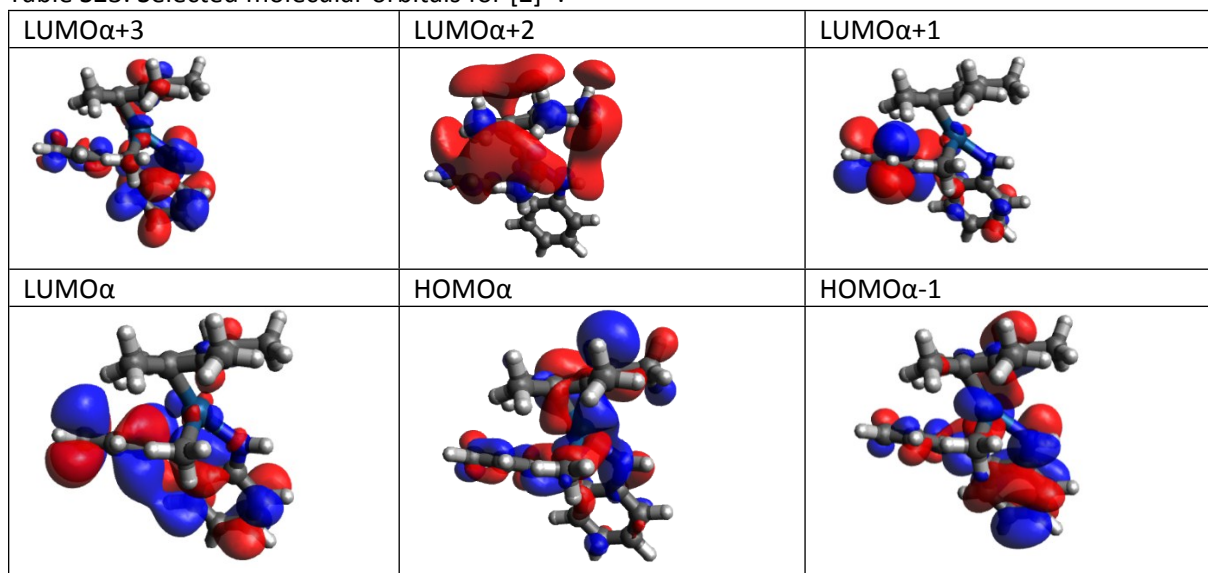


Table S24: Selected molecular orbitals for $[2]^2$.

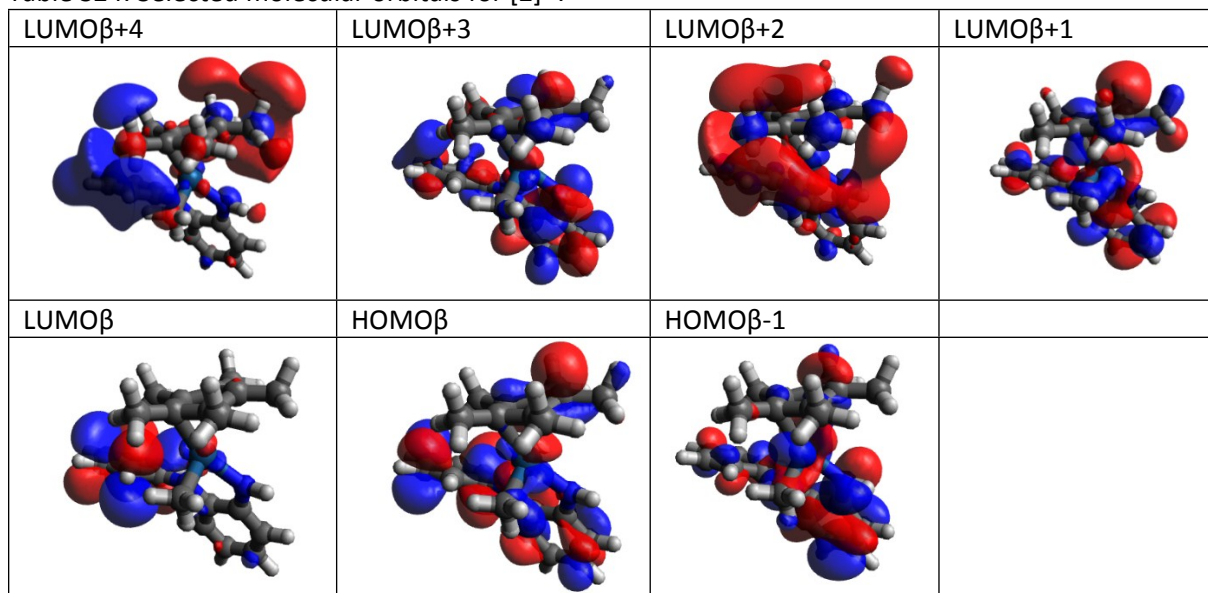


Table S25. Orbital energies of $[2]^2$ for selected molecular orbitals.

Spin up Orbitals alpha				Spin down orbitals beta			
Orbital No.	Orbital	Energy (Eh)	Energy (eV)	Orbital No.	Orbital	Energy (Eh)	Energy (eV)
127	HOMO α -2	-0.094693	-2.5767	127	HOMO β -1	-0.089895	-2.4462
128	HOMO α -	-0.070057	-1.9063	128	HOMO β	-0.065503	-1.7824
129	HOMO α	-0.022785	-0.6200	129	LUMO β	0.035628	0.9695
130	LUMO α	0.039168	1.0658	130	LUMO β +1	0.042805	1.1648
131	LUMO α +1	0.042582	1.1587	131	LUMO β +2	0.050174	1.3653
132	LUMO α +2	0.066167	1.8005	132	LUMO β +3	0.068563	1.8657
133	LUMO α +3	0.075235	2.0473	133	LUMO β +4	0.078047	2.1238
134	LUMO α +4	0.084832	2.3084	134	LUMO β +5	0.085907	2.3377
135	LUMO α +5	0.085475	2.3259	135	LUMO β +6	0.086927	2.3654

11.8 DFT Calculation for [3]⁺ (singlet state)

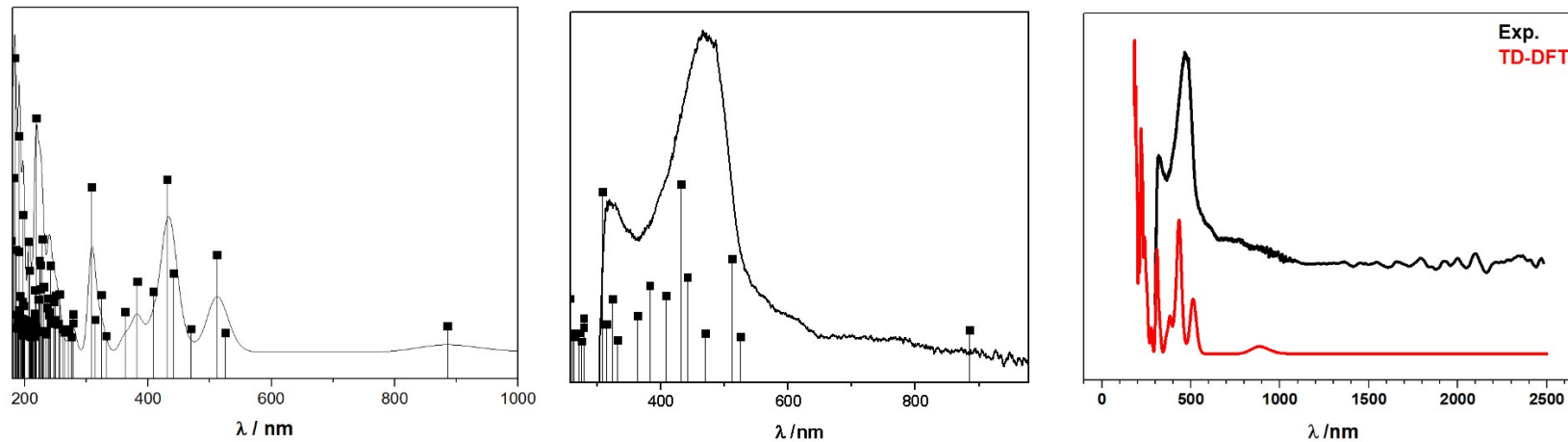


Figure S83: Calculated TD-DFT spectrum with discrete transitions (left), experimental spectrum with discrete calculated transitions (middle) and experimental (black) and calculated TD-DFT spectrum (red) (left).

Table S26: TD-DFT calculated eletronic transistions and difference densities of [3]⁺. (Including raw data)

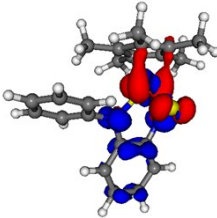
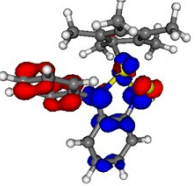
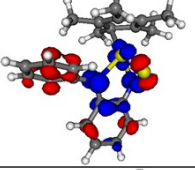
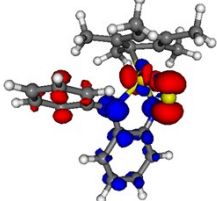
State	Difference densities (iso-value of 0.004)	Transition	Transition homo lumo	Calculated Transition energy	Oscillator strength	Experimental transition energy	Molar absorption coefficient 10^3
1		131a -> 132a (0.90)	HOMO -> LUMO (0.81)	885.3	0.009	776 br	2.1
3		129a -> 132a (0.30) 130a -> 132a (0.30)	HOMO-2 -> LUMO (0.30) HOMO-1 -> LUMO (0.30)	511.7	0.069	469	2.5
5		126a -> 132a (0.35) 129a -> 132a (0.29)	HOMO-5 -> LUMO (0.35) HOMO-2 -> LUMO (0.29)	441.5	0.053		
6		130a -> 132a (0.29)	HOMO-1 -> LUMO (0.29)	431.3	0.132		

Table S27: Composition of selected molecular orbitals of [3]⁺.

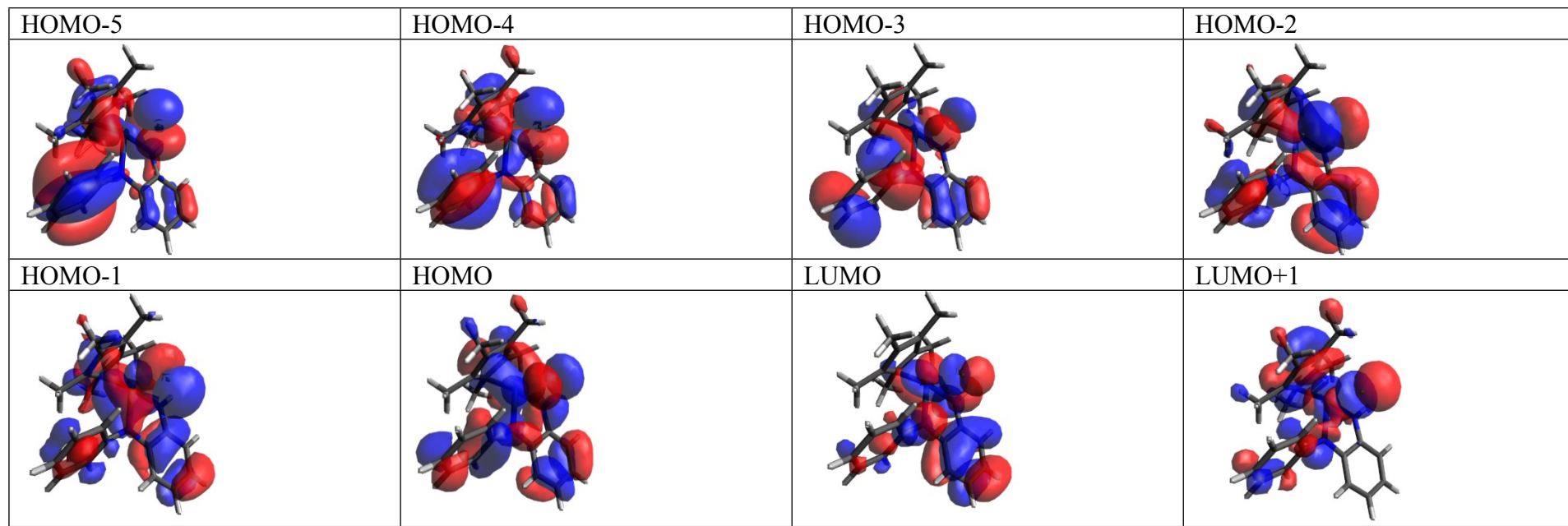


Table S28: Selected molecular orbital energies for [3]⁺.

Orbital No.	HOMO/LUMO	Energy (Eh)	Energy (eV)
126	HOMO-5	-0.287293	-7.8176
127	HOMO-4	-0.284895	-7.7524
128	HOMO-3	-0.281419	-7.6578
129	HOMO-2	-0.273177	-7.4335
130	HOMO-1	-0.266413	-7.2495
131	HOMO	-0.244328	-6.6485
132	LUMO	-0.156737	-4.2650
133	LUMO+1	-0.075974	-2.0674

11.9 Coordinates of optimized structures

IrNPhH native [1]

Ir	-0.67726332572944	-0.06303930746490	-0.20961079613236
N	-1.44850661327445	-0.14203340529253	1.59457938145844
N	0.93085662521545	0.01677503658800	0.94545155610124
C	-0.0187979229998	0.01044501527277	-2.32322165362881
C	0.8657987726948	1.1198934772254	-2.02573388985032
C	0.77698937515257	-1.20934108459474	-2.056184387222021
C	-2.17381603536422	0.61840043781833	-1.62764484474785
C	-2.11978105991776	-0.82006562146650	-1.64722371132467
C	-0.61918782919905	-0.10333170900716	2.67878919687192
C	0.7543661867054	-0.00877728239247	2.31127124621120
C	2.23725631614573	0.123878999215184	0.40603232913086
C	1.3609803922963	0.05473313546414	-2.88083260080010
C	0.46588098658997	2.55514255715373	-2.13519012428338
C	-0.28322861182809	-2.61135770149051	-2.20456678317452
C	3.38217699762713	1.44620414105091	-1.34639478605504
C	3.26449471052481	-1.73568428231291	-1.36731581269857
C	0.98346353484205	-0.14840587364541	4.03644578649556
C	1.74589724149025	0.04467365223607	3.3066184723137
C	2.92407582847282	-1.02830535158292	0.00639030968967
C	2.83055599550450	1.38156570325692	0.23295557605071
C	0.00787420545610	-0.08679465983188	5.0106526801953
C	1.3645413242936	0.00896309171305	4.64529117694994
C	4.09503991209534	1.48133971302715	-0.35016220476967
C	4.19134818303459	-0.92545201248773	-0.57102999046873
C	4.77812899751392	0.33038223077483	-0.75402032050052
H	-2.44465551234042	-0.20308806536354	1.78981465155919
H	1.327047839177	0.03825215448394	-3.98151035613549
H	1.97804941973057	-0.78913596931217	-2.55154821379096
H	1.88419532454797	0.97190368359504	-2.57670696094996
H	0.62659405234956	2.635317068904	-2.09873325333918
H	-0.86888140071683	3.15337897507138	-1.30602079793356
H	0.80580615533250	3.01266807409281	-3.08012300234442
H	-4.0731291146733	1.44098942098675	-2.20739716141411
H	3.12114870068287	2.9472808722491	-1.15674635102265
H	-3.95158341765063	1.07881483039994	-0.48023695049160
H	2.80026904680254	0.10708489109063	3.03822500159843
H	2.12932060635127	0.05543019543955	5.41975686319470
H	-0.25431516268949	-0.12060659533703	6.06822833964000
H	-2.039370879325956	-0.23330617919503	4.30070897735319
H	2.28557984926393	2.26449264807051	0.56933236944033
H	2.43816312916572	-1.99576971398581	0.13794034067351
H	0.81230716323646	-2.64770895057452	-2.15191329925188
H	-0.67104747602675	-3.25663432648436	-1.40443754427702
H	-0.58083296915433	-0.30586072619873	-3.16927043774552
H	-3.96581534471808	-1.76117117288059	-2.21909719242004
H	-2.93186792397181	-2.76697786985699	-1.19337741358102
H	-3.839191787171601	-1.40904921297580	-0.4893632216534
H	5.77108097447552	0.41338100577736	-1.20042946625942
H	4.55790120835501	2.46232163535289	-0.47541228457099
H	4.72811361629776	-1.82455266093749	-0.87963002209754

IrNPhH 2ox sing [1]²⁺

Ir	1.41088720406001	2.92029272859950	-0.52084122656546
N	0.62432480600080	3.30440555846520	1.296732407463397
N	3.05758138251197	2.72989865799167	0.75419368039073
C	1.85368505060539	2.63628272149615	-2.6999258252369
C	0.9355708282671	3.74889930123350	-2.46983366371063
C	1.25155943428491	1.46060867350958	-2.14575757648773
C	-0.28096142664570	3.24829198623914	-1.86401549550671
C	-0.08310238093284	1.84479292423000	-1.61668982944957
C	1.34422020966979	2.96595884009903	2.3599168697230
C	2.76259611423955	2.69116592484193	2.05640688505471
C	4.37389129862140	2.89163356801307	0.3062255176950
C	3.12577478091566	2.75345220819863	-3.47023571158334
C	1.19637837687944	5.16896258161046	-2.81626636277268
C	1.76648168687959	0.70430718160776	-2.18214431496753
C	1.50547243169747	4.04625860850845	-1.58261367385847
C	1.071618747404031	0.91137435326203	-1.02673822128828
C	0.89340556586150	2.92564786992273	3.7094353934579
C	3.66948424900605	2.40700973243585	3.12224522734549
C	4.8331326582764	2.0896525317889	-3.47023571158334
C	5.23240034038481	3.84156367575706	0.90976113433803
C	1.79989683832496	2.6410081750740	4.6962928503729
C	3.1872973989877	2.36847714904177	4.40046011698177
C	6.53697483304088	3.96277981679329	0.45275317639583
C	6.14895708414520	2.19579242446422	-1.18067451991049
C	7.0030478832444	3.1338979916245	-0.5972397461034
H	-0.34270941004978	3.57878803179864	1.47306383589634
H	2.88985582919787	2.82033955942036	-4.54224684774186
H	3.75818191528375	1.85313671323246	-3.34110401396332
H	3.70724008262280	3.62089515842087	-3.18785838051502
H	2.25979892890260	5.35658453416917	-2.99465482241908
H	0.8433780002330	5.84305967101256	-2.02378341273919
H	0.64167565520087	5.43212912069697	-3.73379660159521
H	-2.19718483781878	3.98095982720139	-2.43876782666715
H	-1.28343869037181	5.10932078012168	-1.4410325146135
H	-2.06372051243299	3.68369133102545	-0.70878798815779
H	4.71139354118920	2.17440087145073	2.90631619776324
H	3.88529485495340	2.09565520571418	5.21945098024899
H	1.47861455281002	2.60301010432841	5.73797149967406
H	-0.15538996704973	3.12298194628095	3.92874845978894
H	4.85268549621690	4.50379997643752	1.68888711268683
H	4.15702545744839	1.35015253636415	-1.81137405252710
H	2.8600736402656	0.02672882598132	-2.22678730882504
H	1.43473696927044	-0.5107658912969	-1.31865476223884
H	1.39171184714105	-0.43832045629477	-3.08508912699906
H	-1.57286233052790	0.34064699552623	-1.82644348801163
H	-0.6062989284819	0.18571254719029	-0.34520729498456
H	-1.85151371868343	1.4471191839800	-0.47238813764077
H	8.03656045407368	3.22076034810770	-0.91694852008413
H	7.19859865319625	4.70967535062218	0.89115140551467
H	6.52438373063664	1.54061063832344	-1.96675024579379

IrNPhH 1ox dub [1]⁺

Ir	1.27250370216992	2.66065225100001	-0.40566844950282
N	0.49520576430211	2.566406450252630	1.34364937168755
N	2.92537251931267	2.73850727510534	0.76841702729670
C	1.95610854325084	2.70870688500794	-2.50773442884457
C	1.10190011373429	3.83601676459339	-2.21045907366082
C	1.19344671552481	1.51547307037313	-2.2318295792826
C	-0.21695818632337	3.33704049522214	1.82957052926271
C	-0.16626373052119	1.90831600377806	-1.8448558810112
C	1.329447489020000	2.6223308400392	2.4815137474257
C	2.73426276359927	2.72870831929921	2.09889205212271
C	4.23940176971381	2.84409849901616	0.2493981954717
C	3.33801791722632	2.769889324465793	-3.05547980374675
C	1.5107440547803	5.266975088450638	-2.29502534923277
C	1.68499770519096	0.11554443450638	-2.34731802885851
C	-1.41614668427132	4.17321766991322	-1.54991233922865
C	-1.30667058470230	0.99167404802521	-1.56514895799560
C	0.97544097389569	2.58552708072246	3.85311457482269
C	3.73516167397307	2.80373626869708	3.10515898737266
C	4.90447878368676	1.6848390628306	-0.18304747537225
C	1.971069872082269	4.261732871042235	4.799204469492740
C	3.34955612479330	2.78049464667834	4.4239775332086
C	6.09614886731461	4.19334693937747	-0.51790825698640
C	6.17505156034393	1.784923396563	-0.75344620720380
C	6.76912458218245	3.03868326884718	-0.92549049571773
C	-0.4781289713205052	4.29192327972376	1.64574053468582
C	1.32490172377627	2.7567665001335	-1.35653564246934
H	1.2863566424427702	3.80021984877866	-0.69599212478346
H	4.786365642346324	2.87036486482965	2.830849264467985
H	4.1047214729493	2.839077220952677	5.20591657869100
H	1.725688384257163	5.26466602650235	5.86039807522205
H	1.10370548585231	5.85683857493535	-1.46178375072020
H	1.51736040277762	5.72775128826775	-3.2349122037759
H	-0.09393388208035	4.17034493346362	-2.41995505794618
H	-1.1529174237367597	2.51950746249366	-1.35673564246934
H	-1.99908373673735	3.80021984877866	-0.69599212478346
H	4.786365642346324	2.87036486482965	2.830849264467985
H	1.37126545013383	-0.3413582785458	-3.30134397304620
H	-1.9945611146452	0.96681065471545	-2.42746705270531
C	2.65516485394966	0.28561958723051	-0.9925190586282
C	2.666286323163956	0.85650664803273	0.31965746307846
C	1.5862264474523	0.90979716794091</td	

IrMe 1red [2]•

Ir	0.74723951249808	-0.15099379595432	0.08683820905166
N	0.46551523097126	-2.12523558904867	-0.28308757243802
N	-1.29093264111277	-0.36478947995004	0.21025689756575
C	2.6075285092090	0.22290382408901	-1.04368774622934
C	2.67911049138586	0.85000692781144	0.25143447388366
C	1.54156397161116	0.84697232989112	-1.80729260654532
C	1.61262206056446	0.83901512817993	0.32367498022532
C	0.9243141279827	1.81992164725336	-0.94867705213277
C	-3.14303627689743	1.00149900032426	-0.60370448043728
C	-2.47634991843886	0.74357788750864	0.35166295581987
C	-3.93693137378892	2.14252250727606	-0.50369513650777
C	-1.78195434204010	-1.63796045887244	0.14323147031422
C	3.54360749064813	-0.80936782799780	-1.58007280593461
C	-0.77075947355704	-2.63049323784706	-0.13010497648473
C	3.70426814276669	0.62385295885385	1.31065939685897
C	-3.11871902260324	-2.04305024987679	0.34550351759062
C	-2.47634991843886	-4.35951346609016	-0.04105178141527
C	-1.15075279899262	-3.99002928703979	-0.22427364014807
C	-3.4569309362469	-3.38810802356851	0.25178923794313
C	-0.17301233687796	2.75876076434282	-1.33218976331370
C	1.40768491872711	2.83362155770017	1.41842360341017
C	1.15201890935894	0.55465743291907	-3.22253866318855
C	-3.74825539011198	0.04266675787388	0.54983934826414
C	-2.75989617222788	2.78415388212843	1.50539295038222
C	-1.96227110961672	1.64371034017022	1.41253750789290
H	-3.26094326525402	0.29539630512591	-1.42370074218248
H	-2.74638536060341	-5.41419566893113	-0.09863711269223
H	-0.3815725250883	-4.73597218827842	-0.43305232581998
H	0.25772317383476	3.72841066828302	-1.62900685606064
H	-0.8566494421216	2.92959599966898	-0.49320516109881
H	-0.76734426807383	2.3754860794697	-2.17194748584529
H	-4.4924411341996	-3.68819986733138	0.41531456615563
H	1.21149780342596	-2.80288521537006	-0.43058470513938
H	-3.8687950816713	-1.29012237621939	0.58034497603505
H	4.31865247926130	-0.3339045982825	-2.20399730716275
H	3.0282189972469	-1.53187951578699	-2.23045920835049
H	4.05549057639208	-1.37701308709178	-0.79223587937886
H	4.207969306140	-0.34130153697850	1.18745860776268
H	3.2474250585674	0.65133436096453	2.30759865194804
H	4.4707209674617	1.41611747965424	1.28061693189875
H	-4.37273479432119	3.93221920730841	0.62401995022584
H	-2.60854114062064	3.48286204507233	2.32791189328386
H	1.44312921731169	2.35278908949888	2.40407444906940
H	0.4373770810223	3.33195302157029	1.31038544538892
H	2.1943513973365	3.60401604796171	1.40111789389253
H	-1.17851403310399	1.44800166709825	2.14286437011186
H	0.06237608008782	0.47546475830473	-3.31639449353285
H	1.59694560820371	-0.38588548534499	-3.56656918841871
H	1.48288275360182	1.35805823455103	-3.90141583297964
H	-4.69262854451276	2.33482679456107	-1.26555268892653
C	0.74574136380053	-0.75333383013305	2.11105193919431
H	1.6616644929721	-3.2198463610609	2.3384485874590
H	0.69225332818430	0.08886106254213	2.81896236447769
H	-0.11470201861650	-1.40730700007890	2.30652789827721

IrCl

Ir	3.24416348533836	2.04635464456639	17.51927099940094
Cl	2.50690137004877	4.30905911949233	17.5927830301823
C	4.78182430070674	1.27084718495563	18.89707910342497
N	1.87634105734610	1.74208866912136	16.04106462730468
C	5.32923140982803	2.63299148375957	17.06862548355086
N	1.59360715719865	1.49269452975693	18.51883594667846
C	5.12115494245642	1.31339173691271	16.56968843848080
C	5.1307112067144	2.6067423714185	18.5207987576022
C	4.73982149636683	0.46356034508043	17.68572614335662
H	1.54141262177729	1.40973569173247	19.5366658359171
C	4.52440320272532	0.77277254794519	20.27769012896299
C	0.61044281249386	1.52572988554414	16.41371982464571
C	2.22770028011269	1.85640414694076	14.66929710903545
C	5.78153122062663	3.82670348355280	16.29143478334355
C	0.45495687293880	1.37579058914044	17.85451401737456
C	5.31963669385618	0.85159527267021	15.16945843790352
C	5.34718262238101	3.7595129425597	19.44152587092071
C	4.48708641685280	-1.00429414321327	17.61689799394672
C	-0.5379937631613	1.45101605446576	15.57226611801790
C	2.81714881422226	3.04080367725721	14.20848381923842
C	2.03668104308016	0.76850110855404	13.80681735300224
C	-0.83112934910173	1.11278481162208	18.41119570233812
C	-1.75750187394613	1.20160635378018	16.14798445593499
C	3.20325087184203	3.13627049080533	12.8725665458729
C	2.44543810502105	0.87047250217585	12.47642121420274
C	-1.90406378261180	1.02109154905731	17.56458470950967
C	3.02579614853518	2.05180923931807	12.00571445505140
H	2.95008028667816	3.87196603687276	14.90110458325325
H	3.78383114515351	-0.03716086094206	20.28228198373824
H	4.17444072263997	1.5754888372384	20.9377921311945
H	5.45685614117135	0.37021469589095	20.70241069780821
H	5.59892866995392	3.69565969325572	15.21852862423314
H	6.86202312084704	3.9792312234945	16.43702337175003
H	5.26230165401036	4.73483451044481	16.62389406937705
H	5.17993136032035	1.66406624687338	14.44821365631871
H	4.63603280702232	0.035114014765964	14.90902580681944
H	6.34882211252493	0.47426341292025	15.06430558753267
H	6.42549183108316	3.87530647555767	19.63336708261648
H	4.843785434653847	3.61001456617133	20.40388086205428
H	4.97715931725028	4.69175451546507	18.99764021505261
H	3.81878977358347	-1.33646535999964	18.42002311170512
H	5.44015617341075	-1.54651319365824	17.72412915282936
H	4.0452959573220	-1.29107537417922	16.65502271052546
H	-0.43843171255670	1.60299750472613	14.49963742769645
H	1.60024379900272	-0.15459861746560	14.18915499456737
H	-0.93627074480502	0.9972066558905	19.49018836428845
H	-2.64716482311956	1.15169176999336	15.51999774314230
H	3.64941819219223	4.06202964977836	12.50764478890301
H	2.31458949256838	0.01871615166277	11.80822208262711
H	-2.89765646840763	0.82557727091575	17.96819115568152
H	3.34315772321749	2.1269236890272	10.96531247876784

[2]²⁻. IrMe 3red

Ir	0.74791602017080	-0.06225315437809	0.39384784518322
N	0.48721500373394	-2.11528913810663	0.01792445230411
N	-1.42714789162027	-0.36746827168270	0.33528462827663
C	2.82952545027859	0.46083146588825	-1.21609691287654
C	2.77877152254180	0.70691546346824	0.2311794352206
C	1.626353648203027	0.1022063005954	-1.7373705324159
C	1.77679889056089	1.76101676612894	0.49849626187611
C	1.01500102309501	1.87733411793093	-0.73100590333810
C	-3.34028645774894	0.87598441961181	-0.61850729777762
C	-2.14252250727606	0.35166295581987	0.34210532953344
C	-3.93693137378892	0.14232147031422	0.41268647245574
C	-1.78195434204010	0.14323147031422	-0.161749048555276
C	3.54325295649361	-0.70834674354880	-1.84591129413289
C	-0.77075947355704	0.76796155352595	0.07189679498712
C	3.92393315552850	0.45031045061317	1.1641645827308
C	-3.16590794405109	-2.14473896069326	0.21355415904489
C	-2.43123823220471	0.24311784414552	-0.18807226230471
C	-3.94722813736851	0.34237030108732	0.32943475705693
C	-2.94606856079979	2.85810283322120	1.30693316736224
C	-2.13320363186482	0.2205328552238553	1.30330021311220
C	-0.1979545825247	0.40231087676769	-0.52220952809124
C	-0.04690571475976	0.28956411595331	-1.01831961839956
C	1.789411291870811	2.69249608718794	1.66756315213072
C	1.03290331676611	0.30725435277381	-0.12456763631577
C	-3.94722813736851	0.34237030108732	0.32943475705693
C	-2.94606856079979	2.85810283322120	1.30693316736224
C	-2.13320363186482	0.2205328552238553	1.30330021311220
C	-0.1979545825247	0.40231087676769	-0.52220952809124
C	-0.04690571475976	0.28956411595331	-1.01831961839956
C	1.789411291870811	2.69249608718794	1.66756315213072
C	1.03290331676611	0.30725435277381	-0.12456763631577
C	-3.94722813736851	0.34237030108732	0.32943475705693
C	-2.94606856079979	2.85810283322120	1.30693316736224
C	-2.13320363186482	0.2205328552238553	1.30330021311220
C	-0.1979545825247	0.40231087676769	-0.52220952809124
C	-0.04690571475976	0.28956411595331	-1.01831961